

**DESIGN AND OPTIMIZATION OF HELIOSTAT FIELD USING
SPINNING-ELEVATION SUN TRACKING METHOD BASED ON
COMPUTATIONAL ANALYSIS**

By

TAN MING HUI

A thesis submitted to the
Department of Electrical and Electronic Engineering,
Faculty of Engineering and Science,
Universiti Tunku Abdul Rahman,
in partial fulfillment of the requirements for the degree of
Master of Engineering and Science
July 2011

Universiti Tunku Abdul Rahman
July 2011

ABSTRACT

DESIGN AND OPTIMIZATION OF HELIOSTAT FIELD USING SPINNING-ELEVATION SUN TRACKING METHOD BASED ON COMPUTATIONAL ANALYSIS

Tan Ming Hui

The spinning-elevation (SE) method was first proposed by Ries et al. and then popularized by Chen et al. which provide an alternative method for application in the central power tower system. Before the invention of SE method, azimuth-elevation (AE) sun-tracking method is used in the central power tower system. The implementation of the SE method in the central power tower system was compared to that of the traditional AE method. In the thesis, algorithm to analyze and compute the annual accumulated sun-tracking angles, power consumption and annual field efficiency for both methods has been developed and the data generated were analyzed and compared. Results obtained showed that the total power consumption on the sun-tracking system of SE method can be about 4.8–9.3% lesser than that of AE method while the annual field efficiency of SE method is about 0.8–1% greater than the AE method. The central tower system located at the equator consumes the lowest annual power consumption on sun-tracking system and provides the highest annual field efficiency compared to other latitudes.

ACKNOWLEDGEMENT

First and foremost, I would like to take this opportunity to express my sincere appreciation and deepest gratitude to my supervisor, Dr. Chong Kok Keong, for his guidance, invaluable advice, understanding and considerations on my works. I was able to gain a lot of experiences, skills and knowledge from him.

I wish to express my gratitude to Prof. Dr Faidz bin Abd Rahman, my co-supervisor. He had provided me continuous guidance, directions and advice when I was conducting my works. I would also wish to dedicate special gratitude and deepest thankfulness to my research partners, Wong Chee Woon, Tan Woei Chong, Jessie Siaw Fei Lu, Yew Tiong Keat and Chong Yee How, for their assistances. They always give me support, encouragement, advice, technical expertise and experience.

I appreciate for the encouragement and moral support from my family throughout the duration of my study. Last but not the least, with sincere affection and love to my friends, thank you for your friendship, constant encouragement and invaluable help. I wish you all great blessing.

APPROVAL SHEET

This thesis entitled "**DESIGN AND OPTIMIZATION OF HELIOSTAT FIELD USING SPINNING-ELEVATION SUN TRACKING METHOD BASED ON COMPUTATIONAL ANALYSIS**" was prepared by TAN MING HUI and submitted as partial fulfillment of the requirements for the degree of Master of Engineering and Science at Universiti Tunku Abdul Rahman.

Approved by:

(Dr. CHONG KOK KEONG)
Supervisor
Department of Electrical and Electronic Engineering
Faculty of Engineering and Science
Universiti Tunku Abdul Rahman

Date:.....

(Prof. Dr. FAIDZ BIN ABD RAHMAN)
Co-supervisor
Department of Electrical and Electronic Engineering
Faculty of Engineering and Science
Universiti Tunku Abdul Rahman

Date:.....

FACULTY OF ENGINEERING AND SCIENCE
UNIVERSITI TUNKU ABDUL RAHMAN

Date: 20 July 2011

SUBMISSION OF THESIS

It is hereby certified that **TAN MING HUI** (ID No: **10UEM07352**) has completed this thesis entitled "DESIGN AND OPTIMIZATION OF HELIOSTAT FIELD USING SPINNING-ELEVATION SUN TRACKING METHOD BASED ON COMPUTATIONAL ANALYSIS" under supervision of Dr. Chong Kok Keong (Supervisor) from the Department of Electrical and Electronic Engineering, Faculty of Engineering and Science, and Prof. Dr. Faiz Bin Abd Rahman (Co-Supervisor) from the Department of Electrical and Electronic Engineering, Faculty of Engineering and Science.

I understand that the University will upload softcopy of my thesis in pdf format into UTAR Institutional Repository, which may be made accessible to UTAR community and public.

Yours truly,

(TAN MING HUI)

DECLARATION

I, Tan Ming Hui hereby declare that the dissertation is based on my original work except for quotations and citations which have been duly acknowledged. I also declare that it has not been previously or concurrently submitted for any other degree at UTAR or other institutions.

(TAN MING HUI)

Date : 20 July 2011

TABLE OF CONTENTS

	Page
ABSTRACT	ii
ACKNOWLEDGEMENT	iii
APPROVAL SHEET	iv
SUBMISSION OF THESIS	v
DECLARATION	vi
TABLE OF CONTENTS	vii
LIST OF TABLES	xi
LIST OF FIGURES	xii
LIST OF ABBREVIATIONS	xvii
CHAPTER	
1.0 INTRODUCTION	1
1.1 Research Background	1
1.2 Research Objective	4
1.3 Thesis Overview	4

2.0	LITERATURE REVIEW	6
2.1	Earth-Sun Angles	6
2.1.1	Declination Angle	7
2.1.2	Solar Time	9
2.1.3	Equation of Time	10
2.1.4	Hour Angle	11
2.2	Central Receiver	13
2.2.1	Heliostats	13
2.2.2	Heliostat Field Layout	14
2.2.3	Field Losses	15
2.2.3.1	Cosine Loss	15
2.2.3.2	Shadowing and Blocking Loss	17
2.2.3.3	Atmospheric Transmittance	22
2.2.4	Heliostat Packing Factor	23
3.0	METHODOLOGY	25
3.1	Range of Motion Study	25
3.1.1	Sun-tracking Formula	32
3.1.1.1	Spinning-Elevation Sun-Tracking Method	28
3.1.1.2	Azimuth-Elevation Sun-Tracking Method	31

3.1.2	Heliostat Field Layout	35
3.1.3	Annual Accumulated Sun-Tracking Angles	40
3.1.4	Annual Power Consumption of Heliostat Field on Sun-Tracking System	44
3.2	Field Efficiency Study	44
3.2.1	Unit Vector of Incident and Reflected Ray	45
3.2.2	Coordinate Transformation of Heliostat	47
3.2.2.1	Spinning-Elevation Sun-Tracking Method	49
3.2.2.2	Azimuth-Elevation Sun-Tracking Method	51
3.2.3	Cosine Efficiency and Shadowing and Blocking Efficiency	52
3.2.4	Heliostat Field Layout	54
4.0	RESULT and DISCUSSIONS	60
4.1	Annual Accumulated Angles	60
4.1.1	Comparison of AE and SE Methods for a Single Heliostat	60
4.1.2	Comparison of AE and SE Methods for Heliostat Field	76
4.2	Annual Field Efficiency	78

5.0	CONCLUSION	83
5.1	Concluding Remarks	83
5.2	Future Work	84
	REFERENCES	85
	APPENDIX	90
	Range of Motion Study for Two Different Sun-Tracking	90
	Methods in the Application of Heliostat Field	

LIST OF TABLES

Table		Page
3.1	Specifications and design parameters of the heliostat for range of motion study.	38
3.2	Specification of central power tower and heliostat field layout for range of motion study.	39
3.3	Specification of central power tower and heliostat field layout for field efficiency study.	59
4.1	Annual accumulated sun-tracking angles and power consumption of heliostat field.	77
4.2	Annual efficiencies of heliostat field for both sun-tracking methods.	82

LIST OF FIGURES

Figure		Page
2.1	The ecliptic plane showing variations in the earth-sun distance and the equinoxes and solstices.	7
2.2	(a) The earth is shown in the summer solstice position when the declination angle is 23.45 degrees. (b) The yearly variation of declination angle (δ). Note the definition of the tropics as the intersection of the earth-sun line with the surface of the earth at the solstices and the definition of the Arctic and Antarctic circles by extreme parallel sun rays.	8
2.3	The equation time (<i>EOT</i>). This is the difference between the local apparent solar time and the local mean solar time.	11
2.4	The hour angle (ω) is defined as the angle between the meridian parallel to the sun's rays and the meridian containing the observer	12
2.5	The cosine effect for two heliostats in opposite directions from the tower. For the noontime sun condition shown, heliostat A in the north field has greater cosine efficiency than heliostat B.	16

2.6	Shadow and blocking loss of solar flux.	17
2.7	The radial staggered heliostat pattern developed by the University of Houston.	19
2.8	Heliostat spacing for a field using radial stagger layout pattern.	20
2.9	The idea of the graphical method for a no-blocking radial staggered distribution.	21
2.10	Atmospheric transmittance for a clear day and a hazy atmosphere.	23
3.1	A composite view of coordinate systems attached to both the earth-center and earth-surface reference frames.	27
3.2	Coordinate system attached to the local heliostat reference frame for the Spinning-Elevation (SE) sun-tracking method. The heliostat normal vector \mathbf{H}_{SE} is defined as the function of the angles α_{SE} and ρ_{SE} .	28
3.3	The coordinate system attached to the earth-surface reference frame relative to the central tower and the heliostat for Spinning-Elevation sun-tracking method.	30

3.4	The coordinate system attached to the earth-surface reference frame for the Azimuth-Elevation (AE) sun-tracking method where the heliostat normal vector \mathbf{H}_{AE} is defined as the function of the angles α_{AE} and ρ_{AE} .	32
3.5	The coordinate system attached to earth-surface reference frame relative to the central tower and the heliostat for Azimuth-Elevation sun-tracking method.	35
3.6	Layout of the heliostat field consisted of central tower at the origin and surrounded by 342 heliostats.	37
3.7	The flow chart to show the algorithm to compute the annual accumulated sun-tracking angles for Azimuth-Elevation sun-tracking method.	42
3.8	The flow chart to show the algorithm to compute the annual accumulated sun-tracking angles for Spinning-Elevation sun-tracking method.	43
3.9	Coordinate defining the reflection of the sun's ray by heliostat to a single target point in terms of target angle and facing angle, incident sun's ray in terms of sun altitude angle and azimuth angle, target point and center of the heliostat's frame.	46

3.10	The initial coordinate of the heliostat frames is first defined in a fixed coordinate system. The origin is at the middle of the heliostat and \mathbf{P}_i is the point at the corner edge of the heliostat frame.	48
3.11	Ray/Plane Algorithm method used to compute the shadow area.	55
3.12	Ray/Plane Algorithm method used to compute the blocked area.	55
3.13	The flow chart to show the algorithm of computing the annual field efficiency of the heliostat field.	56
3.14	Layout of the heliostat field consisted of central tower at the origin and surrounded by 317 heliostats.	58
4.1	The annual accumulated tracking angle of a single heliostat versus facing angle in the case of target angle 22.26° , and latitudes 0° , 15°N , 30°N , 45°N , 15°S , 30°S . (a) Annual accumulated elevation angle for SE method ($\Sigma\alpha_{\text{SSE}}$), (b) Annual accumulated spinning angle for SE method ($\Sigma\rho_{\text{SE}}$), (c) Annual accumulated elevation angle for AE method ($\Sigma\alpha_{\text{SAE}}$), (d) Annual accumulated azimuth angle for AE method ($\Sigma\rho_{\text{AE}}$).	64

4.2	The annual accumulated tracking angle of a single heliostat versus facing angle in the case of latitude 0° . (a) Annual accumulated elevation angle for SE method ($\Sigma\alpha_{SSE}$), (b) Annual accumulated spinning angle for SE method ($\Sigma\rho_{SE}$), (c) Annual accumulated elevation angle for AE method ($\Sigma\alpha_{SAE}$), (d) Annual accumulated azimuth angle for AE method ($\Sigma\rho_{AE}$).	70
4.3	The annual accumulated tracking angle of a single heliostat versus facing angle in the case of latitude $45^\circ N$. (a) Annual accumulated elevation angle for SE method ($\Sigma\alpha_{SSE}$), (b) Annual accumulated spinning angle for SE method ($\Sigma\rho_{SE}$), (c) Annual accumulated elevation angle for AE method ($\Sigma\alpha_{SAE}$), (d) Annual accumulated azimuth angle for AE method ($\Sigma\rho_{AE}$).	75
4.4	The annual field efficiency in the case of latitude 0° . (a) SE method (b) AE method.	79
4.5	The annual field efficiency in the case of latitude $15^\circ N$. (a) SE method (b) AE method.	80
4.5	The annual field efficiency in the case of latitude $30^\circ N$. (a) SE method (b) AE method.	81

LIST OF ABBREVIATIONS

δ	Declination angle
ω	Hour angle
Φ	Latitude angle
α	Sun altitude angle
A	Sun azimuth angle
ϕ	Facing angle
λ	Target angle
α_{SE}	Elevation angle for spinning-elevation method
α_{AE}	Elevation angle for azimuth-elevation method
ρ_{SE}	Spinning angle for spinning-elevation method
ρ_{AE}	Azimuth angle for azimuth-elevation method
t_s	Solar time
N	Day number
D	Daylight savings time
LC	Longitude correction
EOT	Equation of time
LCT	Local clock time
H	Target height
h	Height of heliostat

R	Radial distances area of heliostats from the central tower
G_ρ	Gear ratio of the gear train in azimuth or spinning drive
G_α	Gear ratio of the gear train in elevation drive
ω_ρ	Angular speed of azimuth or spinning motor
ω_α	Angular speed of elevation motor
P_ρ	Power rating of azimuth or spinning motor
P_α	Power rating of elevation motor

CHAPTER 1

INTRODUCTION

1.1 Research Background

The largest fixed target solar collector, which is also known as the central power tower system, involves the use of many individual sun-tracking mirrors (or heliostats) to reflect and to superpose the concentrated sunlight at a common target attached to the central tower. According to the thermodynamic law, high conversion efficiency from the solar energy to the electrical energy can only be achieved by this type of solar power plant through Rankine cycle. Unfortunately, it requires a complex control system to operate and to monitor the motors fixed on each heliostat for sun-tracking.

The beginning of the application of heliostats, the sun-tracking method has generally been implemented using the Azimuth-Elevation (AE) method (Stine and Harrigan, 1985). In this tracking method, one of the tracking axes of the heliostat points towards the zenith, namely the azimuth-axis, while the other axis is perpendicular to the first axis and tangent to the heliostat frame called the elevation-axis. During the sun-tracking, the motions of the heliostat are operated by two motors: one motor for the azimuth which provides rotational movement in the

azimuth direction, and another motor which rotates the heliostat in the elevation direction. Before year 1990, this sun-tracking method is more widely used due to its straightforward design learned from the steering mirror used in the optical system and in radar antennae.

The first idea of Spinning-Elevation (SE) method was proposed by Schubnell and Ries in the year 1990 for the application of heliostat in the solar furnace system and was then studied in various applications by several authors (Schubnell and Ries, 1990; Chen *et al.*, 2001, 2002, 2003, 2004, 2005, 2006; Chong, 2002, 2010a, b; Chong *et al.*, 2006, 2011; Guo *et al.*, 2010; Li and Lim, 2009). In this tracking method, one of the tracking axes of the heliostat points towards the target, namely the spinning-axis. In order to maintain the heliostat normal within the tangential plane, while the other axis is perpendicular to the first axis and tangent to the heliostat frame in order to adjust the heliostat normal within the tangential plane until it bisects the sun position vector and the target position vector called the elevation-axis. The motions of this type of heliostat are also operated by two different motors, the motor which provides rotational movement at spinning-axis and another motor which provides rotational movement at elevation-axis. Since 2001, Chen *et al.* and Chong have collectively derived and developed the sun-tracking formula for the SE method by proposing a novel focusing heliostat called non-imaging focusing heliostat (Chen *et al.*, 2001, 2002, 2003, 2004, 2005; Chong, 2002, 2010a,b; Chong *et al.*, 2006, 2011). Unlike the

conventional imaging heliostat design where a fixed geometry approximating spherical surface is used, the non-imaging focusing heliostat is comprised of an array of $m \times n$ facet mirrors which can be maneuvered in line-tilting manner instead of the trivial tip-tilting manner to dynamically correct the first-order astigmatism. Several years later, non-imaging focusing heliostat with a fixed geometry configuration has also been introduced to considerably minimize the complexity of the control system in the heliostat field by excluding all the driving devices for correcting astigmatism (Chen *et al.*, 2004).

The vertical and horizontal sides of the heliostat frame is preserved to be always aligned with the tangential and sagittal planes respectively so that the astigmatism can be corrected using a non-symmetric heliostat with two different radii of curvature as proposed by Zaibel et al. (1995). The geometry of non-imaging focusing heliostat proposed by Chen et al. can be approximated to that of non-symmetric heliostat when the distance between the heliostat and the target is much greater compared to the dimension of the heliostat. In 2004, they have studied the optical performance of the two different sun-tracking methods at the level of a single heliostat and a heliostat field (Chen *et al.*, 2004). The two types of heliostat design are the fixed geometry non-imaging focusing heliostat using SE tracking method and the typical spherical geometry heliostat using AE tracking method. They concluded that the SE tracking method can reduce the receiver spillage loss by 10-30% and also provide a much more uniform concentrated

sunlight at the receiver without huge variations with the time of day compared to the AE tracking method.

1.2 Research Objective

The objectives of the thesis were threefold:

1. To compare the annual accumulated rotational angles for both azimuth-elevation and spinning-elevation sun-tracking methods.
2. To compare the annual power consumption for both sun-tracking methods consumed by the motors in the heliostats.
3. To compare the annual field efficiency for both sun-tracking methods.

1.3 Thesis Overview

The organization of the thesis is as follow: Chapter 1 of this thesis gives a general idea of the research and clarifies the research objectives. Chapter 2 gives the literature reviews about the central receiver. The calculation of sun position is also reviewed. In Chapter 3, the principles of both AE and SE sun-tracking formulas are discussed in detail including the mathematical derivation of tracking

angles. The methodologies for the simulation algorithm also included. The simulation results are shown and discussed in Chapter 4. Chapter 5 ends the thesis with the conclusion.

CHAPTER 2

LITERATURE REVIEW

2.1 Earth-Sun Angles

The earth revolves around the sun every 365.25 days in an elliptical orbit. The plane of the earth's revolution is referred as the ecliptic. The mean distance between the earth and the sun is approximately 1.496×10^{11} m which is also defined as one astronomical unit (1 AU). The maximum earth-sun distance (1.52×10^{11} m), *aphelion*, occurs on about July 3rd, while the minimum earth-sun distance (1.47×10^{11} m), *perihelion*, occurs on about January 2nd. Figure 2.1 depicts these variations in relation to the Northern Hemisphere seasons.

The earth revolves about its polar axis in approximately 24 hours per day. The polar axis is inclined to the ecliptic plane by 23.45 degrees. The direction in which the polar axis points is fixed in space and is aligned with the North Star (Polaris) to within about 45 minutes of arc (13 mrad). The revolution of the earth about its polar axis bring into being the days and nights, whereas the tilt of this axis relative to the ecliptic plane produces four seasons in several countries as the earth rotates about the sun (Stine and Harrigan, 1985).

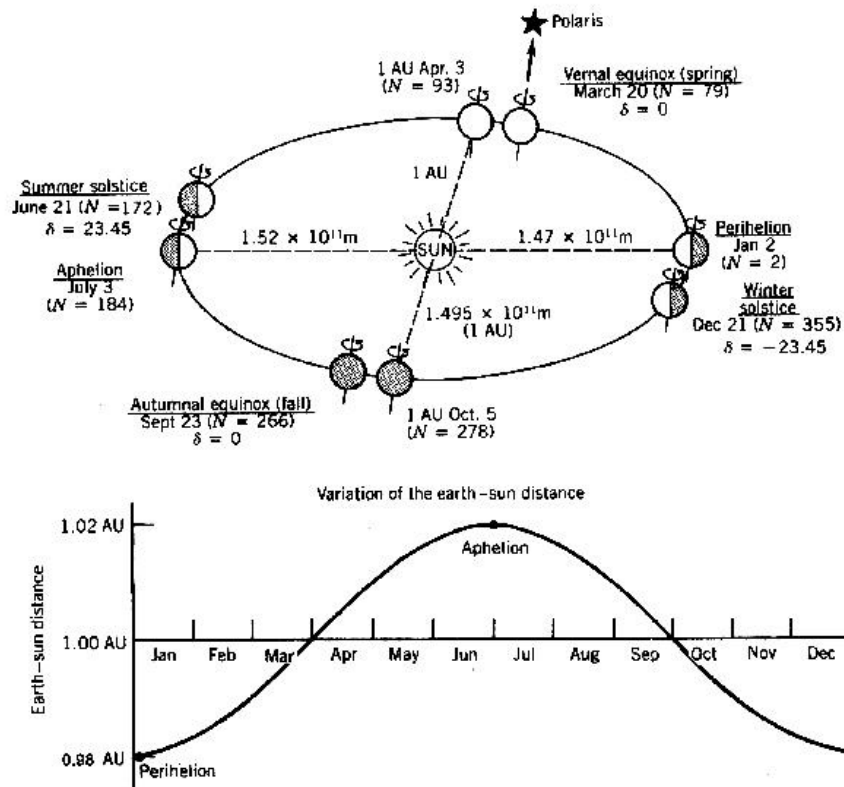


Figure 2.1: The ecliptic plane showing variations in the earth-sun distance and the equinoxes and solstices (Stine and Harrigan, 1985).

2.1.1 Declination Angle

If a line is drawn from the center of the earth to the center of the sun, the angle between this line and the earth's equatorial plane (earth equator) is defined as the declination angle (δ), as revealed in Figure 2.2.

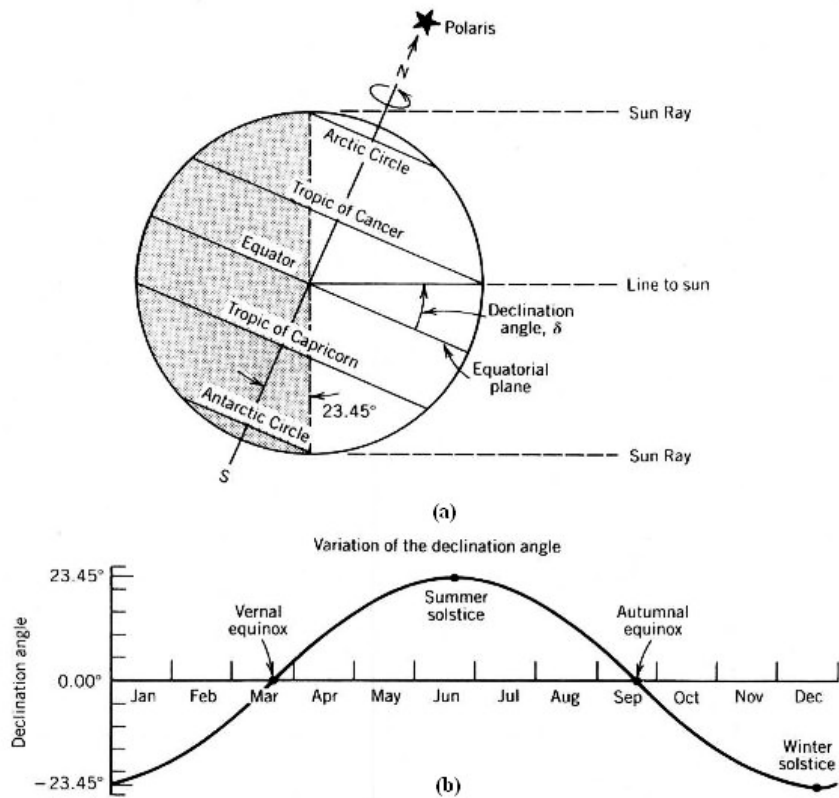


Figure 2.2: (a) The earth is shown in the summer solstice position when the declination angle is 23.45 degrees. (b) The yearly variation of declination angle (δ). Note the definition of the tropics as the intersection of the earth-sun line with the surface of the earth at the solstices and the definition of the Arctic and Antarctic circles by extreme parallel sun rays (Stine and Harrigan, 1985).

About June 21st, the northern part of the earth's rotational axis is inclined toward the sun with the maximum declination angle 23.45 degrees. This situation is known as the summer solstice which symbols the beginning of summer in the Northern Hemisphere. Three months later, the line from the earth to the sun lies on the equatorial plane (δ becomes zero). An observer at the equator would observe

that the sun is directly overhead at noontime. This phenomenon is known as the equinox since the period of day time and night time are equal to 12 hours. There are two such situations during a year: the autumnal equinox on about September 23rd, marking the start of the fall and the vernal equinox around March 22nd, marks the beginning of the spring. The winter solstice occurs around December 22nd and marks the point when the equatorial plane is tilted relative to the earth-sun line such that the northern hemisphere is tilted far away from the sun (δ is -23.45 degrees) (Stine and Harrigan, 1985).

2.1.2 Solar Time

Solar time is a 24-hour clock and it is usually used as a reference in solar energy field. The concept of the solar time is used in calculating the direction of the sun's ray relative to a point on the earth. Solar time is location (longitude) dependent because it is measured from the solar noon, i.e. the time when the sun appears to cross the local meridian. It is generally different from local clock time, which is defined by politically defined time zones and other approximations. The difference between solar time and local clock time can come up to 1 or 2 hours at various locations (Stine and Harrigan, 1985).

Mean time is based on the duration of an average day. A mean second is 1/86,400 of average time between one complete transits of the sun, averaged over

the entire year. In reality, the time-span of any one specific day can be measured by the complete transit of the sun which can vary by up to 30 seconds during the year.

The variation in solar day length is due to four factors listed in order of decreasing importance (Jespersion and Fitz-Randolph, 1977):

- a. The earth's orbit around the sun is not a perfect circle but elliptical, so the earth travels faster when it is nearer the sun than when it is farther away.
- b. The earth's axis is tilted to the plane containing its orbit around the sun.
- c. The earth spins at an irregular rate around its axis of rotation.
- d. The earth wobbles on its axis.

2.1.3 Equation of Time

The difference between mean time and solar time is depicted in Figure 2.3. The difference is called the equation of time (*EOT*). The level of accuracy required in the correlation between time and day and the solar time will depend on whether the designer is doing performance prediction, system correlation, or developing tracking equations. An approximation for the equation of time in minutes, as given by Woolf (1968), is accurate to within about 30 seconds during daylight hours.

$$EOT = 0.258 \cos x - 7.416 \sin x - 3.648 \cos 2x - 9.228 \sin 2x \quad (\text{minutes}) \quad (2.1)$$

where the angle x is a function of the day number N :

$$x = \frac{360(N-1)}{365.242} \quad (\text{degrees}) \quad (2.2)$$

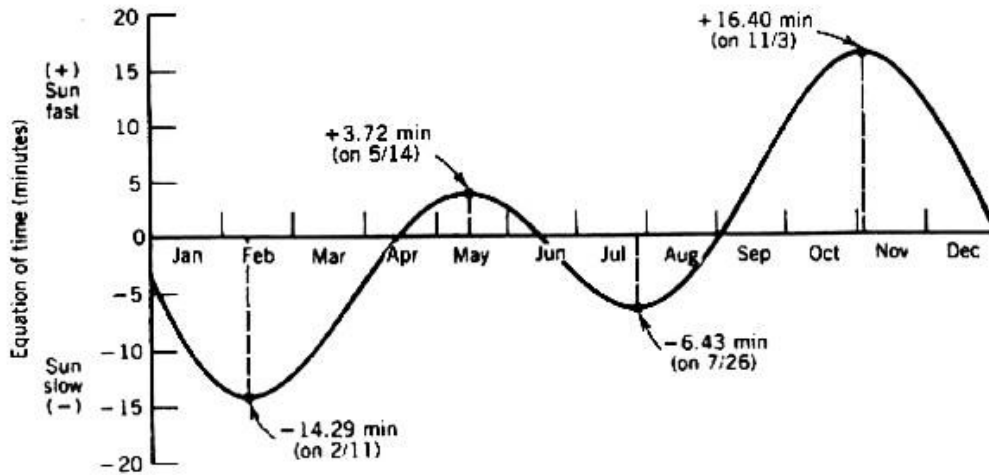
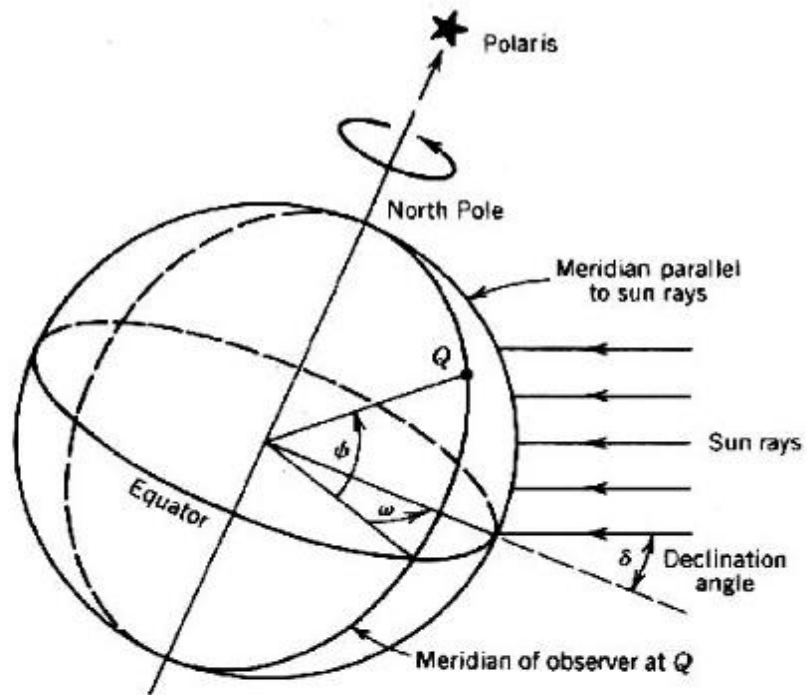


Figure 2.3: The equation time (*EOT*). This is the difference between the local apparent solar time and the local mean solar time (Woolf, 1968).

2.1.4 Hour Angle

The clock is used to describe the earth's rotation about its polar axis. The hour angle (ω) is the angle of rotation associated with the clock. It is the angle between the plane of the meridian containing the point of interest and the meridian that touches the earth-sun line as shown in Figure 2.4. The hour angle is zero at solar noon (when the sun reaches its highest point in the sky). The hour angle increases by 15 degrees every hour and 1 degree every 4 minutes. As an example, when it is 4 hours after the solar noon, the hour angle has a value of 60 degrees.



Variation of the hour angle

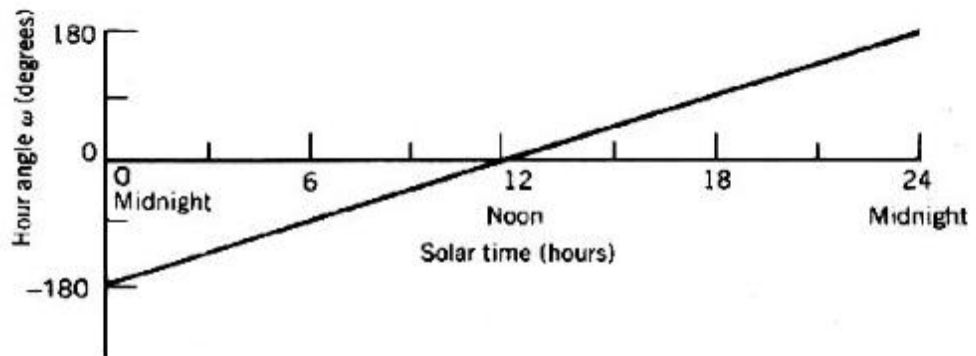


Figure 2.4: The hour angle (ω) is defined as the angle between the meridian parallel to the sun's rays and the meridian containing the observer (Stine and Harrigan, 1985).

2.2 Central Receiver

The central-receiver concept for solar energy concentration and collection is based on a field of individual sun-tracking mirrors which are also known as heliostats that reflect the incident sunlight to a target or receiver located at the top of a central tower. The reflected energy is absorbed into the heat-transfer fluid which is pumped up from the bottom of the tower to the receiver. The heated fluid which return down from the tower will be used for thermal electrical power plant or an industrial process requiring heat.

2.2.1 Heliostats

Heliostats reflect incident light from the sun to a target or receiver located at the top of a central tower. It is composed of several mirror module panels rather than a single large mirror. Currently, two types of sun-tracking methods which implemented in the heliostat are the azimuth-elevation (AE) method and the spinning-elevation (SE) method. The reflective surfaces (mirrors) of the heliostat are mounted or supported on a pedestal which permits the movement about the azimuth and elevation axes for AE method or the spinning and elevation axes for SE method. Movement about each axis is supplied by a fractional-horsepower motor through a gearbox drive. These motors receive signals from a central control

computer that accurately points the reflective surface normal intermediate between the sun and the receiver. The power consumed by the motors is known as the parasitic energy. It is better to minimize the power usage from the motors to obtain higher energy output from the central power tower system.

2.2.2 Heliostat Field Layout

Heliostat field layout is the pattern or arrangement of heliostats in the heliostat field. The layout must be well designed to maximize the field efficiency for the central power tower system. Most of the heliostat field layout designs have a radial stagger pattern (Lipps and Vant-hull, 1978; Segal and Epstein, 1996; Siala and Elayeb, 2001; Sanchez and Romero, 2006). This pattern is based on an assumption that every single heliostat will be able to move freely in a circular space without collision with their respective adjacent heliostats. The diameter of the circle is given by the diagonal of the reflector of the heliostat with the addition of security distance (Collado and Turégano, 1989; Collado, 2009).

2.2.3 Field Losses

The energy losses associated specifically with the heliostat field include cosine loss, shadowing loss, blocking loss, reflectance loss from the mirror and atmosphere attenuation loss.

2.2.3.1 Cosine Loss

The largest source of field energy loss is the cosine loss. Even though cosine losses can be minimized with appropriate field layout design, it is still the single most important field loss mode.

Cosine losses depend on both the sun's position and the location of the individual heliostat relative to the receiver or target. The heliostat's reflector is positioned by the sun-tracking mechanism so that its surface normal bisects the angle between the sun's incident rays and a line from the center reflector of the heliostat to the target located on top of the central tower. The effective reflective area of the heliostat is reduced by the cosine of one-half of this angle. This may be visualized by considering heliostats at two positions in a field as shown in Figure 2.5. Heliostat A has a lower cosine loss since it has a smaller reflecting angle, θ_i compare with Heliostat B which has a higher cosine loss because it has a larger reflecting

angle. It is noted that the most efficient heliostats are located just opposite the sun (Stine and Harrigan, 1985).

In the morning, heliostats located at the west of the central tower will have lower cosine loss compare to those heliostats which are at the east of the central tower. On the contrary, heliostats located at the east field have lower cosine loss compare to those at the west field during the afternoon.

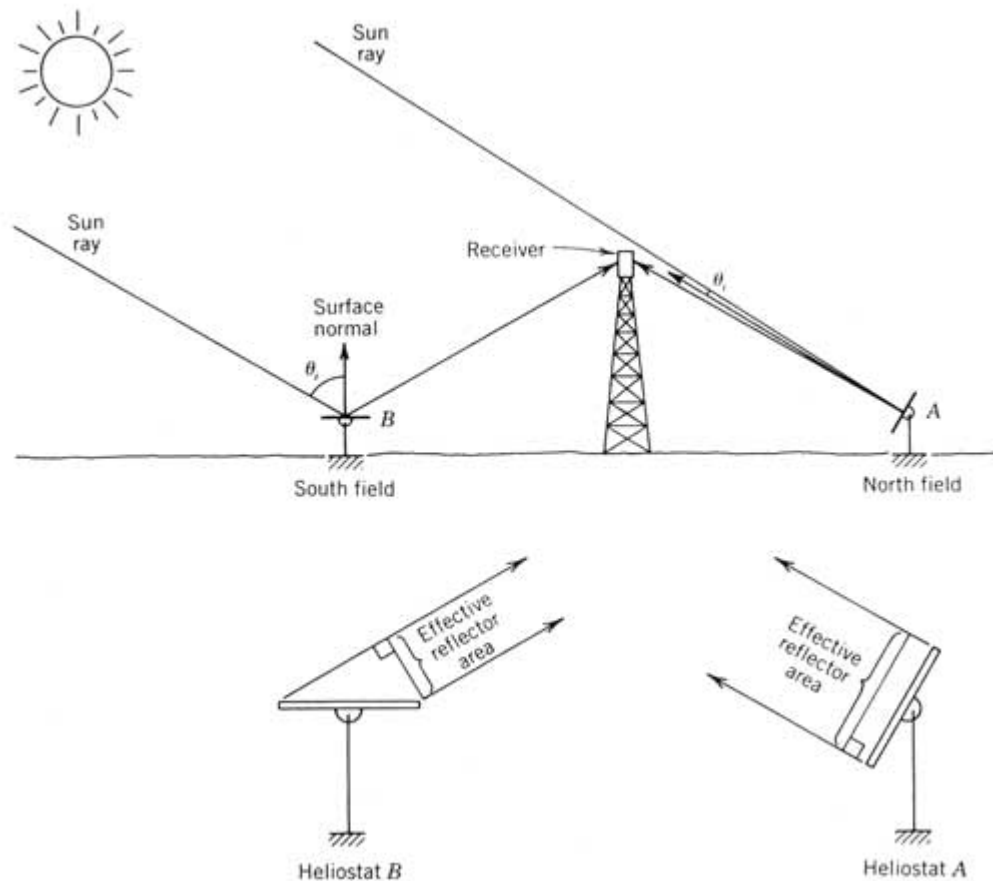


Figure 2.5: The cosine effect for two heliostats in opposite directions from the tower. For the noontime sun condition shown, heliostat A in the north field has greater cosine efficiency than heliostat B (Stine and Harrigan, 1985).

2.2.3.2 Shadowing and Blocking Loss

For central receiver systems, besides cosine loss which causes the reduction of heliostat field efficiency, there are two vital factors that will reduce the amount of energy reaching the receiver or target located at the top of the central tower. They are the shadowing and blocking caused by the adjacent heliostats.

Shadowing occurs at low sun angles when a heliostat casts its shadow on the heliostats located behind it. Therefore, not all the incident solar flux from the sun reaches the reflector. Blocking occurs when a heliostat in front of another heliostat blocks the reflected flux on its way to the receiver. Both processes are illustrated in Figure 2.6. Blocking can be observed in a heliostat field by noting reflected light on the backs of heliostats.

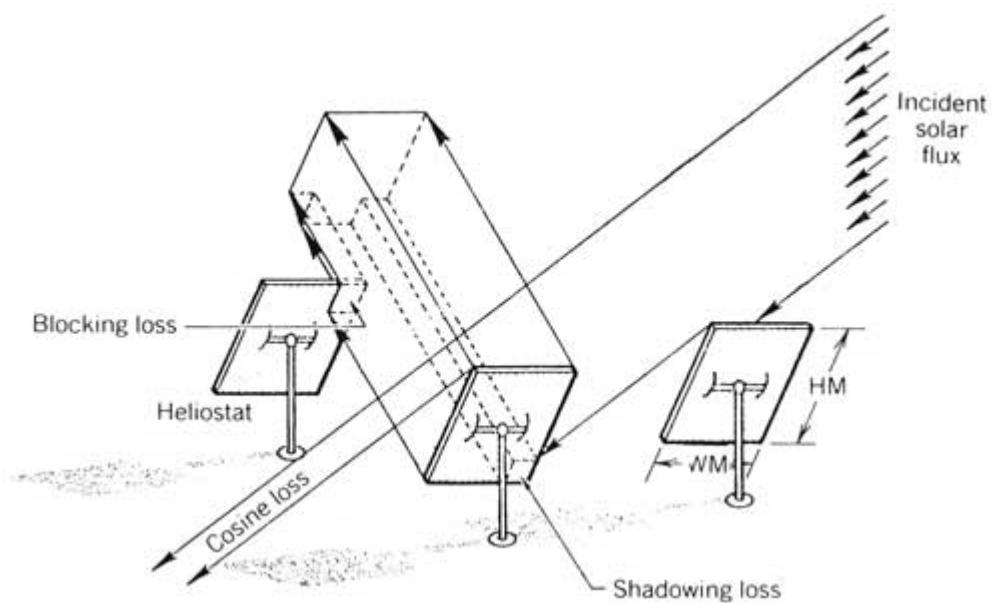


Figure 2.6: Shadow and blocking loss of solar flux (Stine and Harrigan, 1985).

It is generally good to arrange heliostats in a radial staggered pattern as shown in Figure 2.7. This pattern minimizes land usage as well as shadowing and blocking losses. Heliostats are tightly packed near the tower but must be sufficiently separated to prevent mechanical interference or collision. For heliostats located farther away from the central tower, the spacing between heliostats increases to minimize blocking of the reflected rays. Additional heliostats are added when spacing becomes too huge and a new stagger pattern is established.

Optimized heliostat layouts developed at the University of Houston (Lipps and Vant-Hull, 1978) have produced a means of determining spacing and average field density for preliminary field layouts. The radial spacing ΔR and the azimuthal spacing ΔA , as shown in Figure 2.8, are given by Dellin et al. (1981) for high-reflectance heliostats (about 90 percent) in large fields as:

$$\Delta R = HM(1.44 \cot \theta_L - 1.094 + 3.068\theta_L - 1.1256\theta_L^2) \quad (\text{m}), \quad (2.3)$$

$$\Delta A = WM \left(1.749 + 0.6396\theta_L + \frac{0.2873}{\theta_L - 0.04902} \right) \quad (\text{m}), \quad (2.4)$$

where HM and WM are the height and width of the heliostat, respectively, as shown in Figure 2.6. The angle θ_L is the altitude angle to the receiver from the heliostat location of concern and may be calculated as

$$\theta_L = \tan^{-1} \left(\frac{1}{r} \right) \quad (\text{degree}), \quad (2.5)$$

where r is the normalized distance from the tower to the heliostat location measured in "Tower Heights."

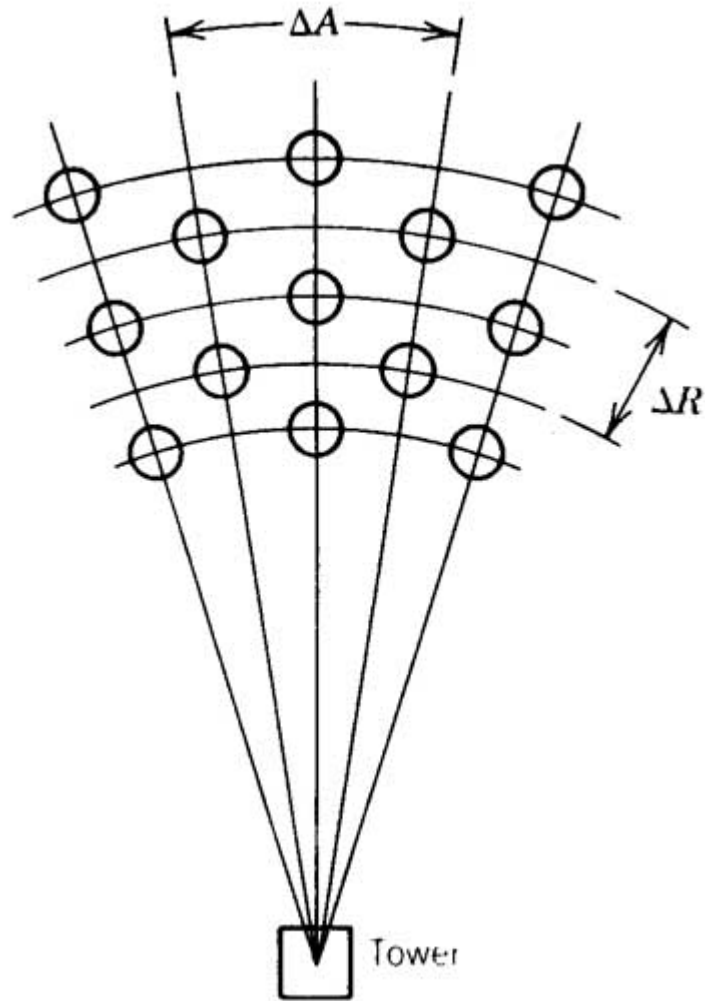


Figure 2.7: The radial staggered heliostat pattern developed by the University of Houston (Lipps and Vant-Hull, 1978).

Figure 2.8 shows the spacing predicted by Equations (2.3) and (2.4). It was shown that for the heliostats farther from the tower, the radial spacing increases, whereas the azimuthal spacing decreases to the point where the heliostats at a particular radial distance have one heliostat width between them ($\Delta A = 2$).

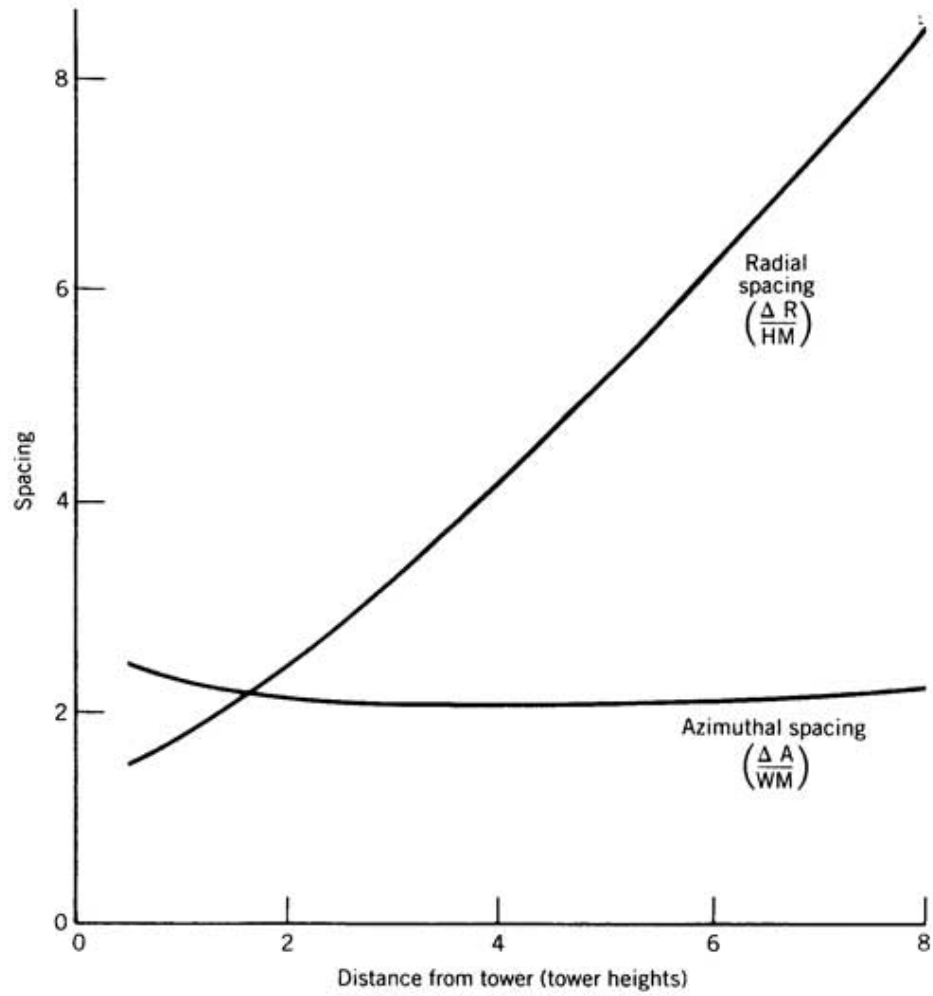


Figure 2.8: Heliostat spacing for a field using radial stagger layout pattern (Dellin et al., 1981).

Based on the criterion by Al-Rabghi and Elsayed (1990) of no blocking and no shadowing, the heliostat field is subdivided into zones which are characterized by a predominant shadowing and blocking effect. The minimum yearly radial spacing for no blocking and no shadowing condition is computed for all zones.

The idea of graphical method for a no-blocking radial staggered layout was introduced within the joint work between the Center For Solar Studies (CSES), Tripoli and Atlantis Energy Ltd, Bern. It placed the heliostats in the field of central power tower system so that no blocking losses occur over the entire year (Siala and Elayeb, 2001). Figure 2.9 shows the idea of the graphical method being proposed.

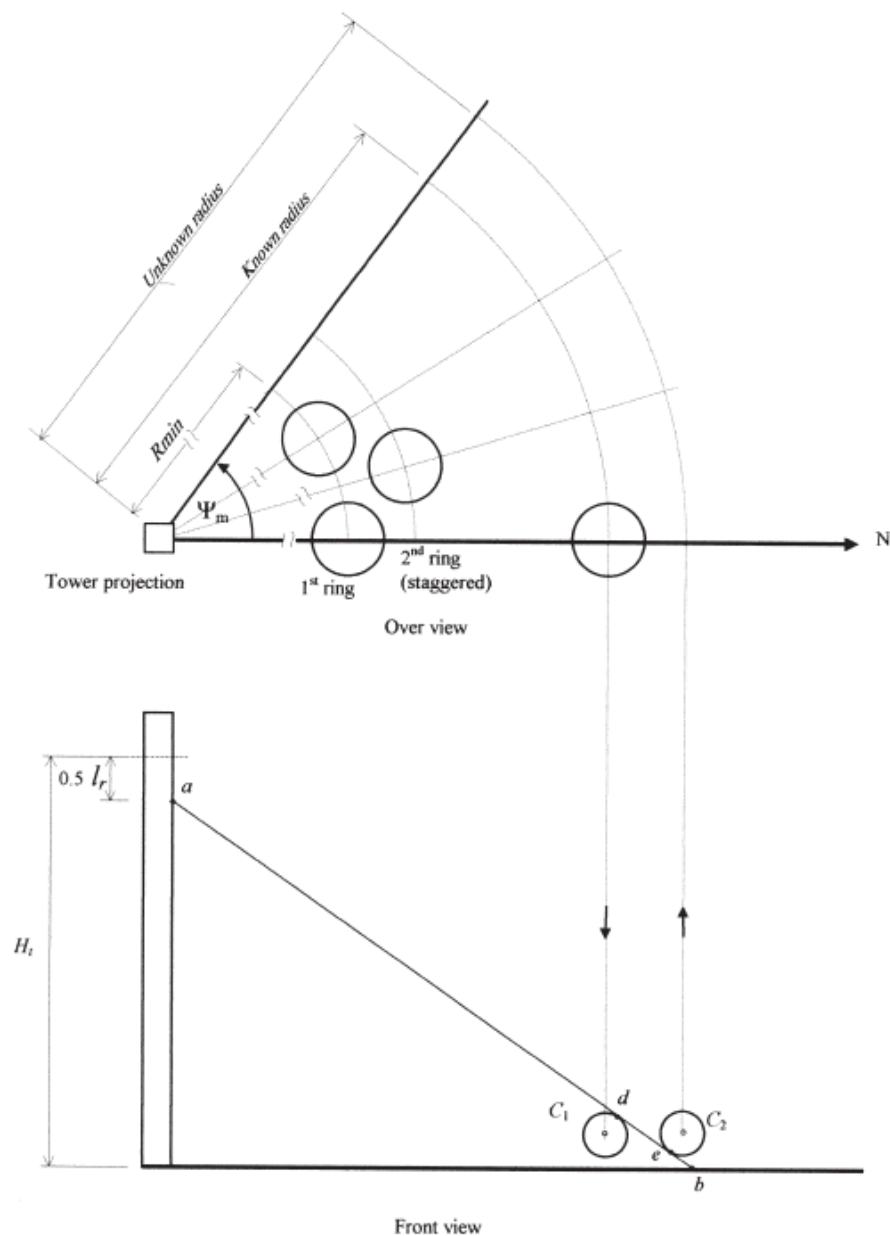


Figure 2.9: The idea of the graphical method for a no-blocking radial staggered distribution (Siala and Elayeb, 2001).

2.2.3.3 Atmospheric Transmittance

Many factors in field layout suggest that the field should extend far to the north of a very high tower. The major limitation on the distance a heliostat is located away from the tower is the attenuation of the reflected rays as they travel from the heliostat to the receiver.

Atmospheric transmittance has been approximated by Vittitoe and Biggs (1978) for a clear day (23-km visibility) and a hazy day (5-km visibility). For a clear day with 23-km visibility, the atmospheric transmittance is

$$\tau_a = 0.99326 - 0.1046S + 0.017S^2 - 0.002845S^2, \quad (2.6)$$

where S is the slant range from heliostat to the receiver in kilometers. For a hazy day with only 5-km visibility, the atmospheric transmittance is

$$\tau_a = 0.98707 - 0.2748S + 0.3394S^2. \quad (2.7)$$

Even though these expressions were derived for a specific site's altitude, they are strongly reliant on the aerosol distribution at ground level (visibility) and only slightly dependent on site's altitude. The effect of atmospheric attenuation is shown graphically in Figure 2.10. Conversely, larger fields are envisioned in the near future where atmospheric attenuation will be even more significant.

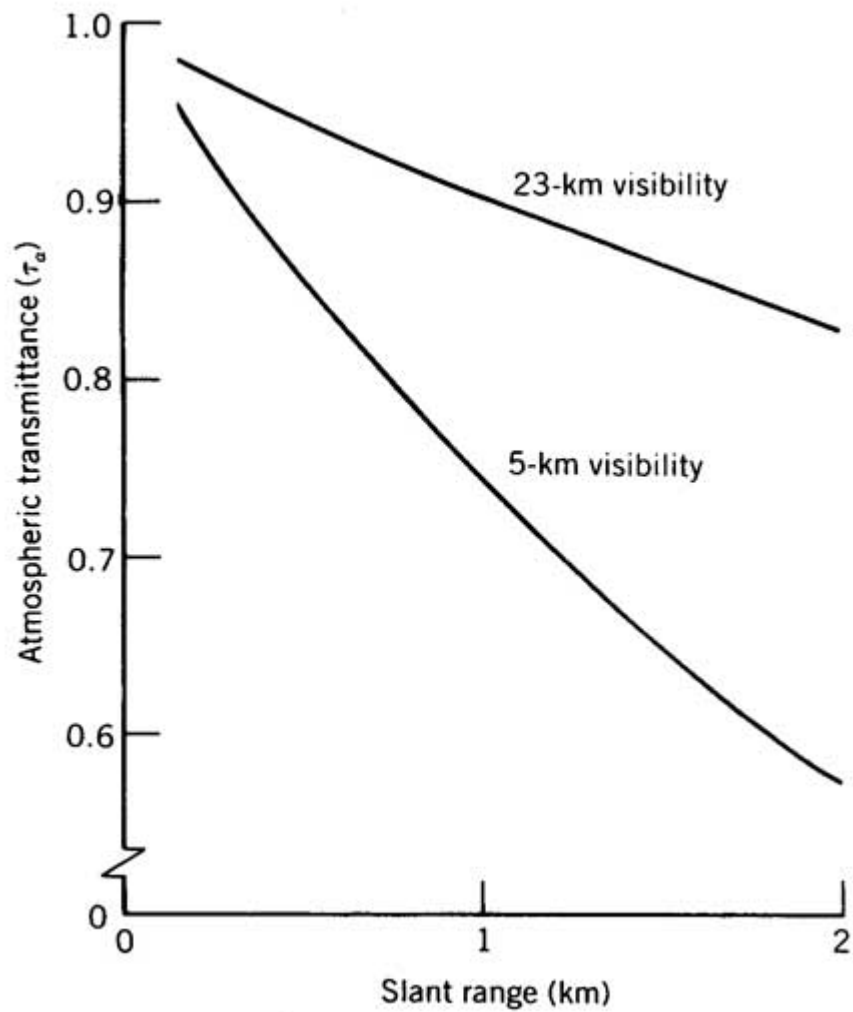


Figure 2.10: Atmospheric transmittance for a clear day and a hazy atmosphere (Vittitoe and Biggs, 1978).

2.2.4 Heliostat Packing Factor

Heliostat packing factor is the ratio of mirror area to field area. A high heliostat packing factor can have the advantage of more heliostats being installed in

the most favorable region combined with low cosine losses, low astigmatism and a shorter distance between the reflector and the receiver aperture. Unfortunately, it will increase shadowing and blocking effect.

The average heliostat packing factor from optimized ray trace analyses of shadowing and blocking is normally in the range of 0.2 to 0.25 (Battleson, 1981). Recently, the CSIRO solar tower system in Australia has a heliostat packing factor approximately 0.53 which was optimized to have the highest performance for the time frame from 10:00 to 14:00 (Schramek et al., 2009).

CHAPTER 3

METHODOLOGY

3.1 Range of Motion Study

There are two types of sun-tracking methods implemented in the heliostat field for the central solar power tower system, the azimuth-elevation (AE) method and the spinning-elevation (SE) method. Further exploration on the range of motion for the two different sun-tracking methods is done in this study. The characteristics of both rotational angles in the AE and SE methods are analyzed to compare which sun-tracking method has the minimum accumulated rotational angles throughout the year.

3.1.1 Sun-tracking formula

To analyze the range of motion for the two different sun-tracking methods in the application of central tower system, the formulas of sun-tracking angles of both methods must be obtained first. In fact, the mathematical expressions of the sun-tracking formulas for AE and SE methods were previously derived by Stine and Harrigan in year 1985 and Chen et al. in year 2001 respectively. In central tower system, sun rays that impinge on a field of heliostats (each heliostat is an

array of $m \times n$ facet mirrors attached to a movable mechanical frame) are reflected to a single point in space namely fixed target or central receiver. Thus, sun-tracking formulas of both methods have to involve a sun position vector (incident sun ray), a target position vector (reflected sun ray) and a heliostat normal vector. Since the sun is a moving object and the target is a fixed object, the heliostat normal must be adjusted from time to time when the sun position changes with time. The sun's position relative to any location on the earth's surface can be mathematically described as sun altitude angle (α) and sun azimuth angle (A). The ultimate position of the heliostat normal regardless of any sun-tracking method should be the same during sun-tracking whilst the only difference between the AE and the SE methods is the orientation of tracking axes for rotating the heliostat normal to that position. Before deriving the sun-tracking formulas of both methods, the sun position angles must be presented first. Figure 3.1 shows the composite view of coordinate systems attached to both the earth-centre and earth-surface reference frames. In earth-centre frame, the vector \mathbf{S}' that points towards the sun is described in terms of hour angle ω and declination angle δ . Given that the observer Q is located on the earth surface with latitude Φ , the sun position vector \mathbf{S} is defined in the earth-surface frame in terms of the sun altitude angle α and the sun azimuth angle A . According to Stine and Harrigan (1985), the derivation of sun's altitude and azimuth angles can be obtained by multiplying the latitude transformation matrix Φ on the vector \mathbf{S}' as follow:

$$\begin{bmatrix} \sin \alpha \\ \cos \alpha \sin A \\ \cos \alpha \cos A \end{bmatrix} = \begin{bmatrix} \cos \Phi & 0 & \sin \Phi \\ 0 & 1 & 0 \\ -\sin \Phi & 0 & \cos \Phi \end{bmatrix} \begin{bmatrix} \cos \delta \cos \omega \\ -\cos \delta \sin \omega \\ \sin \delta \end{bmatrix} \quad (3.1)$$

$$= \begin{bmatrix} \sin \delta \sin \Phi + \cos \delta \cos \omega \cos \Phi \\ -\cos \delta \sin \omega \\ \sin \delta \cos \Phi - \cos \delta \cos \omega \sin \Phi \end{bmatrix}. \quad (3.2)$$

The sun's altitude angle is defined as

$$\alpha = \sin^{-1}(\sin \delta \sin \Phi + \cos \delta \cos \omega \cos \Phi). \quad (3.3)$$

The sun azimuth angle is defined as

$$A = \cos^{-1}\left(\frac{\sin \delta \cos \Phi - \cos \delta \cos \omega \sin \Phi}{\cos \alpha}\right). \quad (3.4)$$

$$\text{If } \sin \omega > 0 \text{ then } A = 2\pi - A. \quad (3.5)$$

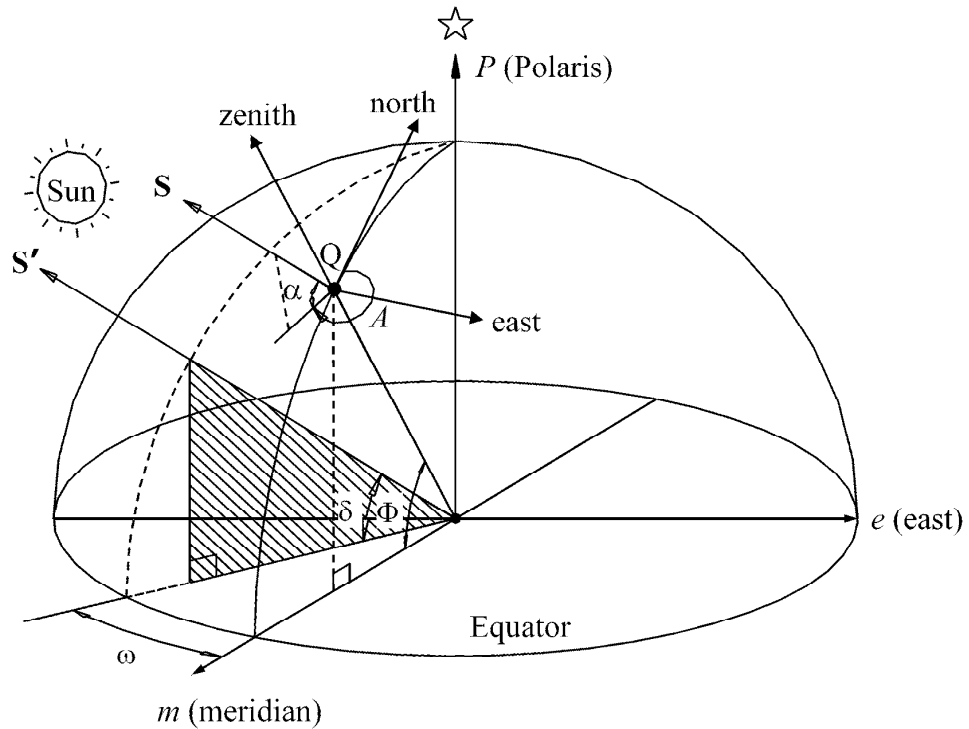


Figure 3.1: A composite view of coordinate systems attached to both the earth-center and earth-surface reference frames.

The declination angle, δ , can be calculated by using the following formula:

$$\delta = 23.45 \times \sin \left[\frac{360}{365} \times (284 + N) \right] \quad (3.6)$$

The hour angle, ω , can be calculated as follow:

$$\omega = 15 \times (t_s - 12) \quad (3.7)$$

where N is number of day in a calendar year, $N = 1$ for January 1 and $N = 42$ for February 11, t_s is the solar time in 24-hour rather than AM/PM.

3.1.1.1 Spinning-Elevation Sun-Tracking Method

For the Spinning-Elevation (SE) sun-tracking method, the coordinate system being referred to the local heliostat reference frame as shown in Figure 3.2 with

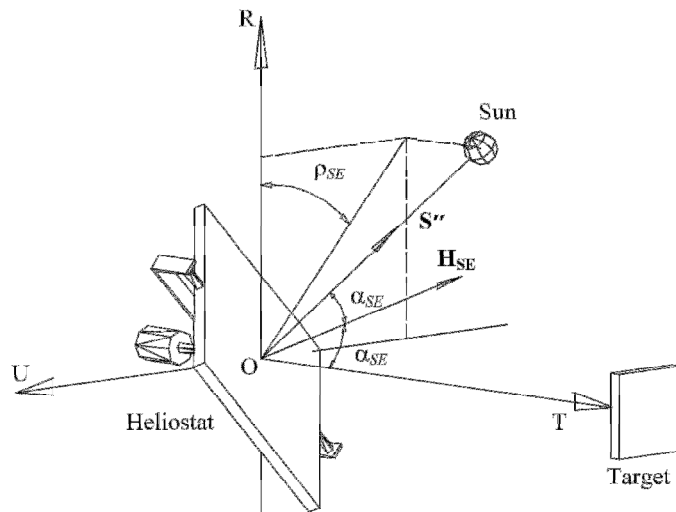


Figure 3.2: Coordinate system attached to the local heliostat reference frame for the Spinning-Elevation (SE) sun-tracking method. The heliostat normal vector \mathbf{H}_{SE} is defined as the function of the angles α_{SE} and ρ_{SE} .

the origin, O, defined as the cross-section point of the two sun-tracking axes. OR, OU and OT are three fixed orthogonal axes with the OT axis pointing out from the origin towards the target direction. The initial orientation of heliostat is defined in such a way that the mirrors along the central column and central row are aligned to be parallel with the OR and OU axes respectively. The heliostat normal vector \mathbf{H}_{SE} is defined as the function of the angles α_{SE} and ρ_{SE} . From Figure 3.3, the spinning angle (ρ_{SE}) and elevation angle (α_{SE}) of the heliostat can be interrelated to the sun position vector through the coordinate transformations of facing angle, ϕ , and then followed with that of the target angle, λ , as expressed in the following:

$$\begin{bmatrix} \cos(\frac{\pi}{2} - 2\alpha_{SE}) \cos \rho_{SE} \\ -\cos(\frac{\pi}{2} - 2\alpha_{SE}) \sin \rho_{SE} \\ \sin(\frac{\pi}{2} - 2\alpha_{SE}) \end{bmatrix} = \begin{bmatrix} \cos \lambda & 0 & -\sin \lambda \\ 0 & 1 & 0 \\ \sin \lambda & 0 & \cos \lambda \end{bmatrix} \begin{bmatrix} 1 & 0 & 0 \\ 0 & \cos \phi & -\sin \phi \\ 0 & \sin \phi & \cos \phi \end{bmatrix} \begin{bmatrix} \sin \alpha \\ \cos \alpha \sin A \\ \cos \alpha \cos A \end{bmatrix} \quad (3.8)$$

$$= \begin{bmatrix} \cos \lambda \sin \alpha - \sin \lambda \sin \phi \cos \alpha \sin A - \sin \lambda \cos \phi \cos \alpha \cos A \\ \cos \phi \cos \alpha \sin A - \sin \phi \cos \alpha \cos A \\ \sin \lambda \sin \alpha + \cos \lambda \sin \phi \cos \alpha \sin A + \cos \lambda \cos \phi \cos \alpha \cos A \end{bmatrix}, \quad (3.9)$$

when $\phi = 0^\circ$, the heliostat is due south of the target and it is of a positive value if the spinning-axis is rotated from the north to the east. $\lambda = 0^\circ$ if the heliostat is of the same height as the target and it is of a positive value when the spinning-axis is rotated so that the target is higher than the heliostat. It is noted that the angle λ in this thesis is defined in the opposite direction compared with the definition by Chen et al. (Chen *et al.*, 2001, 2002, 2003, 2004, 2005, 2006). The direction of λ is hereby being redefined as a positive value in a way that the elevation of the target is always above the heliostat field.

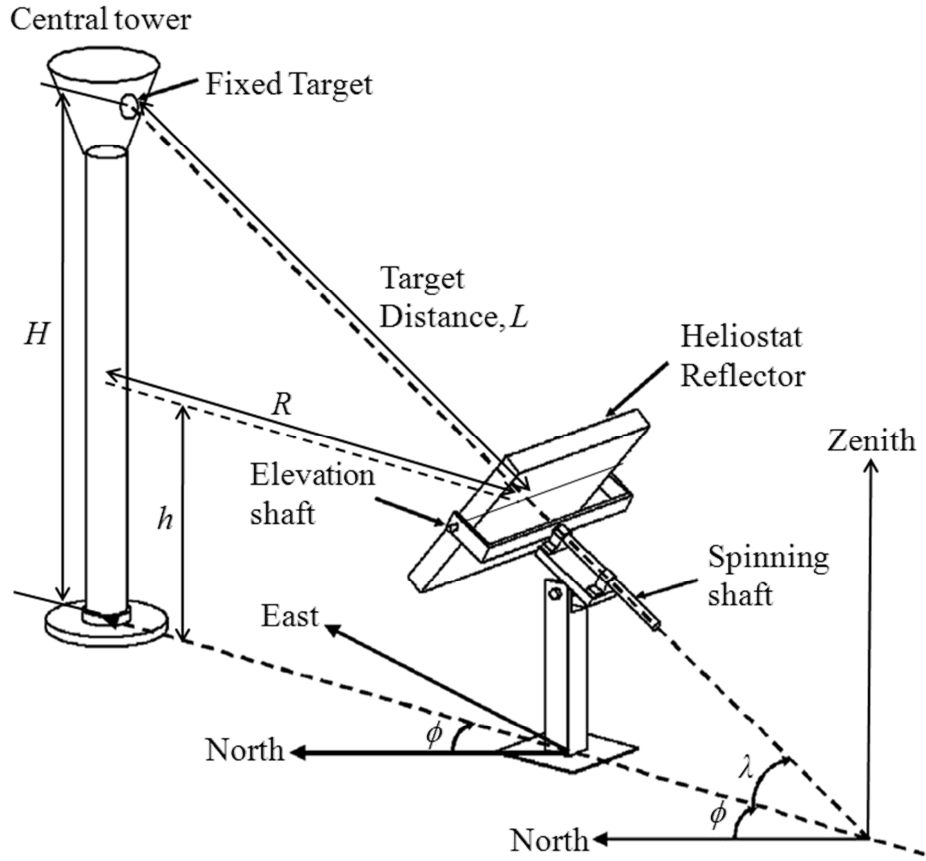


Figure 3.3: The coordinate system attached to the earth-surface reference frame relative to the central tower and the heliostat for Spinning-Elevation sun-tracking method.

The elevation and spinning angles of heliostat using the SE method can be expressed as follow:

$$\alpha_{SE} = \frac{\pi}{4} - \frac{1}{2} \sin^{-1} (\sin \lambda \sin \alpha + \cos \lambda \sin \phi \cos \alpha \sin A + \cos \lambda \cos \phi \cos \alpha \cos A). \quad (3.10)$$

In the case of $\cos \rho_{SE} > 0$,

$$\rho_{SE}^+ = \sin^{-1} \left\{ \frac{\sin \phi \cos \alpha \cos A - \cos \phi \cos \alpha \sin A}{\cos(\frac{\pi}{2} - 2\alpha_{SE})} \right\}. \quad (3.11)$$

In the case of $\cos \rho_{SE} < 0$,

$$\rho_{SE}^- = \pi - \rho_{SE}^+, \quad (3.12)$$

where

$$\cos \rho = \frac{\cos \lambda \sin \alpha - \sin \lambda \sin \phi \cos \alpha \sin A - \sin \lambda \cos \phi \cos \alpha \cos A}{\cos(\frac{\pi}{2} - 2\alpha_{SE})}. \quad (3.13)$$

Note: equation (3.10) is obtained from the third row of equation (3.9), equations (3.11) and (3.12) are derived from the second row of equation (3.9) and equation (3.13) is derived from the first row of equation (3.9).

From equations (3.10) - (3.12), both the angles ρ_{SE} and α_{SE} are exactly 0° when the elevation axis is aligned to be parallel with the OU axis and the top of heliostat frame facing towards OR axis.

3.1.1.2 Azimuth-Elevation Sun-Tracking Method

For the Azimuth-Elevation (AE) sun-tracking method, the coordinate system being referred to the earth-surface reference frame where the heliostat normal vector \mathbf{H}_{AE} is defined as the function of the angles α_{AE} and ρ_{AE} as shown in Figure 3.4. The azimuth angle ρ_{AE} and the elevation angle α_{AE} can be derived solely based on the reflection law that relates the sun position vector, the target position vector and the heliostat normal vector in the earth-surface coordinate system. The

sun position vector can be recalled from the equation (3.1) in the matrix form as follow:

$$\mathbf{S} = \begin{bmatrix} \sin \alpha \\ \cos \alpha \sin A \\ \cos \alpha \cos A \end{bmatrix}. \quad (3.14)$$

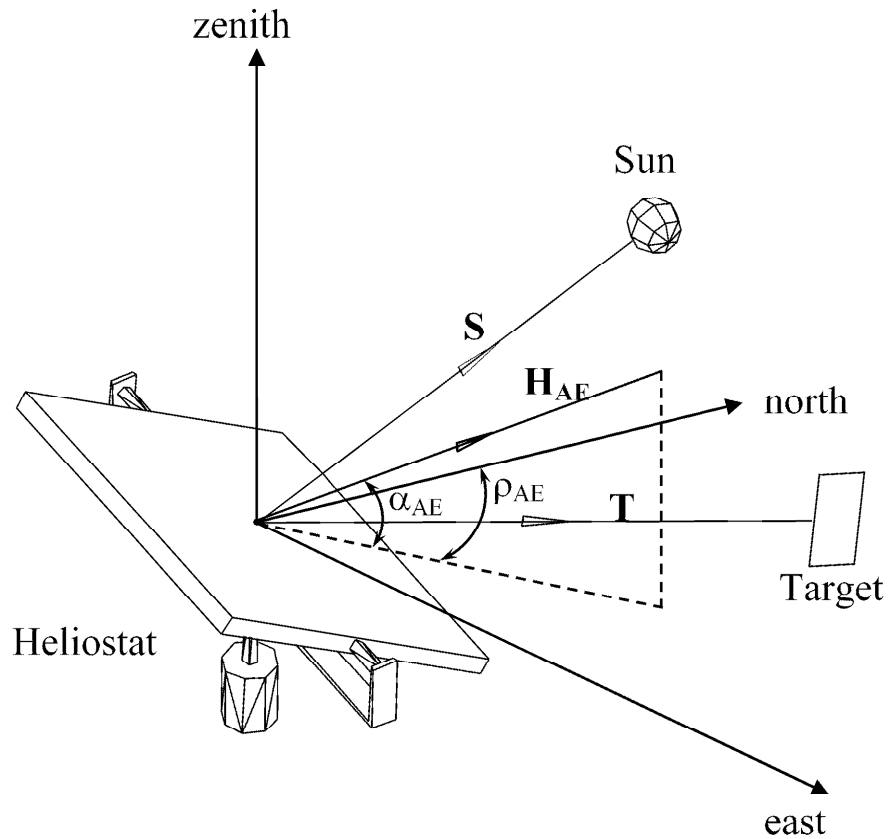


Figure 3.4: Coordinate system attached to the earth-surface reference frame for the Azimuth-Elevation (AE) sun-tracking method where the heliostat normal vector \mathbf{H}_{AE} is defined as the function of the angles α_{AE} and ρ_{AE} .

The target position vector expressed in terms of angles λ and ϕ is as follow:

$$\mathbf{T} = \begin{bmatrix} \sin \lambda \\ \cos \lambda \sin \phi \\ \cos \lambda \cos \phi \end{bmatrix}. \quad (3.15)$$

The heliostat normal vector expressed in terms of angles α_{AE} and ρ_{AE} is as follow:

$$\mathbf{H}_{AE} = \begin{bmatrix} \sin \alpha_{AE} \\ \cos \alpha_{AE} \sin \rho_{AE} \\ \cos \alpha_{AE} \cos \rho_{AE} \end{bmatrix}. \quad (3.16)$$

From the reflection law, the relationship of the three vectors is as follow:

$$\mathbf{H}_{AE} = \frac{1}{2 \cos \theta} (\mathbf{S} + \mathbf{T}) \quad (3.17)$$

$$\begin{bmatrix} \sin \alpha_{AE} \\ \cos \alpha_{AE} \sin \rho_{AE} \\ \cos \alpha_{AE} \cos \rho_{AE} \end{bmatrix} = \frac{1}{2 \cos \theta} \begin{bmatrix} \sin \alpha + \sin \lambda \\ \cos \alpha \sin A + \cos \lambda \sin \phi \\ \cos \alpha \cos A + \cos \lambda \cos \phi \end{bmatrix}, \quad (3.18)$$

where $\cos 2\theta = (\mathbf{S} \cdot \mathbf{T})$ so that the incident angle can be obtained as

$$\theta = \frac{1}{2} \cos^{-1} (\sin \alpha \sin \lambda + \cos \alpha \sin A \cos \lambda \sin \phi + \cos \alpha \cos A \cos \lambda \cos \phi). \quad (3.19)$$

From eqn (3.18), the elevation and azimuth angles of AE method can be derived as

follow:

$$\alpha_{AE} = \sin^{-1} \left(\frac{\sin \alpha + \sin \lambda}{2 \cos \theta} \right). \quad (3.20)$$

In the case of $\cos \rho_{AE} > 0$,

$$\rho_{AE}^+ = \sin^{-1} \left(\frac{\cos \alpha \sin A + \cos \lambda \sin \phi}{2 \cos \theta \cos \alpha_{AE}} \right). \quad (3.21)$$

In the case of $\cos \rho_{AE} < 0$,

$$\rho_{AE}^- = \pi - \rho_{AE}^+, \quad (3.22)$$

given that

$$\cos \rho_{AE} = \frac{\cos \alpha \cos A + \cos \lambda \cos \phi}{2 \cos \theta \cos \alpha_{AE}}. \quad (3.23)$$

Note: equation (3.20) is obtained from the first row of equation (3.18), equations (3.21) and (3.22) are derived from the second row of equation (3.18) and equation (3.23) is derived from the third row of equation (3.18).

From equations (3.20) - (3.22), both the angles ρ_{AE} and α_{AE} are exactly 0° when the elevation axis is aligned to be parallel along the east-west axis and heliostat frame facing the north.

According to the definition of AE sun tracking angle as shown in Figure 3.5, heliostats located in the northern, eastern and western fields of the central tower have a problem of large azimuth angle because of the initial position of the heliostat's reflector is referenced towards the north instead of towards the central tower, thus additional power consumption to the azimuth motor for driving the heliostat's reflector to face the central tower during sun-tracking for heliostats located in these fields. In order to avoid the aforementioned problem, the initial orientation of heliostat's reflector is redefined to face the central tower and thus the azimuth angle in this case has to be rewritten as

$$\rho_{AE}' = \rho_{AE} - \phi. \quad (3.24)$$

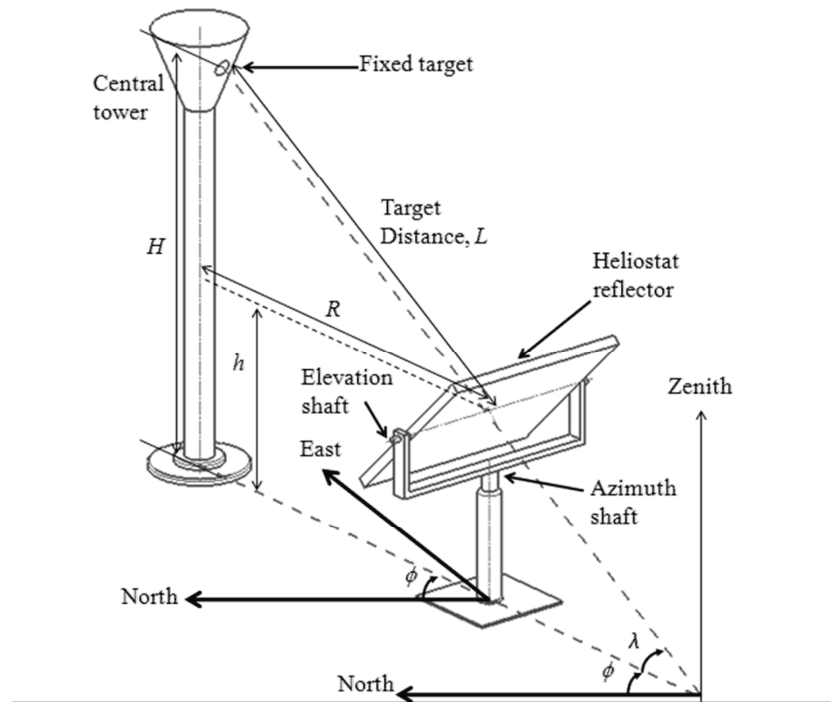


Figure 3.5: The coordinate system attached to the earth-surface reference frame relative to the central tower and the heliostat for Azimuth-Elevation sun-tracking method.

3.1.2 Heliostat Field Layout

In Figure 3.6, a layout of heliostat field consisted of central tower surrounded by 342 heliostats with the specifications as listed in Tables 3.1 and 3.2 is designed for the range of motion study. In the field layout, the heliostats are arranged into nine rings with radial staggered pattern surrounding the central tower. The specifications of each ring, such as number of heliostat's per ring, radial distance and target angle, are listed in Table 3.2 and the heliostats along each ring are separated with equal azimuthal spacing. According to the sun-tracking formulas

stated earlier, the local coordinate of the heliostat can be represented by two position angles, i.e. the facing angle ϕ and the target angle λ .

Alternatively, the position of the heliostat's central point (defined as the cross-section point of two sun-tracking axes) can also be represented by the Cartesian coordinate and the position of target located at the center of heliostat field as $(0, 0, H)$. The relationship between the Cartesian coordinate and the position angles of heliostat are as below:

$$H_{cx} = -R \sin \phi \quad (3.25)$$

$$H_{cy} = -R \cos \phi \quad (3.26)$$

$$H_{cz} = h, \quad (3.27)$$

provided that

$$R = \frac{H - h}{\tan \lambda}, \quad (3.28)$$

where H_{cx} is the distance of the heliostat in east-west direction (it is positive value if the heliostat is located on the east of the tower), H_{cy} is the distance of the heliostat in north-south direction (it is in positive value if the heliostat is located on the north of the tower), R is the perpendicular distance between the central point of the concerned heliostat and the central line of central tower (or known as the radial distance), H is the target height, and h is the height of the heliostat.

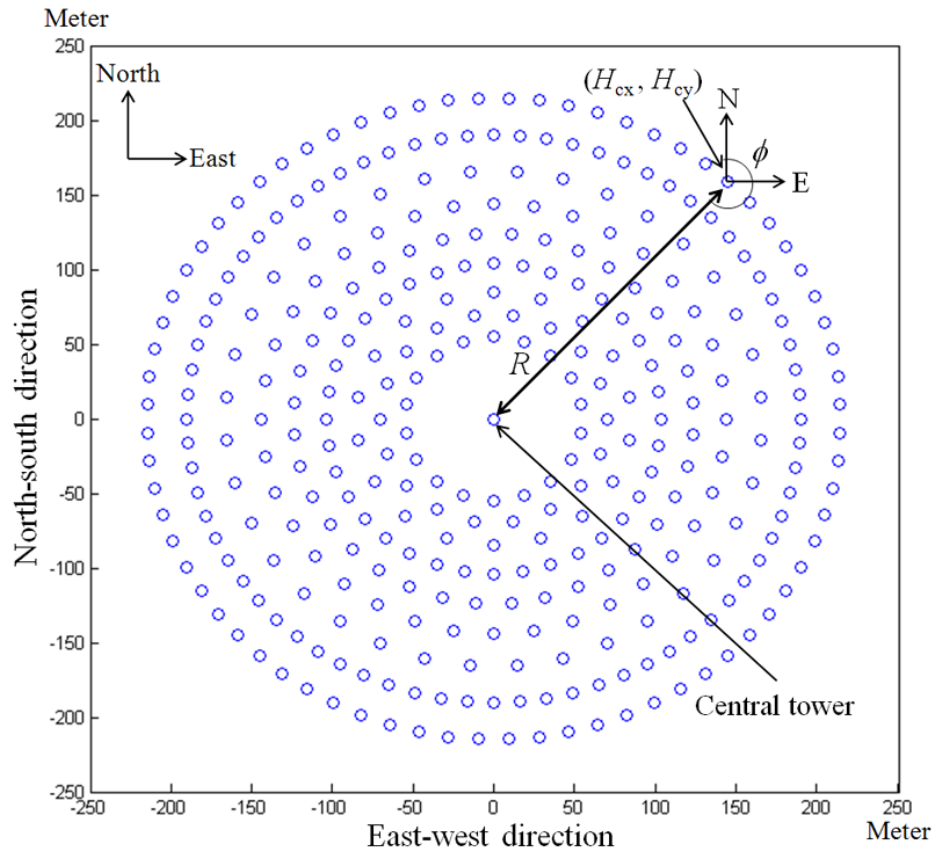


Figure 3.6: Layout of the heliostat field consisted of central tower at the origin and surrounded by 342 heliostats.

Table 3.1: Specifications and design parameters of the heliostat for range of motion study.

Reflective area of heliostat	11 m x 11 m
Height of heliostat, h	7 m
Gear ratio of the gear train in the azimuth or spinning drive, G_ρ	4400
Gear ratio of the gear train in the elevation drive, G_α	4400
Angular speed of the azimuth or spinning motor, ω_ρ	120 rpm
Angular speed of the elevation motor, ω_α	120 rpm
Power rating of azimuth or spinning motor, P_ρ	66 Watt
Power rating of the elevation motor, P_α	99 Watt

Table 3.2: Specification of central power tower and heliostat field layout for range of motion study.

Total number of heliostats	342								
Target (or tower) height, H	95 m								
Total reflective area of heliostat field	41,382 m ²								
Total land area	156,016.6 m ² (15.60166 hectare)								
Ring Number	1	2	3	4	5	6	7	8	9
Radial distances of heliostats from the central tower, R	55m	70m	85m	104m	124m	144m	166m	190m	216m
Target angle, λ	57.99°	51.50°	45.99°	40.24°	35.36°	31.43°	27.93°	24.85°	22.26°
Field layout (Number of heliostats per ring)	18	18	18	36	36	36	36	72	72

3.1.3 Annual Accumulated Sun-Tracking Angles

Since the orientation of sun-tracking axes for AE and SE methods are quite different, the sun-tracking angles, α_{AE} and ρ_{AE} of AE method will be definitely different from α_{SE} and ρ_{SE} of SE method. In practice, the reflector of the heliostat is set to be in the stowed orientation also known as the storage position, i.e. facing the sky, when it is not in operation for minimizing the wind load acting on the reflector. Hence, to simulate the actual operation of heliostat field, the computation of accumulated sun-tracking angle should be started from the stowed orientation during the sunrise as well as returned to this orientation during the sunset. To fully understand the range of motion for the two different methods, the annual accumulated sun-tracking angles are calculated for both the cases of a single heliostat and the heliostat field.

The annual accumulated sun-tracking angle of any heliostat is defined as the summation of angular movement of the particular heliostat for the daily operation with solar time from 0700 Hours (or $t_s = 7$) to 1700 Hours (or $t_s = 17$) and throughout the year with the calendar day from Jan 1 (or $N = 1$) to Dec 31 (or $N = 365$) provided that the heliostat is started from and returned to the stowed position during the daily tracking. Furthermore, the heliostat is consider only using an open-loop sun-tracking system where the angular movement of heliostat is strictly based on the calculated tracking angles using two optical encoders as position sensors and therefore the heliostat movement is not affected by windy or cloudy

weather.

To differentiate between the elevation angles relative to their respective origins, α_{AE} and α_{SE} showed in Figure 3.2 and Figure 3.4, α_{SAE} and α_{SSE} are defined as the elevation angles relative to the stowed orientation for AE and SE methods respectively, $\alpha_{SAE} = 90^\circ - \alpha_{AE}$ and $\alpha_{SSE} = 90^\circ - \lambda - \alpha_{SE}$. The annual accumulated elevation and azimuth angles of a single heliostat for AE method are represented by $\Sigma\alpha_{SAE}$ and $\Sigma\rho_{AE}$ respectively, while the annual accumulated elevation and spinning angles of a single heliostat for SE method are represented by $\Sigma\alpha_{SSE}$ and $\Sigma\rho_{SE}$ respectively. To differentiate from the case of a single heliostat, the annual accumulated elevation and azimuth angles of heliostat field are indicated by using a double summation, e.g. $\Sigma\Sigma\alpha_{SAE}$, $\Sigma\Sigma\rho_{AE}$, $\Sigma\Sigma\alpha_{SSE}$ and $\Sigma\Sigma\rho_{SE}$.

Algorithm to compute the annual accumulated sun-tracking angles of the heliostat field is presented in the flow chart as illustrated in Figure 3.7 and Figure 3.8. In this algorithm, the computation is always considered the shortest pathway for the heliostat to reach the tracking position in each interval during period of sun-tracking in order to optimize the annual accumulated sun-tracking angles.

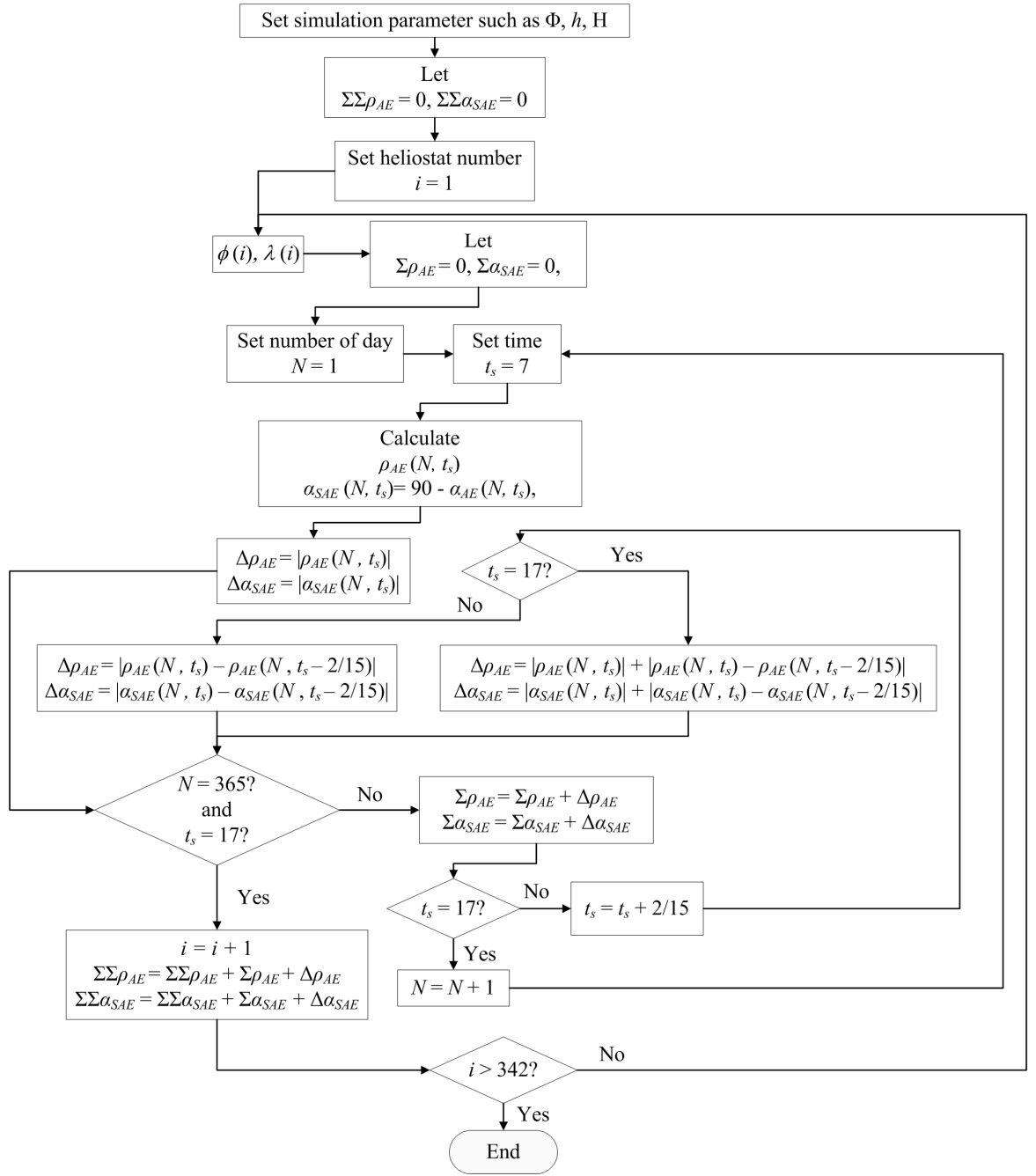


Figure 3.7: The flow chart to show the algorithm to compute the annual accumulated sun-tracking angles for Azimuth-Elevation sun-tracking method.

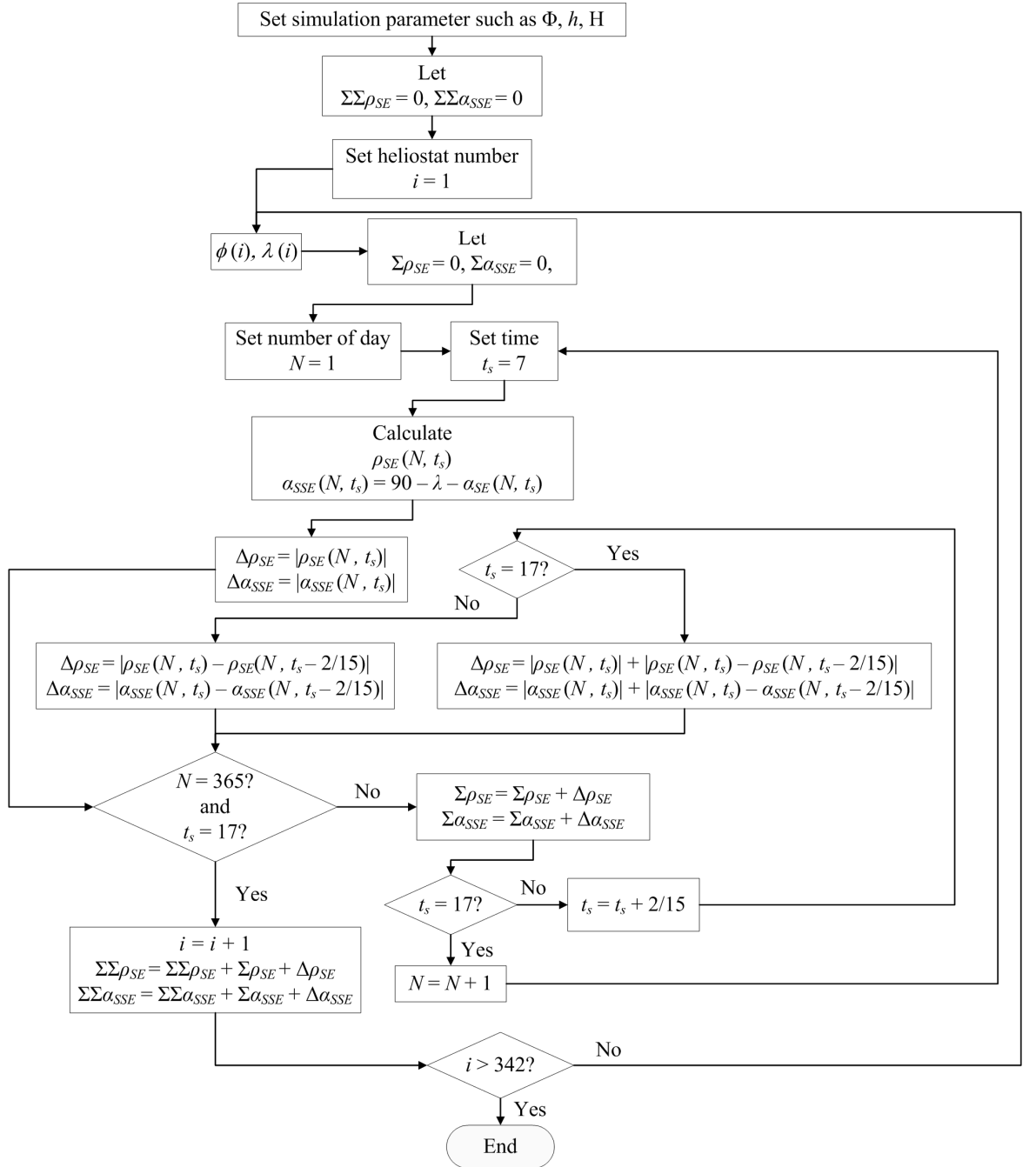


Figure 3.8: The flow chart to show the algorithm to compute the annual accumulated sun-tracking angles for Spinning-Elevation sun-tracking method.

3.1.4 Annual Power Consumption of Heliostat Field on Sun-Tracking System

For the AE method, the annual power consumption of the heliostat field on sun-tracking system can be computed using equation (3.29).

$$\Sigma P_{AE} = \left(\frac{\Sigma \alpha_{AE} \times G_{elev}}{\omega_{\alpha} (rpm) \times 60 \times 360} \times P_{\alpha} (kW) \right) + \left(\frac{\Sigma \rho_{AE} \times G_{azim}}{\omega_{\rho} (rpm) \times 60 \times 360} \times P_{\rho} (kW) \right). \quad (3.29)$$

For the SE method, the annual power consumption of the heliostat field on sun-tracking system can be computed using equation (3.30).

$$\Sigma P_{SE} = \left(\frac{\Sigma \alpha_{SE} \times G_{elev}}{\omega_{\alpha} (rpm) \times 60 \times 360} \times P_{\alpha} (kW) \right) + \left(\frac{\Sigma \rho_{SE} \times G_{spin}}{\omega_{\rho} (rpm) \times 60 \times 360} \times P_{\rho} (kW) \right). \quad (3.30)$$

where G_{azim} is the gear ratio of the gear train in the azimuth drive, G_{spin} is the gear ratio of the gear train in the spinning drive, G_{elev} is the gear ratio of the gear train in the elevation drive, ω_{α} is the angular speed of the elevation motor, ω_{ρ} is the angular speed of the azimuth or spinning motor, P_{α} is the power rating of the elevation motor, and P_{ρ} is the power rating of azimuth or spinning motor.

3.2 Field Efficiency Study

Azimuth-elevation sun-tracking method is widely implemented in the application of heliostat since the development in central tower solar power plant systems. Therefore, the field efficiency of AE sun-tracking method was broadly studied by many authors. Unfortunately, the field efficiency for SE sun-tracking method remains unknown to us. Hence, further exploration on the field efficiency

of SE sun-tracking method is done in this study. The field efficiency of both AE and SE sun-tracking methods are compared and analyzed to compare which sun-tracking method has the highest field efficiency throughout the year.

3.2.1 Unit Vector of Incident and Reflected Ray

Let define the origin at the base of the central tower, it can be assumed that the east is the positive direction of X-axis, north as the positive direction of Y-axis and the zenith as the positive direction of Z-axis. From Figure 3.9, the components of the unit vector for the sun incident ray can be obtained as:

$$S_x = \cos \alpha \sin A \quad (3.31)$$

$$S_y = \cos \alpha \cos A \quad (3.32)$$

$$S_z = \sin \alpha, \quad (3.33)$$

where α and A are the sun altitude and azimuth angle respectively.

The reflected sun rays by the heliostat can be easily described by using the target angle and the facing angle of the heliostat. In Figure 3.9, the direction of the unit vector \mathbf{R} is defined pointing from the heliostat toward the target, which can be described in terms of direction cosines R_x , R_y and R_z relative to the X, Y and Z-axes, respectively. Finally, the components of the unit vector of the sun reflected ray are found as:

$$R_x = \cos \lambda \sin \phi \quad (3.34)$$

$$R_y = \cos \lambda \cos \phi \quad (3.35)$$

$$R_z = \sin \lambda . \quad (3.36)$$

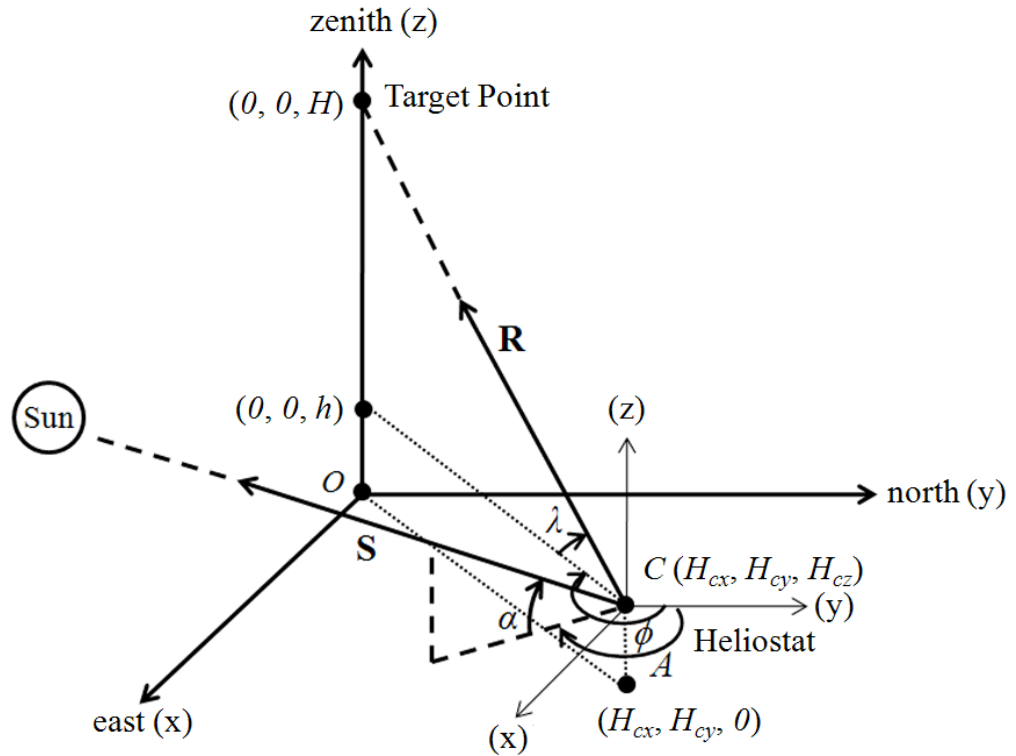


Figure 3.9: Coordinate defining the reflection of the sun's ray by heliostat to a single target point in terms of target angle and facing angle, incident sun's ray in terms of sun altitude angle and azimuth angle, target point and center of the heliostat's frame.

3.2.2 Coordinate Transformation of Heliostat

Given that the sun is a moving object while the target is a fixed object, the heliostat's normal has to be adjusted from time to time when the sun position changes with time. To determine the blocking and shadowing effects of the heliostat, the position of the heliostat frame must be known. The altered orientation of the heliostat frame during the sun tracking period in three-dimensional space can be modeled by applying the coordinate transformation. For the convenience of the three-dimensional coordinate transformation, an additional dimension of space is added to make all the transformations linear.

The initial coordinate of the heliostat frame is first defined in a fixed coordinate system shown in Figure 3.10 where the center of the heliostat frame's surface in which all the facet mirrors are attached is defined as (0, 0, 0). In this analysis, the heliostat frame is presented by four points assigned for the four corner edges of the moving frame. The coordinate of the points will be treated as a vector in the coordinate space and it is written as

$$\mathbf{P}_i = \begin{bmatrix} P_{ix} \\ P_{iy} \\ P_{iz} \\ 1 \end{bmatrix}, \quad (3.37)$$

where $i = 1$ (upper left of the moving frame), 2 (upper right of the moving frame), 3 (lower right of the moving frame), and 4 (lower left of the moving frame).

The final coordinate of the points for the heliostat frame after the transformation will be treated as a vector in matrix form written as

$$\mathbf{P}'_i = \begin{bmatrix} P'_{ix} \\ P'_{iy} \\ P'_{iz} \\ 1 \end{bmatrix} . \quad (3.38)$$

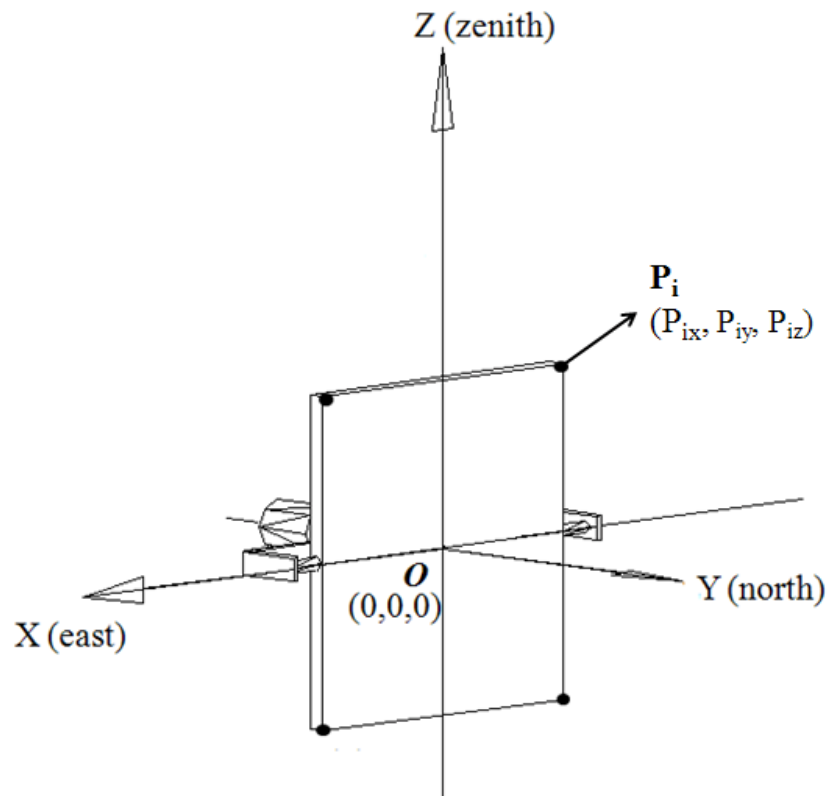


Figure 3.10: The initial coordinate of the heliostat frames is first defined in a fixed coordinate system. The origin is at the middle of the heliostat and \mathbf{P}_i is the point at the corner edge of the heliostat frame.

3.2.2.1 Spinning-Elevation Sun-Tracking Method

In the coordinate transformation for the SE method, there are two angular movements of the heliostat frame relative to the spinning and elevation axes, two initial positioning of the heliostat named as the target angle and the facing angle, one translational transformation which transforms the heliostat frame from the fixed coordinate system to the real coordinate in the heliostat field. Therefore, the first rotation transformation by the angle α_{SE} about the X-axis will transform the point from the fixed coordinate system to an elevation-movement coordinate system. The rotation transformation matrix can be written as

$$[\alpha_{SE}] = \begin{bmatrix} 1 & 0 & 0 & 0 \\ 0 & \cos \alpha_{SE} & -\sin \alpha_{SE} & 0 \\ 0 & \sin \alpha_{SE} & \cos \alpha_{SE} & 0 \\ 0 & 0 & 0 & 1 \end{bmatrix}. \quad (3.39)$$

The second rotation transformation for the rotational movement by the angle ρ_{SE} about the Y-axis will transform the point from the elevation-movement coordinate system to a spinning-movement coordinate system. This spinning transformation matrix can be written as

$$[\rho_{SE}] = \begin{bmatrix} \cos \rho_{SE} & 0 & -\sin \rho_{SE} & 0 \\ 0 & 1 & 0 & 0 \\ \sin \rho_{SE} & 0 & \cos \rho_{SE} & 0 \\ 0 & 0 & 0 & 1 \end{bmatrix}. \quad (3.40)$$

The third rotation transformation by the target angle λ about the X-axis will transform the heliostat frame facing upward to the target. The target angle transformation matrix can be written as

$$[\lambda] = \begin{bmatrix} 1 & 0 & 0 & 0 \\ 0 & \cos \lambda & -\sin \lambda & 0 \\ 0 & \sin \lambda & \cos \lambda & 0 \\ 0 & 0 & 0 & 1 \end{bmatrix}. \quad (3.41)$$

The fourth rotation transformation by the facing angle ϕ about the Z-axis will transform the heliostat frame facing toward the target. The target angle transformation matrix can be written as

$$[\phi] = \begin{bmatrix} \cos \phi & \sin \phi & 0 & 0 \\ -\sin \phi & \cos \phi & 0 & 0 \\ 0 & 0 & 1 & 0 \\ 0 & 0 & 0 & 1 \end{bmatrix}. \quad (3.42)$$

After all the rotational transformation, the points will be transformed from the fixed coordinate system to the real coordinate system in the heliostat field under a translation transformation. The translation transformation matrix can be written as

$$[T_1] = \begin{bmatrix} 1 & 0 & 0 & H_{cx} \\ 0 & 1 & 0 & H_{cy} \\ 0 & 0 & 1 & H_{cz} \\ 0 & 0 & 0 & 1 \end{bmatrix}. \quad (3.43)$$

After all the transformations, the final position of the points of the SE heliostat frame can be expressed by using the formula below

$$P'_i = M_{SE} P_i, \quad (3.44)$$

where the net matrix for SE coordinate transformations of the point is

$$M_{SE} = [T_1][\phi][\lambda][\rho_{SE}][\alpha_{SE}]. \quad (3.45)$$

3.2.2.2 Azimuth-Elevation Sun-Tracking Method

In the coordinate transformation for the AE sun-tracking method, there are two angular movements of the heliostat frame about the azimuth axis and the elevation axis, one translational transformation which transforms the heliostat frame from the fixed coordinate system to the real coordinate in the heliostat field. The first rotation transformation by the angle α_{AE} about the X-axis will transform the point from the fixed coordinate system to an elevation-movement coordinate system. The rotation transformation matrix can be written as

$$[\alpha_{AE}] = \begin{bmatrix} 1 & 0 & 0 & 0 \\ 0 & \cos \alpha_{AE} & -\sin \alpha_{AE} & 0 \\ 0 & \sin \alpha_{AE} & \cos \alpha_{AE} & 0 \\ 0 & 0 & 0 & 1 \end{bmatrix}. \quad (3.46)$$

The second rotation transformation for the rotational movement by the angle ρ_{AE} about the Z-axis will transform the point from the elevation-movement coordinate system to azimuth-movement coordinate system. This azimuth transformation matrix can be written as

$$[\rho_{AE}] = \begin{bmatrix} \cos \rho_{AE} & \sin \rho_{AE} & 0 & 0 \\ -\sin \rho_{AE} & \cos \rho_{AE} & 0 & 0 \\ 0 & 0 & 1 & 0 \\ 0 & 0 & 0 & 1 \end{bmatrix}. \quad (3.47)$$

After all the rotational transformation, the points will be transformed from the fixed coordinate system to the real coordinate system in the heliostat field under a translational transformation which is similar with equation (3.43).

After all the transformations, the final position of the points of the AE heliostat frame can be calculated by substituting the net matrix for coordinate transformations, M_{SE} in equation (3.44) with M_{AE} . The net matrix for AE coordinate transformations of the point is

$$M_{AE} = [T_I][\rho_{AE}][\alpha_{AE}]. \quad (3.48)$$

3.2.3 Cosine Efficiency and Shadowing and Blocking Efficiency

The major factor to determine the optical efficiency of the heliostat field is the cosine effect of the heliostat. The efficiency depends on both the sun's position and the position of the heliostat relative to the receiver. The effective reflection area of the heliostat is reduced by the cosine of one-half of the angle between the sun rays and a line from the heliostat to the receiver. Therefore, the cosine efficiency for SE and AE heliostats are

$$\eta_{\cos} = \cos \theta. \quad (3.49)$$

Besides that, shadowing and blocking efficiency also contribute optical losses to heliostat field. The heliostat field optical efficiency caused by shadow and block can be computed by using ray tracing techniques.

After computing the sun tracking angles and coordinate transformation for the “Adjacent Heliostat” (heliostat which block the incident sun ray and reflected ray) and the “Test Heliostat” (heliostat which is tested for the shadow and block efficiency) in the heliostat field, the tracking positions of both heliostats’ frames is known.

The Ray/Plane Algorithm is used to determine whether the shadow of the “Adjacent Heliostat” will cast on the surface plane of the “Test Heliostat” as illustrated in Figure 3.11. Besides that, it is also used to determine whether the reflected ray from the “Test Heliostat” is blocked by the “Adjacent Heliostat” as illustrated in Figure 3.12. For blocking efficiency testing, reflected ray of the “Test Heliostat” is used while sun incident ray is used for the shadow efficiency testing. Note that the direction of the incident ray used in the computer algorithm is $-\mathbf{S}$ instead of \mathbf{S} as sun ray is originated from the sun to the heliostat. Furthermore, the reflected ray used in the computer algorithm is $-\mathbf{R}$ instead of \mathbf{R} for the purpose of standardisation the computer algorithm for both shadowing and blocking efficiency testing. Finally, the area of shadowing, A_s which is the intersection area for the “Test Heliostat” frame and shadow of the “Adjacent Heliostat” and the area of blocking, A_b is being computed. The shadowing efficiency is

$$\eta_{shadow} = (A_t - A_s) / A_t . \quad (3.50)$$

The shadowing efficiency is

$$\eta_{block} = (A_t - A_b) / A_t . \quad (3.51)$$

where A_r is the total area of the reflector.

The operating period for the flow chart in Figure 3.13 is from solar time 0800 Hours to 1600 Hours and throughout the year with the calendar day from Jan 1 to Dec 31. In this study, three significant efficiency terms not to be included are heliostat reflectivity, spillage loss and atmospheric attenuation. Reflectivity and spillage are excluded as they are independent of the location of the heliostat field (Noone, C.J. *et al.*, 2011). For atmospheric attenuation, it is strongly dependent on the aerosol distribution at ground level (Stine and Harrigan, 1985).

3.2.4 Heliostat Field Layout

In Figure 3.14, a heliostat field made up of 317 heliostats and a center tower is design with accordance to the specifications listed in Table 3.3 for this field study. The heliostats are packed in a way to maximize blocking and shadowing effects while avoiding collision between heliostats.

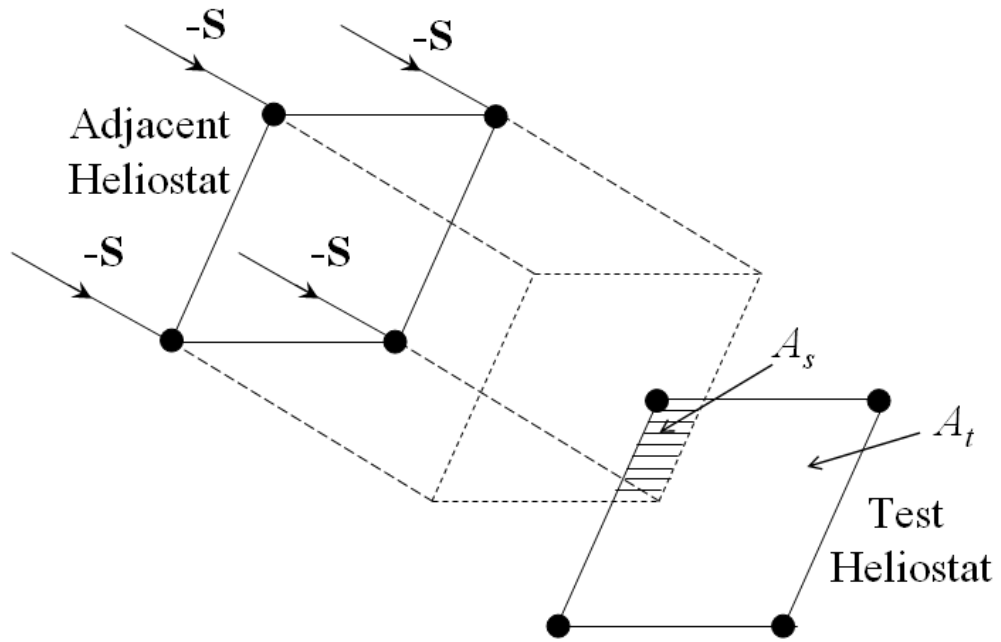


Figure 3.11: Ray/Plane Algorithm method used to compute the shadow area.

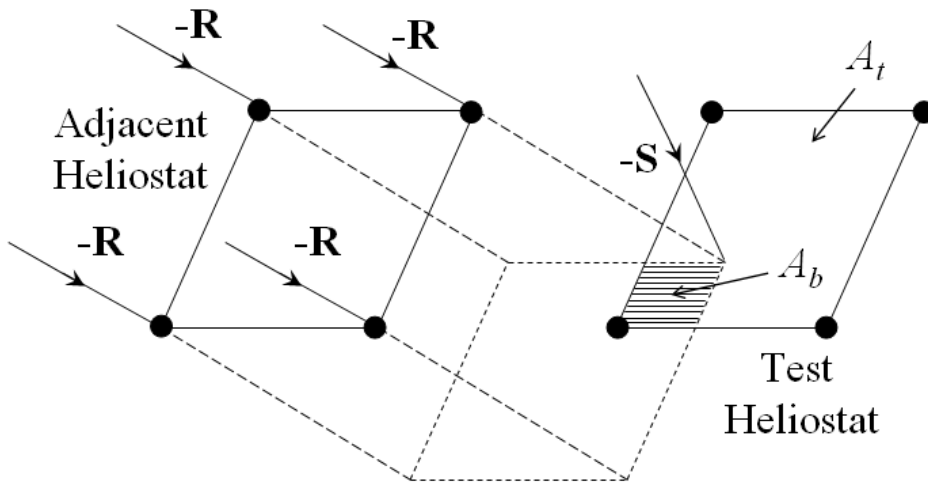


Figure 3.12: Ray/Plane Algorithm method used to compute the blocked area.

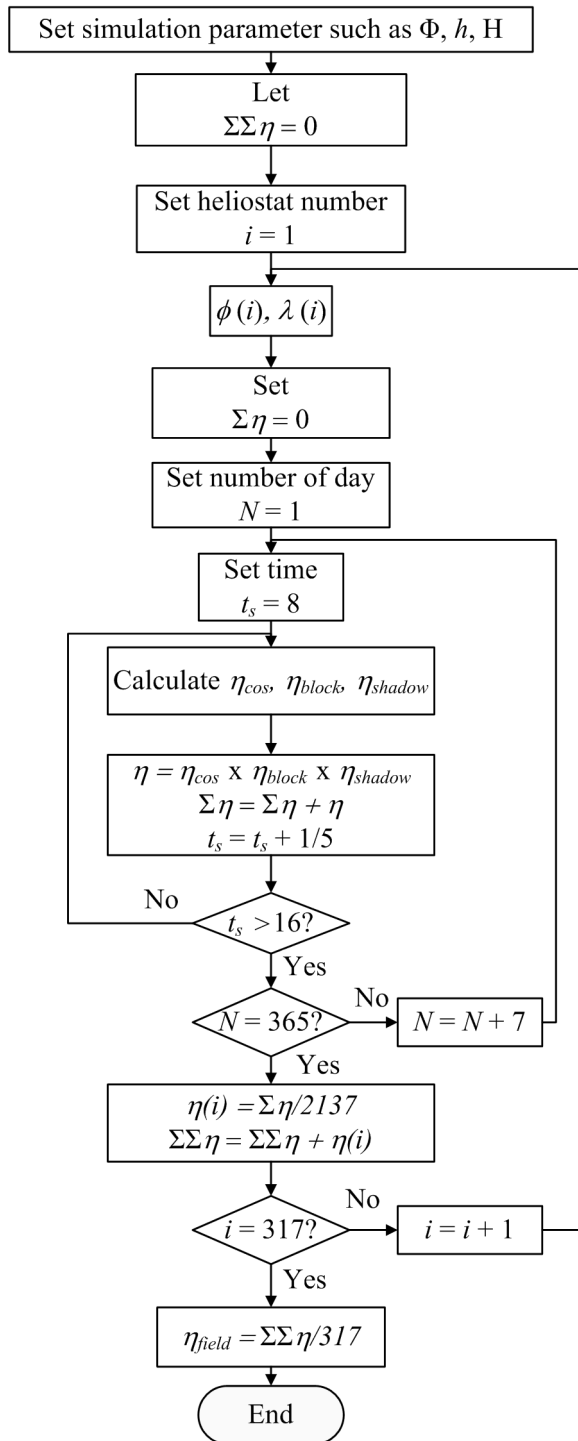


Figure 3.13: The flow chart to show the algorithm of computing the annual field efficiency of the heliostat field.

The previous heliostat field layout is not used in this study due to low field packing factor. Field with low packing factor has significantly lower effect on shadowing and blocking. Therefore, the comparison of shadowing and blocking effect between the two sun-tracking methods will not be significant. In the field layout, the heliostats are arranged into nine rings with radial staggered pattern surrounding the central tower. The specifications of each ring, such as the number of heliostat's per ring, radial distance and target angle, are listed in Table 3.3. Note that the heliostats at the first four rings closest to the central tower are separated with equal azimuthal spacing. For the 5th, 6th, 7th, 8th, and 9th rings, the heliostats are also separated with equal azimuthal spacing except at the south field due to insufficient spacing for additional heliostats to be inserted.

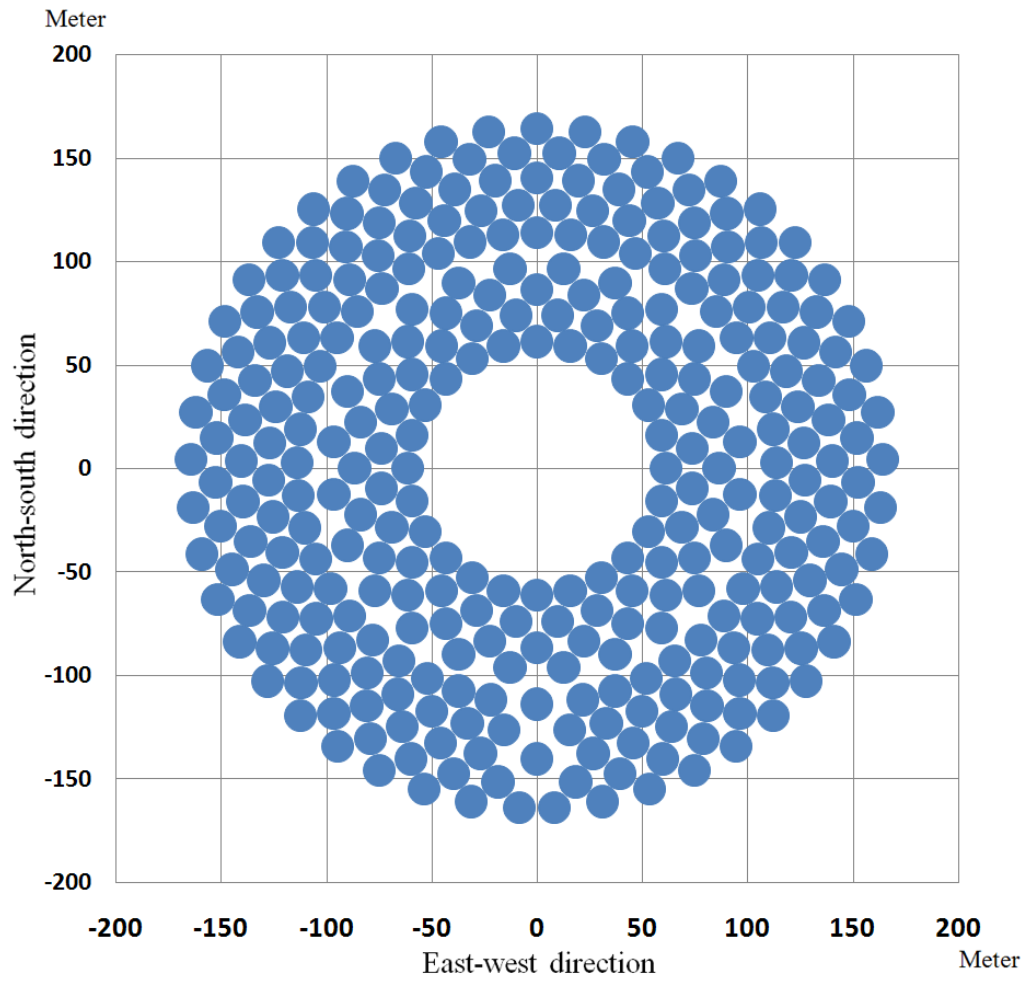


Figure 3.14: Layout of the heliostat field consisted of central tower at the origin and surrounded by 317 heliostats.

Table 3.3: Specification of central power tower and heliostat field layout for field efficiency study.

Total number of heliostats	317								
Reflective area of a heliostat	11 m x 11 m								
Target (or tower) height, H	95 m								
Height of heliostat, h	7 m								
Total reflective area of heliostat field	38,357 m ²								
Total land area	90,792.03 m ² (9.0792 hectare)								
Packing Factor	42.247%								
Ring Number	1	2	3	4	5	6	7	8	9
Radial distances of heliostats from the central tower in meter, R	61.3	74.6	86.6	97.2	114	127.6	140.5	152.8	164.3
Target angle, λ	55.16°	49.72°	45.45°	42.15°	37.67°	34.60°	32.06°	29.94°	28.18°
Field layout (Number of heliostats per ring)	24	24	24	24	44	44	44	44	45

CHAPTER 4

RESULTS and DISCUSSIONS

4.1 Annual Accumulated Angles

To simulate the annual accumulated angles of the two different sun-tracking methods, the algorithm as shown in Figure 3.7 and 3.8 are applied in which equations (3.10)-(3.13) and equations (3.20)-(3.24) are used for SE and AE methods respectively. The three major parameters that affect the annual accumulated tracking angles are analyzed in this study, the latitude (Φ), facing angle (ϕ) and the target angle (λ). Besides that, a detailed comparison has also been carried out for both cases of a single heliostat and heliostat field.

4.1.1 Comparison of AE and SE Methods for a Single Heliostat

The simulation of the annual accumulated angles of a single heliostat has been performed to calculate $\Sigma\alpha_{SSE}$ & $\Sigma\rho_{SE}$ for SE method and $\Sigma\alpha_{SAE}$ & $\Sigma\rho_{AE}$ for AE method based on the specification as listed in Table 3.1. Firstly, the characteristics of the annual accumulated angle of a single heliostat at different latitudes are analyzed. Figures 4.1 (a)-(b) show the annual accumulated elevation ($\Sigma\alpha_{SSE}$) and spinning angles ($\Sigma\rho_{SE}$) of a heliostat versus facing angle with the target angle being

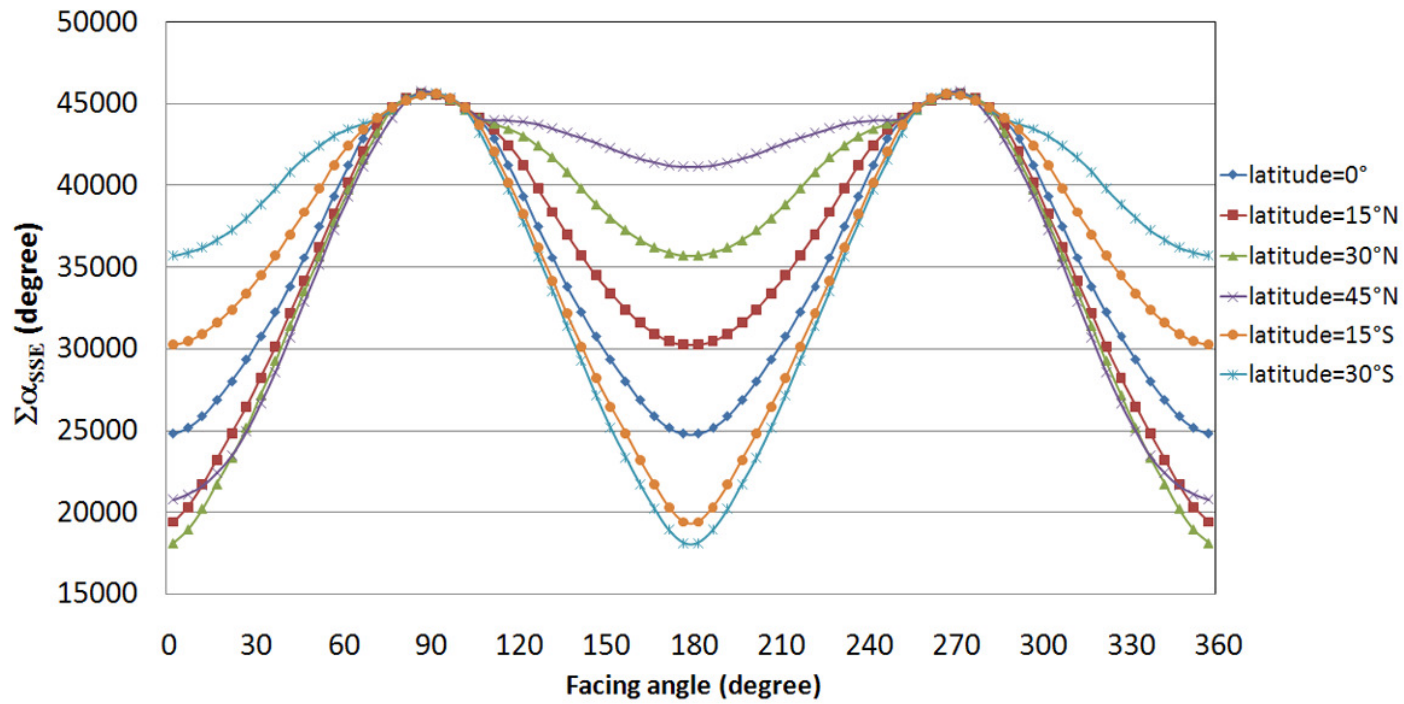


Figure 4.1 (a)

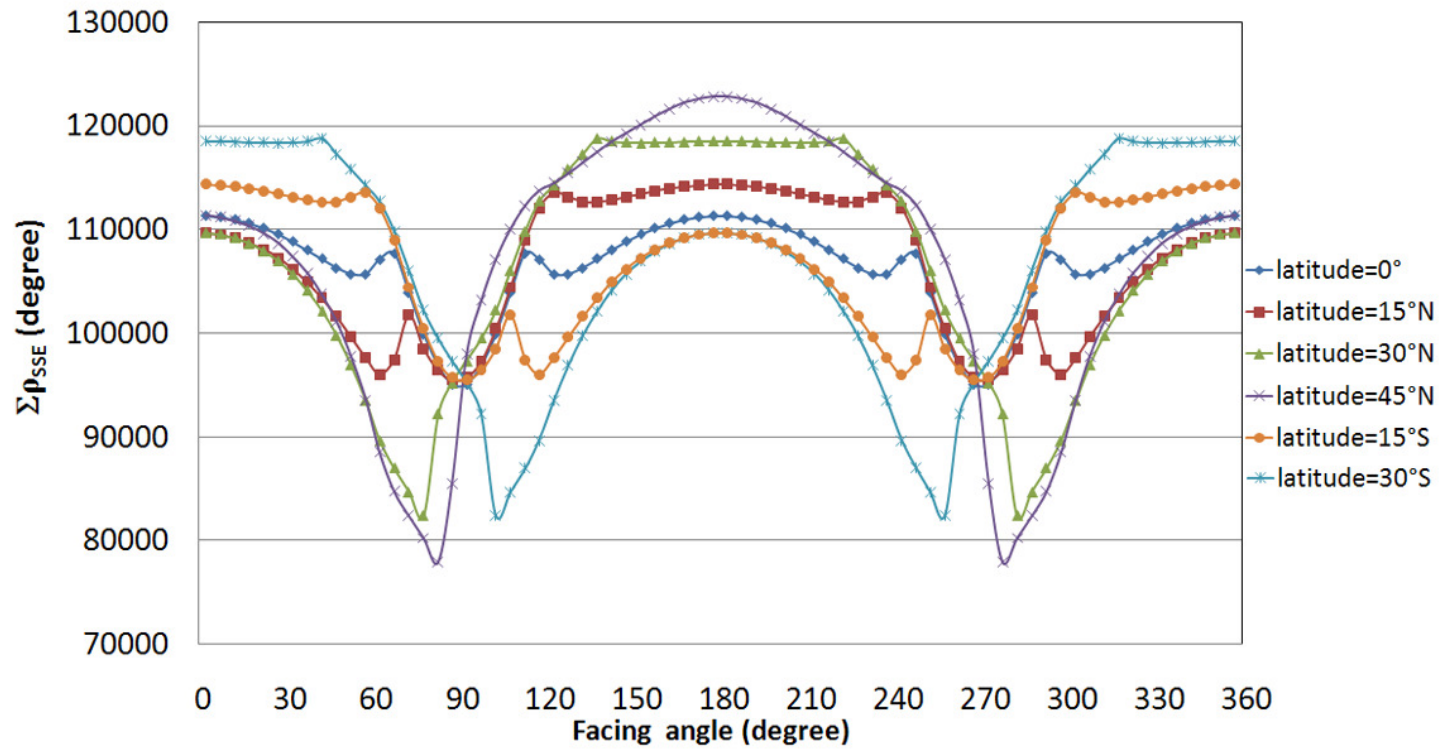


Figure 4.1 (b)

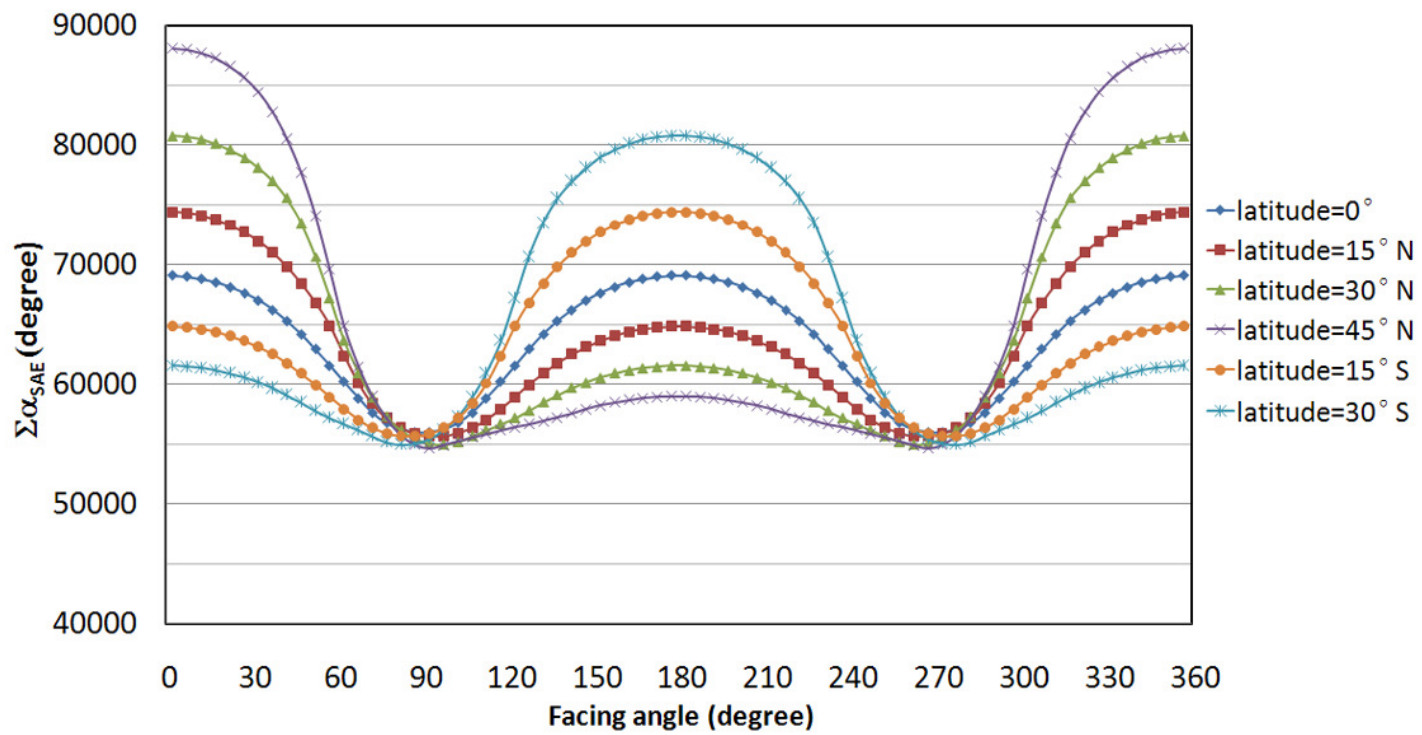


Figure 4.1 (c)

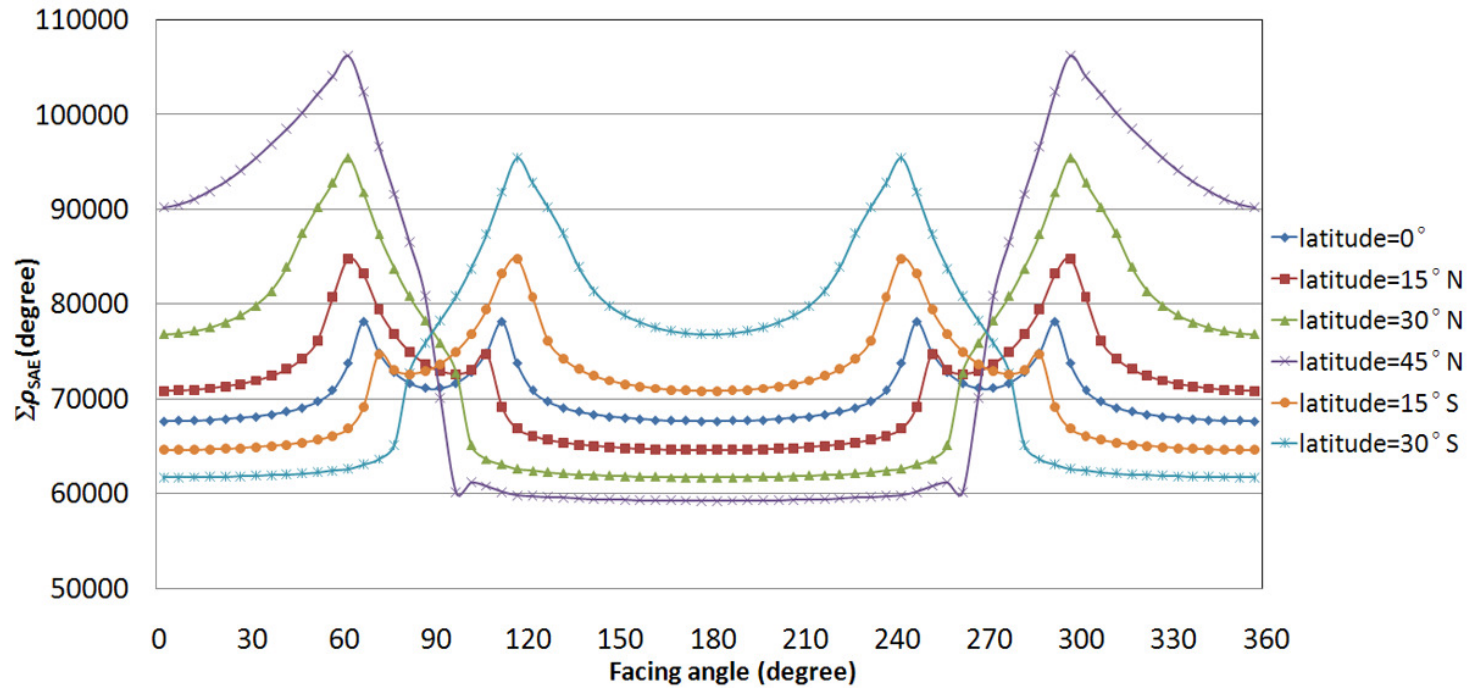


Figure 4.1 (d)

Figure 4.1: The annual accumulated tracking angle of a single heliostat versus facing angle in the case of target angle 22.26° , and latitudes 0° , 15°N , 30°N , 45°N , 15°S , 30°S . (a) Annual accumulated elevation angle for SE method ($\Sigma\alpha_{\text{SE}}$), (b) Annual accumulated spinning angle for SE method ($\Sigma\rho_{\text{SE}}$), (c) Annual accumulated elevation angle for AE method ($\Sigma\alpha_{\text{SAE}}$), (d) Annual accumulated azimuth angle for AE method ($\Sigma\rho_{\text{AE}}$).

fixed at 22.26° for SE method. For AE method, Figures 4.1(c)-(d) show the annual accumulated elevation ($\Sigma\alpha_{SAE}$) and azimuth angles ($\Sigma\rho_{AE}$) of a heliostat against facing angle with the same target angle. For the equator (or latitude 0°), the graphs in Figures 4.1(a)-(d) have shown perfect symmetrical patterns between the north field and the south field as well as east field and west field. On the other hand, for the other latitudes, such as 15°N , 30°N , 45°N , 15°S and 30°S , the graphs only show symmetrical patterns between the east field and the west field. There is another relationship between the corresponding latitudes in northern and southern hemispheres shown in Figures 4.1 (a)-(d) where the graphs of annual accumulated tracking angles at northern hemisphere will be identical to that of southern hemisphere by simply displacing one of them with 180° of facing angle. In other words, the north field in the northern hemisphere behaves identically to the south field in the southern hemisphere. For a comparison of the annual accumulated elevation angle between SE and AE methods, it is obvious that $\Sigma\alpha_{SSE}$ with the range of $18,088^\circ$ to $45,718^\circ$ is about half of $\Sigma\alpha_{SAE}$ with the range of $54,641^\circ$ to $88,113^\circ$. Nevertheless, $\Sigma\rho_{SE}$ with the range of $77,977^\circ$ to $122,842^\circ$ is about 20% more than $\Sigma\rho_{AE}$ with the range of $59,298^\circ$ to $106,247^\circ$.

Furthermore, the characteristic of the annual accumulated angle of a single heliostat with different position angles (combination of target angle and facing angle) is carefully analyzed as well. All the possible position angles of 342 heliostats in the field layout as shown in Figure 3.6 are considered in our analysis

for the latitudes 0° and 45°N . This study let us understand more about the contribution of individual heliostat with different position angles to the total annual accumulated angles of the heliostat field. Since the simulated result of the surrounding heliostat field located at southern hemisphere and northern hemisphere is just a mirror image of each other with a displacement of 180° of facing angle, we only need to show the graphs of the heliostat field located at equator and northern hemisphere.

Figures 4.2 (a)-(d) show the variations in annual accumulated sun-tracking angles against facing angles with different target angles for both methods at the Equator. The figures have shown perfect symmetry between the east and west fields as well as between the north and south fields for all target angles. Figure 4.2 (c) shows that $\Sigma\alpha_{\text{SAE}}$ is inversely proportional to the target angle (or lambda) at all facing angles. Contrarily, Figure 4.2 (d) shows that $\Sigma\rho_{\text{SAE}}$ is proportional to the target angle (or lambda) at all facing angles. From Figures 4.2 (a)-(b), SE method has also shown the same tendency as that of AE method except for the facing angles around both 0° and 180° . For a comparison between SE and AE methods as shown in Figures 4.2 (a) and 4.2 (c) respectively, it is obvious that $\Sigma\alpha_{\text{SSE}}$ with the range of $17,311^\circ$ to $45,502^\circ$ is lesser than $\Sigma\alpha_{\text{SAE}}$ with the range of $50,303^\circ$ to $69,080^\circ$. Nonetheless, for Figures 4.2 (b) and 4.2 (d), $\Sigma\rho_{\text{SE}}$

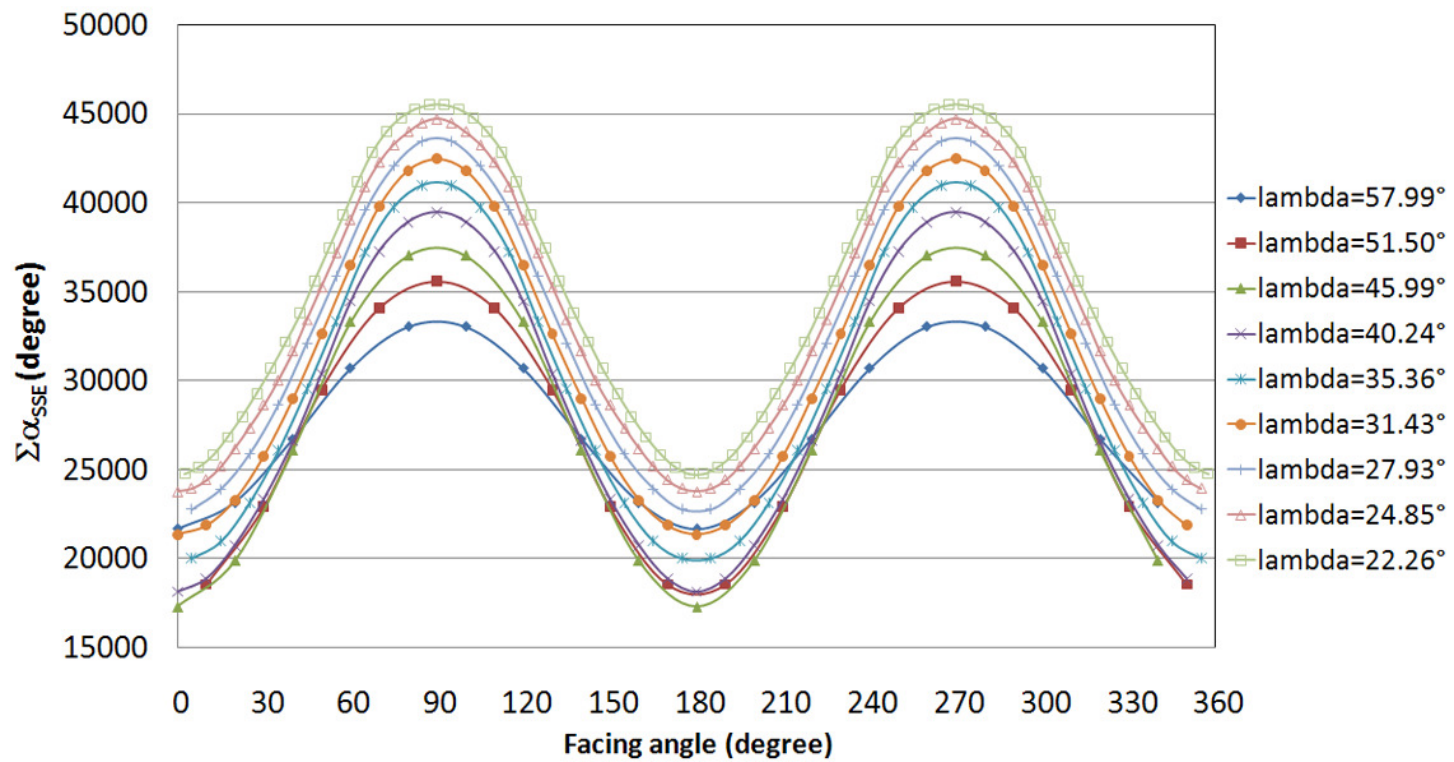


Figure 4.2 (a)

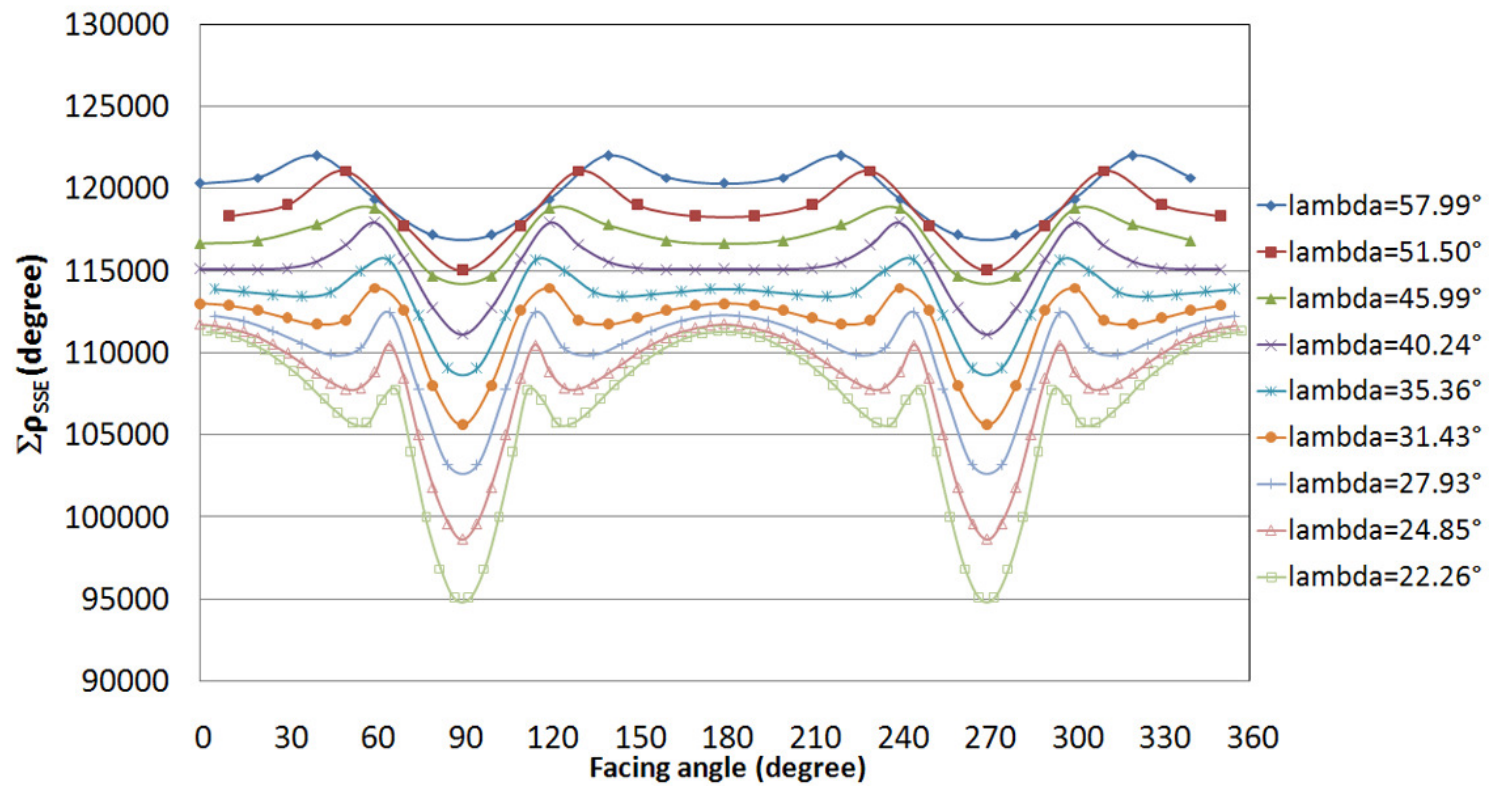


Figure 4.2 (b)

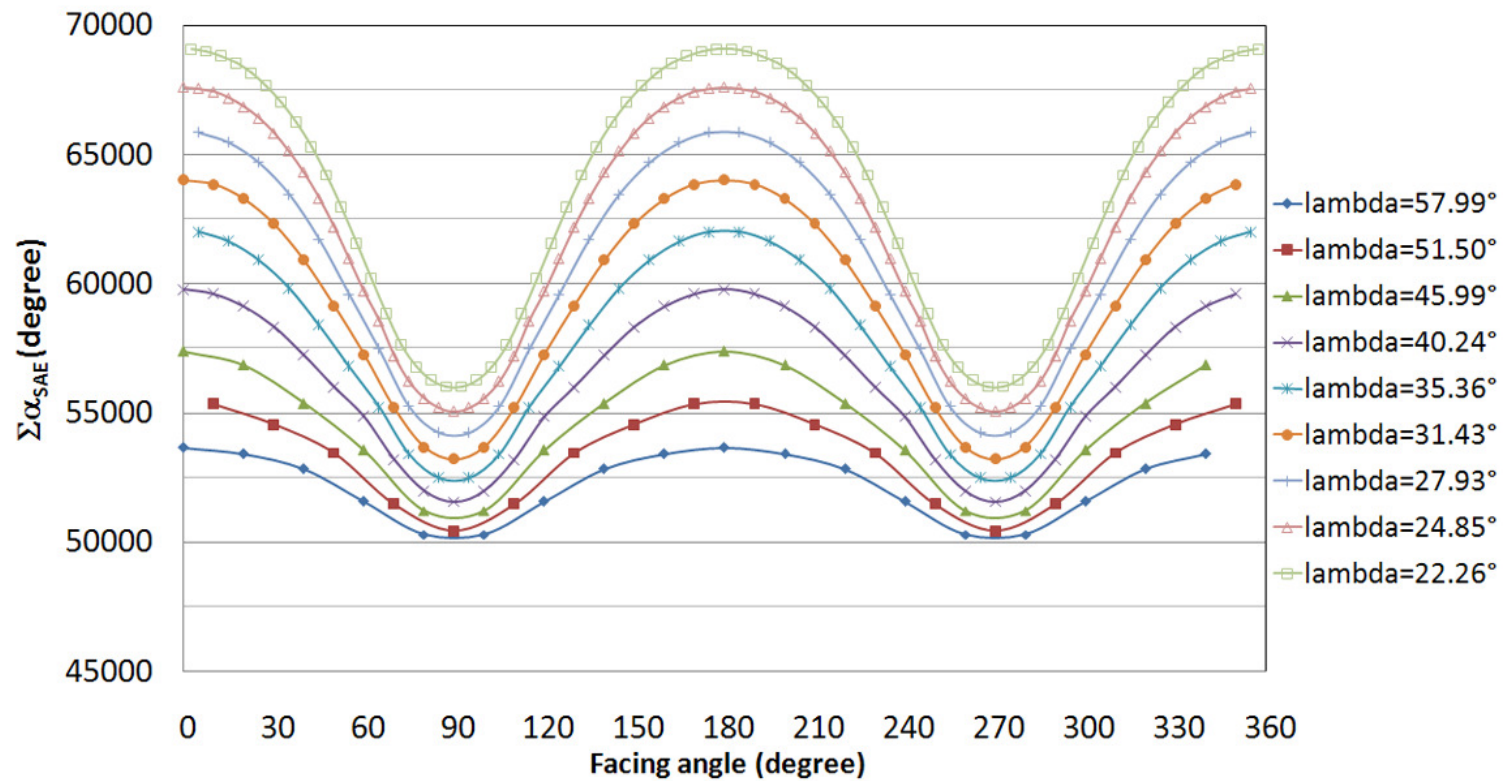


Figure 4.2 (c)

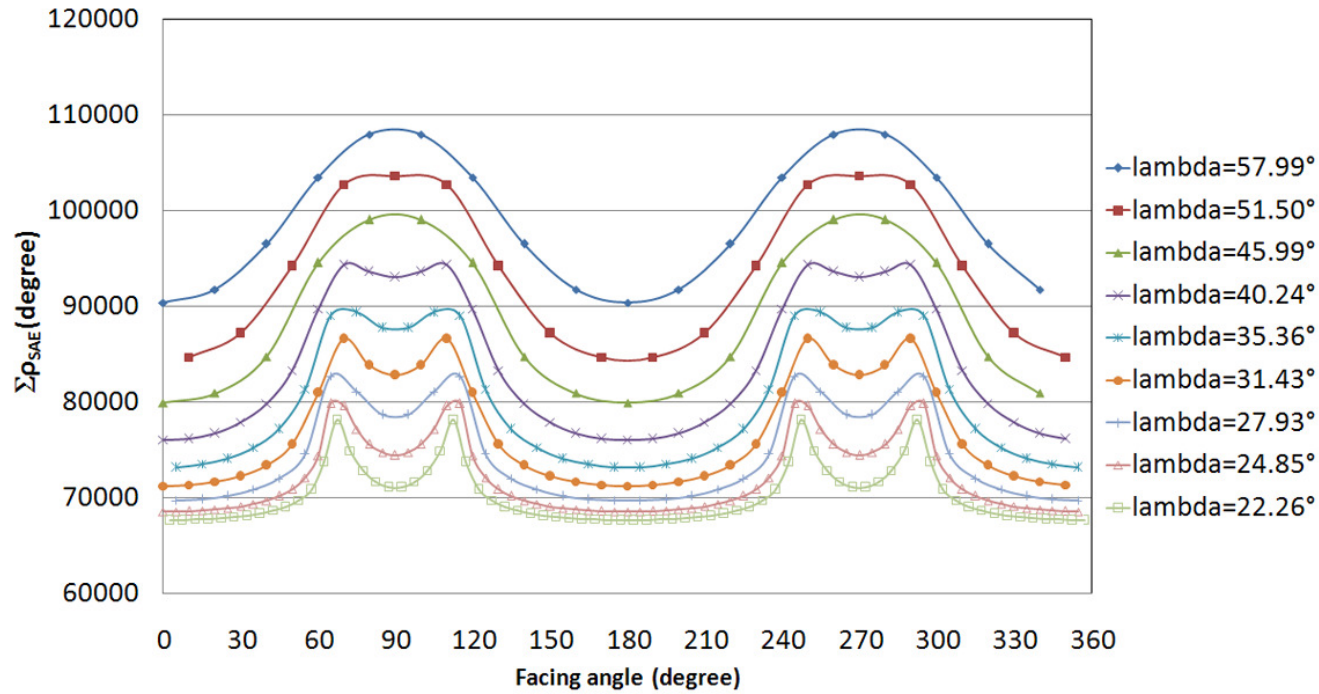


Figure 4.2 (d)

Figure 4.2: The annual accumulated tracking angle of a single heliostat versus facing angle in the case of latitude 0° . (a) Annual accumulated elevation angle for SE method ($\Sigma\alpha_{SSE}$), (b) Annual accumulated spinning angle for SE method ($\Sigma\rho_{SE}$), (c) Annual accumulated elevation angle for AE method ($\Sigma\alpha_{SAE}$), (d) Annual accumulated azimuth angle for AE method ($\Sigma\rho_{AE}$).

with the range of $95,075^\circ$ to $122,055^\circ$ is more than $\Sigma\rho_{AE}$ with the range of $67,704^\circ$ to $107,962^\circ$.

Figures 4.3(a)-(d) show the annual accumulated sun-tracking angles varying against both facing and target angles for a comparison of the two methods at the latitude $45^\circ N$. In northern hemisphere, the graphs of the annual accumulated angle show perfect symmetry between east and west fields for all target angles. Figure 4.3 (c) shows that $\Sigma\alpha_{SAE}$ is inversely proportional to the target angle at all facing angles. Contrarily, Figure 4.3 (d) shows that $\Sigma\rho_{SAE}$ is proportional to the target angle at all facing angles. From Figures 4.3 (a)-(b), SE method has also shown the same tendency as that of AE method except the heliostat located at north and south fields. To compare between SE and AE methods as shown in Figures 4.3 (a) and 4.3 (c) respectively, it is obvious that $\Sigma\alpha_{SSE}$ with the range of $5,732^\circ$ to $45,718^\circ$ is lesser than $\Sigma\alpha_{SAE}$ with the range of $42,478^\circ$ to $88,113^\circ$. For Figures 4.3 (b) and 4.3 (d), $\Sigma\rho_{SE}$ with the range of $77,977^\circ$ to $131,400^\circ$ is more than $\Sigma\rho_{AE}$ with the range of $59,298^\circ$ to $131,400^\circ$.

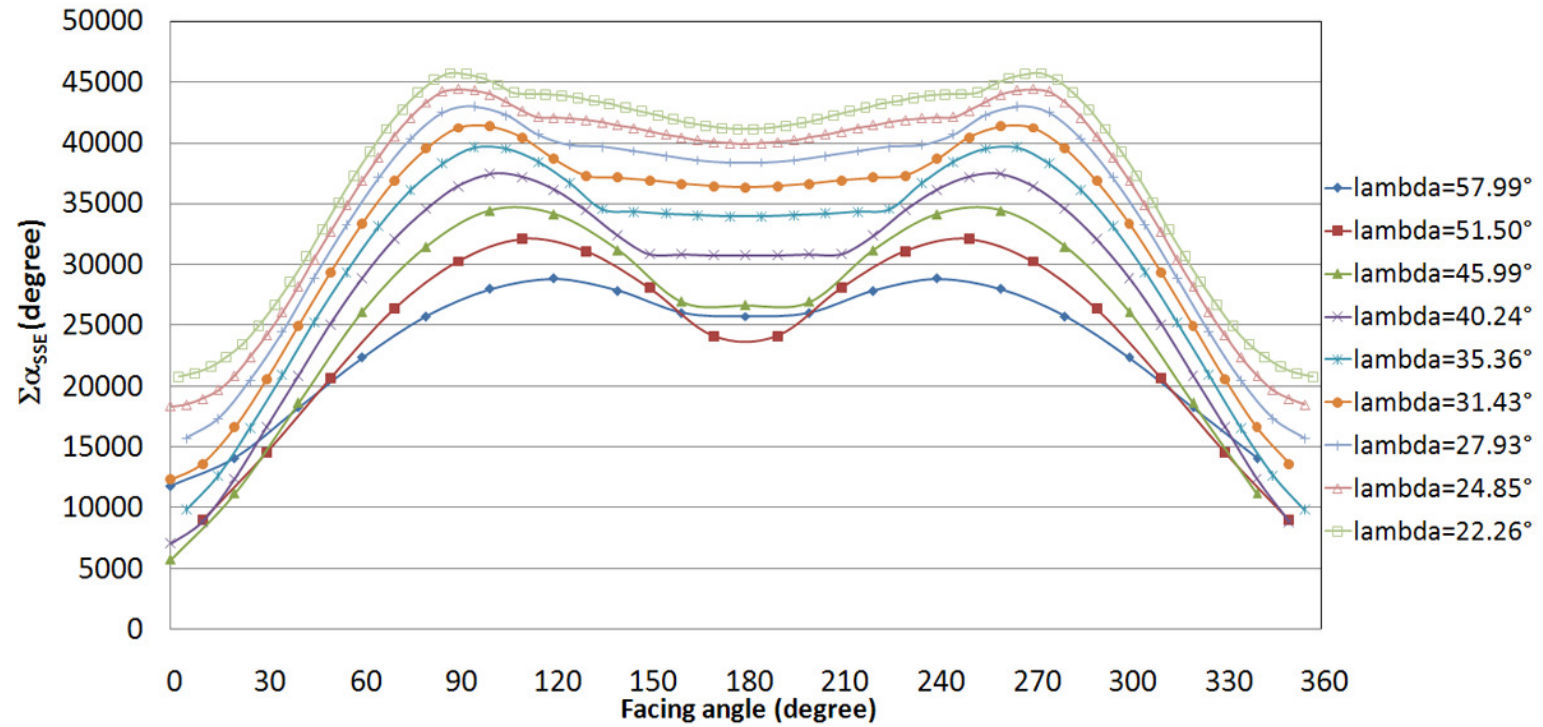


Figure 4.3 (a)

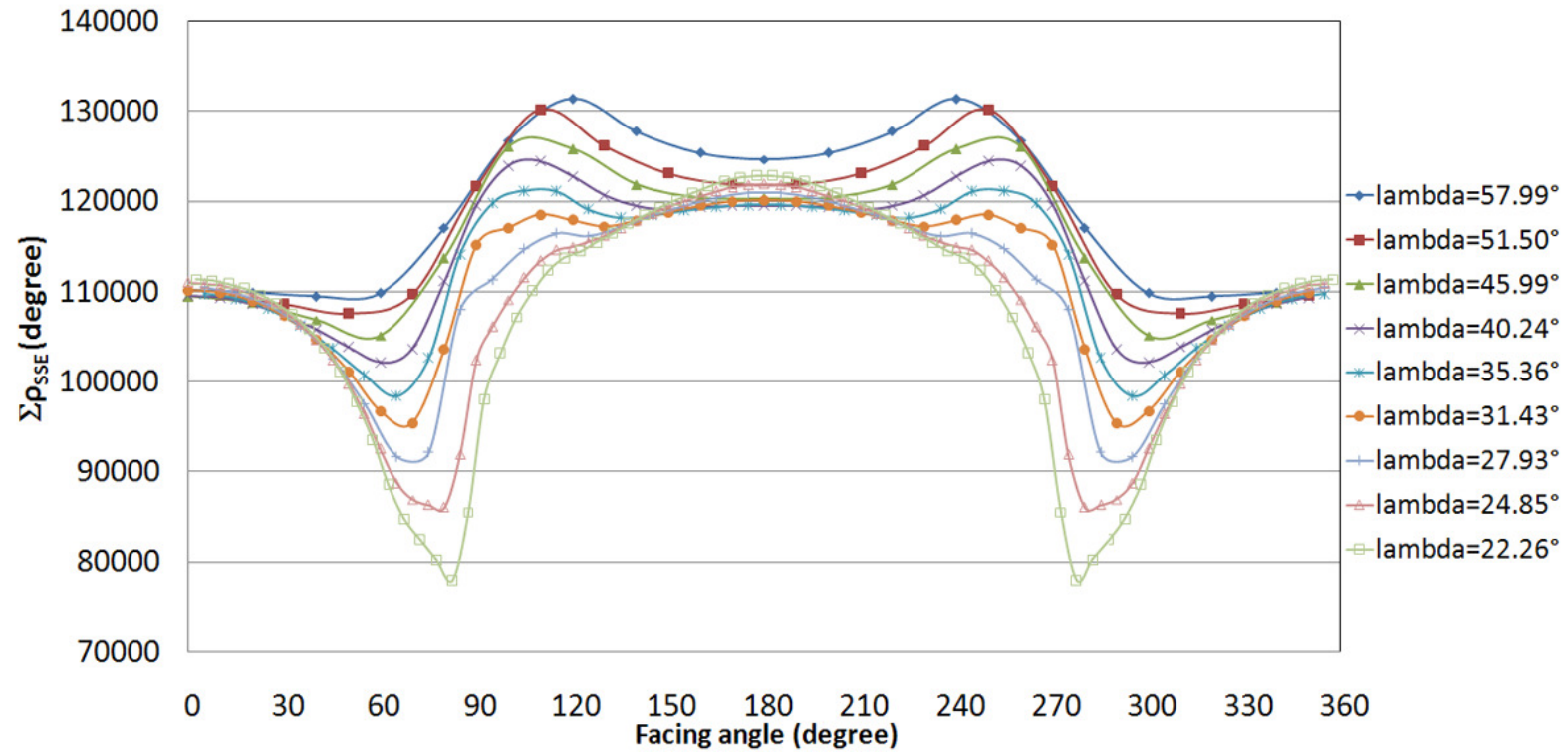


Figure 4.3 (b)

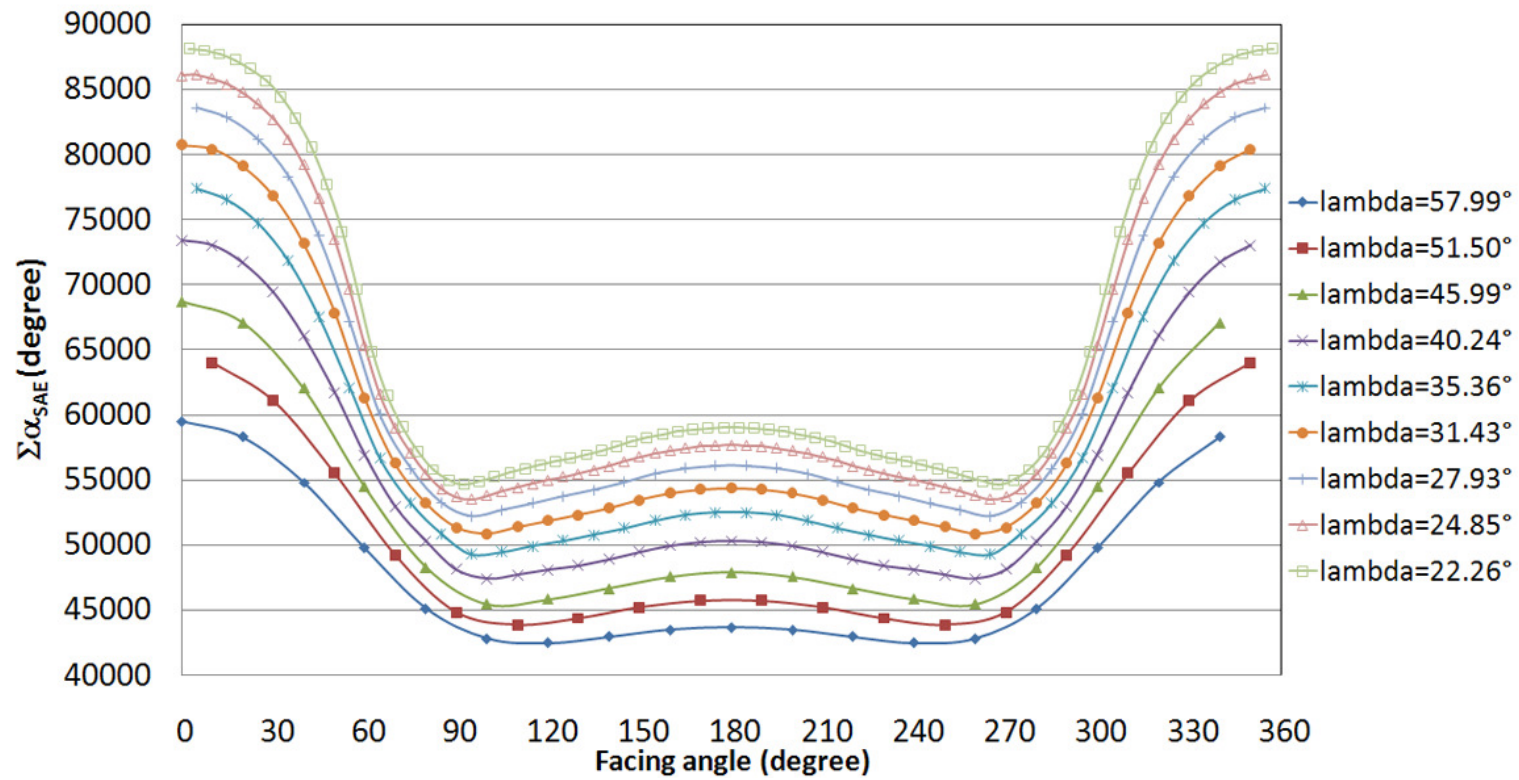


Figure 4.3 (c)

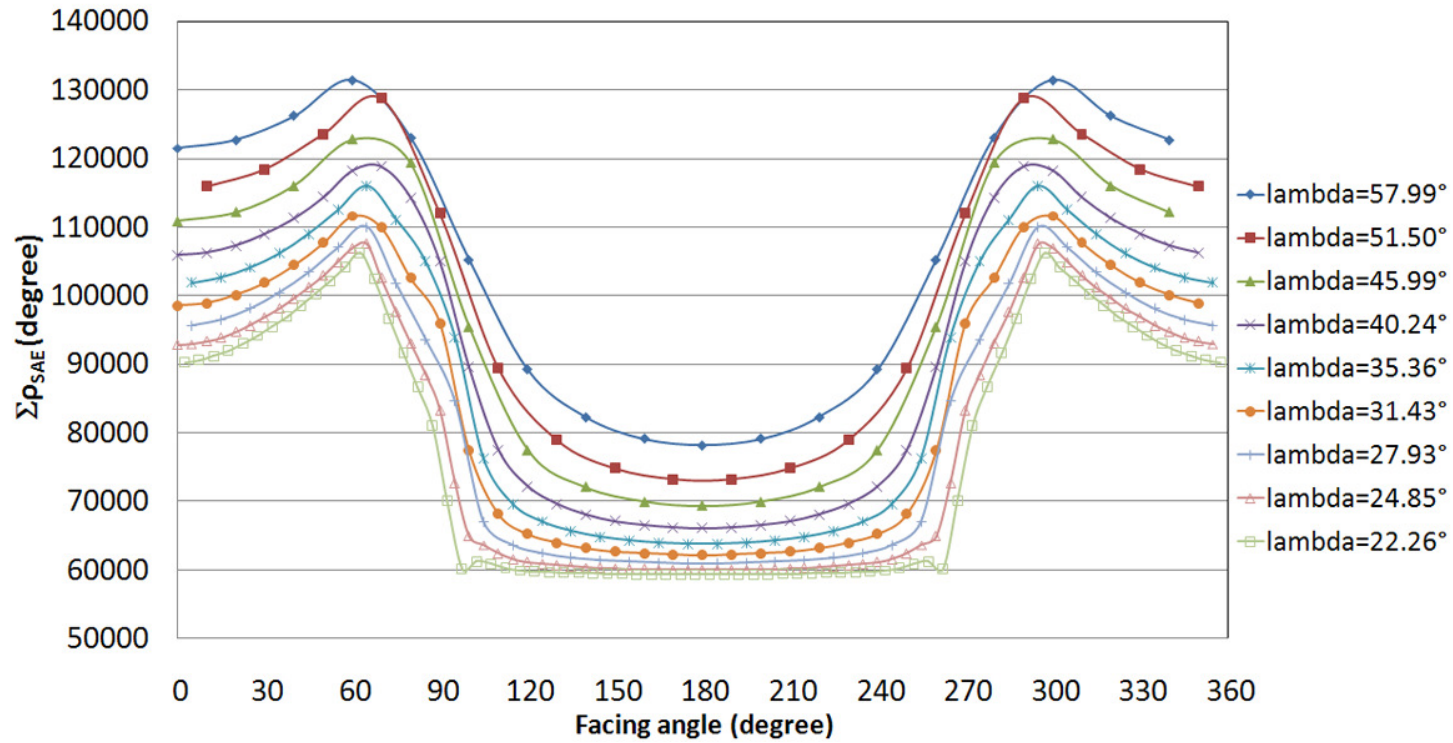


Figure 4.3 (d)

Figure 4.3: The annual accumulated tracking angle of a single heliostat versus facing angle in the case of latitude $45N^\circ$. (a) Annual accumulated elevation angle for SE method ($\Sigma\alpha_{SSE}$), (b) Annual accumulated spinning angle for SE method ($\Sigma\rho_{SE}$), (c) Annual accumulated elevation angle for AE method ($\Sigma\alpha_{SAE}$), (d) Annual accumulated azimuth angle for AE method ($\Sigma\rho_{AE}$).

4.1.2 Comparison of AE and SE Methods for Heliostat Field

The simulation of the annual accumulated angles of heliostat field has been performed to compute $\Sigma\Sigma\alpha_{SSE}$, $\Sigma\Sigma\rho_{SE}$, $\Sigma\Sigma\alpha_{SAE}$ and $\Sigma\Sigma\rho_{AE}$ for both SE and AE methods correspondingly based on the specifications and design parameters as revealed in Table 3.2 and Figure 3.6. Figures 3.7 and 3.8 show the complete algorithms of simulation programs designed to compute the annual accumulated tracking angles of heliostat field for SE and AE tracking methods respectively. The simulated results of $\Sigma\Sigma\alpha_{SAE}$, $\Sigma\Sigma\rho_{AE}$, $\Sigma\Sigma\alpha_{SSE}$ and $\Sigma\Sigma\rho_{SE}$ at different latitudes, i.e. 0° , 15°N , 30°N , 45°N , 15°S and 30°S are listed in Table 4.1. Overall, the annual accumulated elevation angle for the SE method $\Sigma\Sigma\alpha_{SSE}$ is around 53.5% to 54.1 % of the annual accumulated elevation angle for the AE method $\Sigma\Sigma\alpha_{SAE}$. Meanwhile, the annual accumulated azimuth angle for the AE method $\Sigma\Sigma\rho_{AE}$ is about 70.1% to 74.0 % of the annual accumulated spinning angle for the SE method $\Sigma\Sigma\rho_{SE}$. Putting this aspect in a more practical sense, the corresponding power consumption of the heliostat field for both sun-tracking methods are also calculated based on the annual accumulated angles using the equations (3.29) and (3.30). From the calculated result shown in Table 4.1, the central tower system located at latitude 0° consumes the lowest annual power consumption on sun-tracking system compared to those of other latitudes. In general, the annual power consumption for SE method is lower than that of AE method in all latitudes.

Table 4.1: Annual accumulated sun-tracking angles and power consumption of heliostat field.

latitude	SE method				
	$\Sigma\Sigma\alpha_{SSE}$	$\Sigma\Sigma\rho_{SE}$	Annual power consumption on elevation movement	Annual power consumption on spinning movement	Annual total power consumption
0	10,898,727°	38,068,016°	1.83 MWh	4.27 MWh	6.10 MWh
15°N	10,930,488°	38,036,573°	1.84 MWh	4.26 MWh	6.10 MWh
30°N	11,040,512°	37,957,837°	1.86 MWh	4.25 MWh	6.11 MWh
45°N	11,161,685°	37,990,854°	1.88 MWh	4.26 MWh	6.13 MWh
15°S	10,930,488°	38,036,573°	1.84 MWh	4.26 MWh	6.10 MWh
30°S	11,040,512°	37,957,837°	1.86 MWh	4.25 MWh	6.11 MWh
latitude	AE method				
	$\Sigma\Sigma\alpha_{SAE}$	$\Sigma\Sigma\rho_{AE}$	Annual power consumption on elevation movement	Annual power consumption on azimuth movement	Annual total power consumption
0	20,379,193°	26,672,585°	3.42 MWh	2.99 MWh	6.41 MWh
15°N	20,404,920°	27,058,546°	3.43 MWh	3.03 MWh	6.46 MWh
30°N	20,491,149°	28,092,050°	3.44 MWh	3.15 MWh	6.59 MWh
45°N	20,620,319°	29,445,112°	3.47 MWh	3.30 MWh	6.76 MWh
15°S	20,404,920°	27,058,546°	3.43 MWh	3.03 MWh	6.46 MWh
30°S	20,491,149°	28,092,050°	3.44 MWh	3.15 MWh	6.59 MWh

4.2 Annual Field Efficiency

The simulation of the annual field efficiency of heliostat field has been performed to compute cosine efficiency, shadowing and blocking efficiency for both SE and AE methods based on the specifications and design parameters as revealed in Table 3.3 and Figure 3.13. Figure 3.12 shows the complete algorithms of simulation programs designed to compute the annual field efficiency of heliostat field for SE and AE tracking methods respectively.

Figures 4.4(a)-(b) show the annual field efficiency for a comparison of the two methods at the latitude 0° (or at equator). The graphs have shown that the annual field efficiency is perfectly symmetrical for both east-west and north-south fields for both sun-tracking methods. For the SE sun-tracking method, the annual field efficiency of the heliostats in the layout shown in Figure 3.13 is equal to or higher than 77.5%. For AE sun-tracking method, the annual field efficiency of the heliostats in this configuration is equal to or higher than 75.0%. This shows that SE sun-tracking method has better field efficiency than AE sun-tracking method at latitude 0° . Figures 4.5(a)-(b) show the annual field efficiency for a comparison of two methods at latitude 15°N while Figures 4.6(a)-(b) show the annual field efficiency for a comparison of the two methods at latitude 30°N . The graphs have shown that the annual field efficiency of the east and west field is perfectly symmetrical for both sun-tracking methods. Furthermore, the north field has the highest annual field efficiency while the south field has the lowest for both sun-tracking methods.

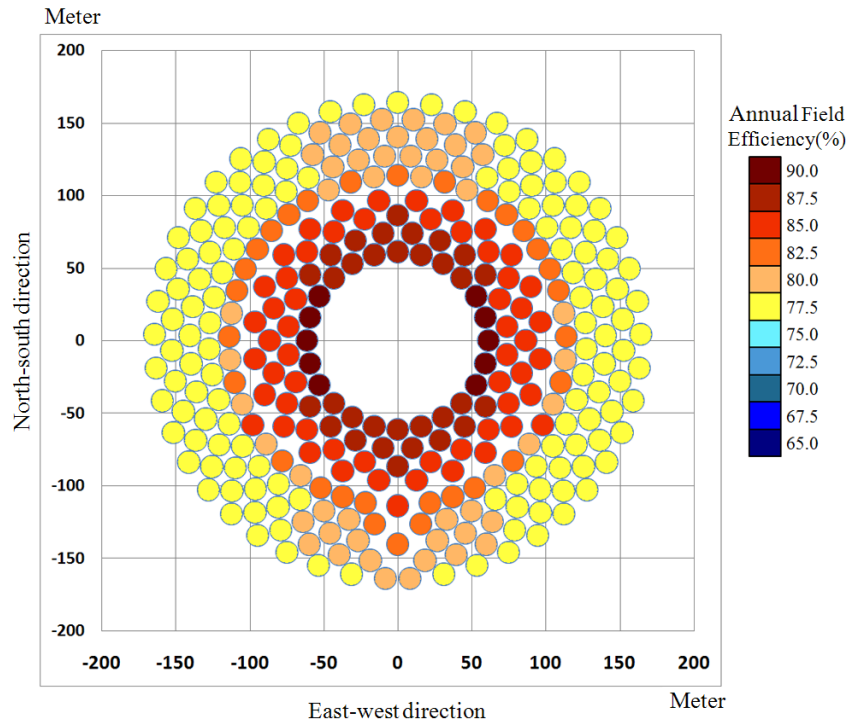


Figure 4.4 (a)

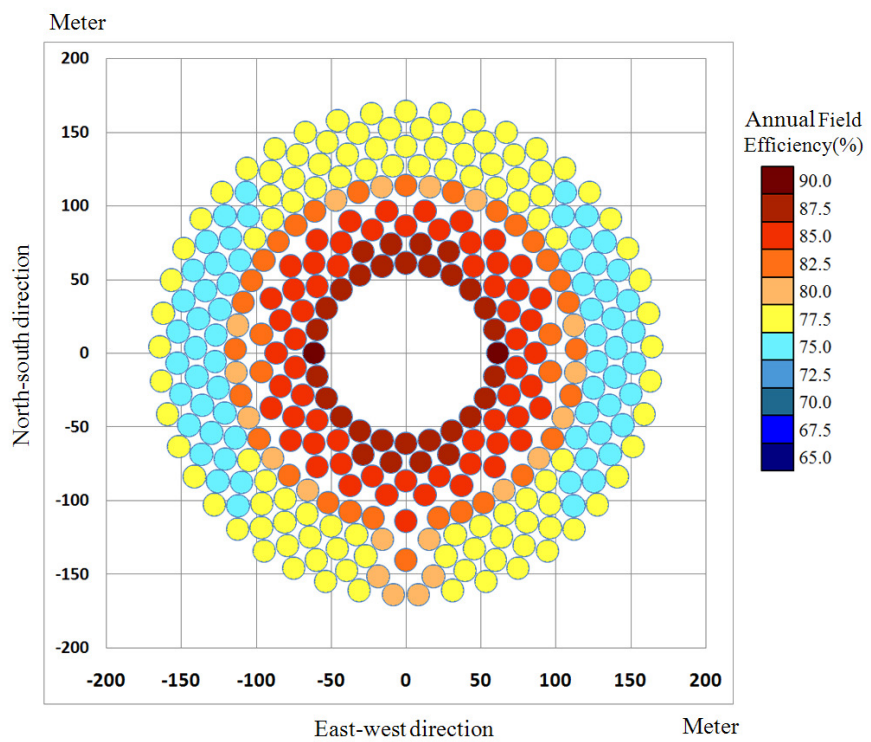


Figure 4.4 (b)

Figure 4.4: The annual field efficiency in the case of latitude 0° . (a) SE method
(b) AE method.

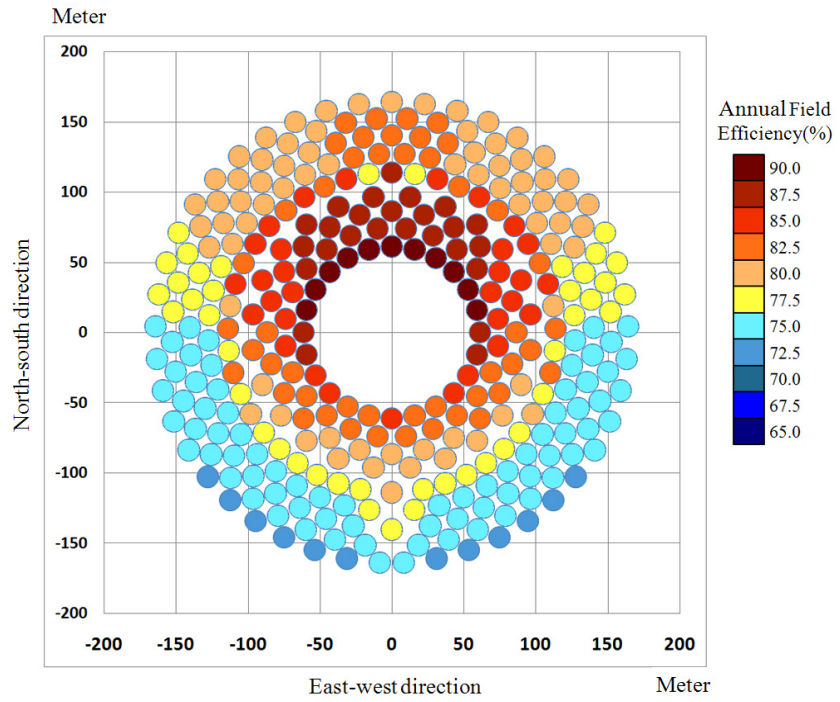


Figure 4.5 (a)

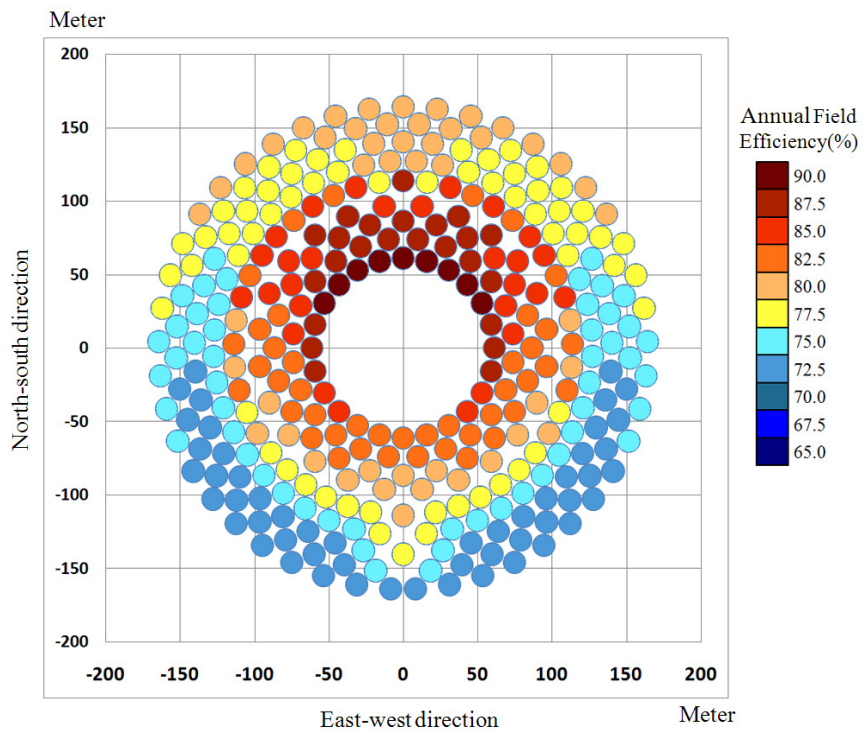


Figure 4.5 (b)

Figure 4.5: The annual field efficiency in the case of latitude 15°N . (a) SE method
(b) AE method.

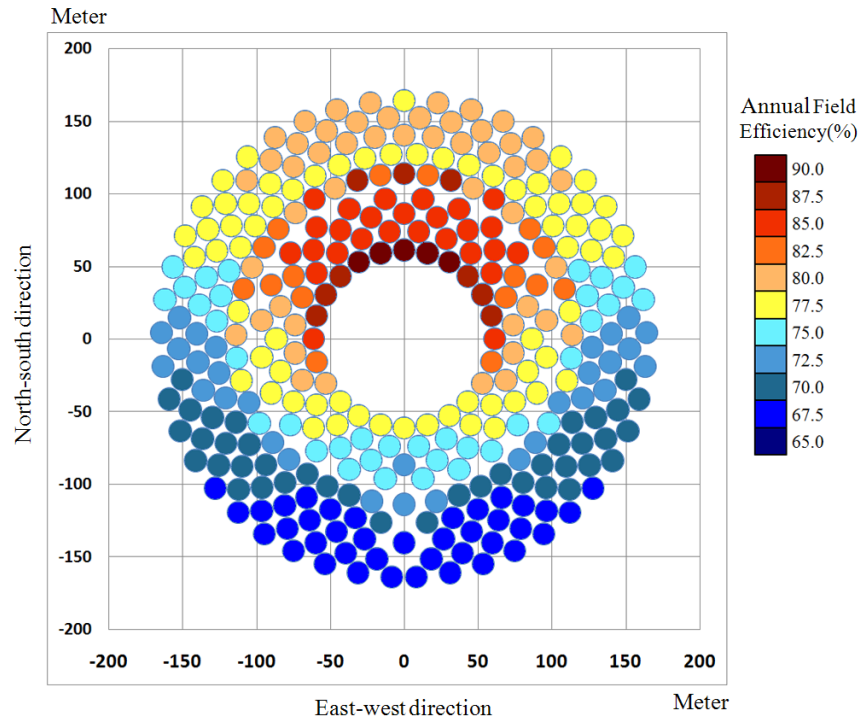


Figure 4.6 (a)

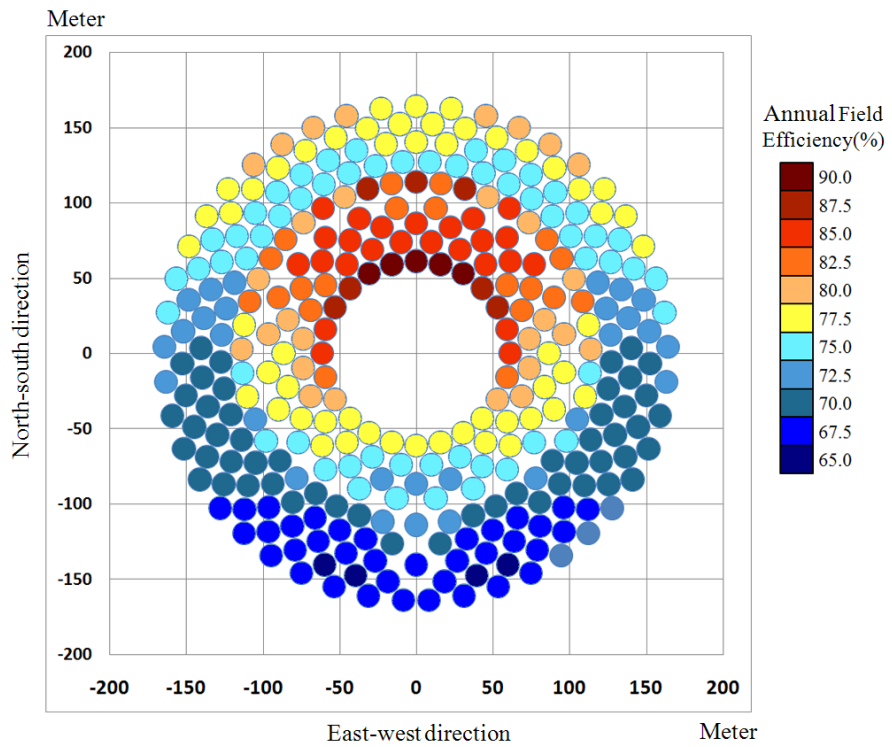


Figure 4.6 (b)

Figure 4.6: The annual field efficiency in the case of latitude 30°N . (a) SE method
(b) AE method.

The simulated results of annual field efficiency for both SE and AE sun-tracking methods at different latitudes, i.e. 0°, 15°N, and 30°N are listed in Table 4.2. From the calculated result shown in Table 4.2, central tower system located at latitude at 0° has the highest annual field efficiency compared to those of other latitudes. Besides that, the latitude is inversely proportional to the annual field efficiency for both sun-tracking methods which means the higher the latitude of the central power tower, the lower the annual field efficiency of the heliostat field.

Moreover, the cosine efficiency for both sun-tracking methods is equal to each other at all latitudes. This is because the positions of the sun, heliostats and target are located at the similar positions which provide same incident and reflected angles. Table 4.2 also shows that SE sun-tracking method has better shadowing and blocking efficiency compared to AE sun-tracking method at all latitudes. In general, the annual field efficiency for SE method is higher than that of AE method in all latitudes.

Table 4.2: Annual efficiencies of heliostat field for both sun-tracking methods.

Latitude	SE			AE		
	0°	15°N	30°N	0°	15°N	30°N
Cosine Efficiency	84.99%	84.45%	82.86%	84.99%	84.45%	82.86%
Blocking Efficiency	98.14%	98.07%	98.03%	97.11%	97.13%	97.24%
Shadowing Efficiency	98.71%	98.11%	95.63%	98.56%	97.93%	95.41%
Annual Field Efficiency	82.33%	81.25%	77.67%	81.35%	80.33%	76.88%

CHAPTER 5

CONCLUSION

5.1 Concluding Remarks

The study on the range of motion for two different sun-tracking methods at the level of single heliostat and heliostat field has been conducted in details. The algorithms to analyze the annual accumulated sun-tracking angles for both methods have also been developed. For a comparison of the two sun-tracking methods, $\Sigma\Sigma\alpha_{SSE}$ is about half of $\Sigma\Sigma\alpha_{SAE}$ but $\Sigma\Sigma\rho_{AE}$ is about 70–74% of $\Sigma\Sigma\rho_{SE}$. As a result, total power consumption on the sun-tracking system of SE method can be about 4.8–9.3% lesser than that of AE method.

Besides that, the algorithms to compute the annual field efficiency for both methods have also been developed. For a comparison of the two sun-tracking methods, the cosine efficiency are equal for both methods and SE method provides better shadowing and blocking efficiency compared to AE method. As a result, the annual field efficiency of SE method is about 0.8–1% better than the AE method. Even though the difference of the annual field efficiency for both methods is small, SE method is still recommended due to low power consumption on sun-tracking method compared to AE method.

Despite the mechanical design of the heliostat using SE sun-tracking method is different from that of the AE sun-tracking method, both types of

heliostats in fact contain exactly the same basic driving mechanism such as motor, gearbox, optical encoder and control system. The manufacturing, assembly and alignment procedures are quite similar for both methods. Comparing the construction cost of both SE and AE methods is not the main aim of this study because it depends on many factors such as the mechanical design, optical design, labor cost (very much dependent on the country), the quantity of heliostats to be manufactured, quality of materials, etc.

However, the materials cost for the heliostat with different tracking methods could be almost the same because both tracking methods require almost the same types of materials such as steel structure, driving mechanism, sensors, and mirrors. Therefore, the final construction cost can be very much dependent on the innovative design of the heliostat and it will remain as a great challenge for the solar systems engineers and scientists in the future.

5.2 Future Work

To further extend the current research work, a thorough study on the flux distribution can be conducted. Since the spinning-elevation method is dominant compared to the azimuth-elevation method, the spinning-elevation method will be selected as the parameter for this future study. The aim of the study is to determine the maximum sun concentration and temperature that can be achieved at the receiver by implementing spinning-elevation method on the heliostat field.

REFERENCES

- Battleson, K. W. (1981). Solar power tower design guide: Solar thermal central receiver power systems, a source of electricity and/or process heat. *Sandia National Labs Report SAND 81-8005*.
- Chen, Y.T., Chong, K.K., Bligh, T.P., Chen, L.C., Yunus, J., Kannan, K.S., Lim, B.H., Lim, C.S., Alias, M.A., Bidin, N., Aliman, O., Salehan, S., Rezan, S.A.H. Shk. Abd., Tam, C.M., Tan, K.K. (2001). Non-imaging focusing heliostat. *Solar Energy*, 71 (3), 155–164.
- Chen, Y.T., Chong, K.K., Lim, B.H., Lim, C.S. (2003). Study of residual aberration for non-imaging focusing heliostat. *Solar Energy Materials and Solar Cells*, 79 (1), 1–20.
- Chen, Y.T., Chong, K.K., Lim, C.S., Lim, B.H., Tan, B.K., Lu, Y.F. (2005). Report on the second prototype of non-imaging focusing heliostat and its application in food processing. *Solar Energy*, 79 (3), 280–289.
- Chen, Y.T., Chong, K.K., Lim, C.S., Lim, B.H., Tan, K.K., Aliman, Omar, Bligh, T.P., Tan, B.K., Ismail, Ghazally. (2002). Report of the first prototype of non-imaging focusing heliostat and its application in high temperature solar furnace. *Solar Energy*, 72 (6), 531–544.

- Chen, Y.T., Kribus, A., Lim, B.H., Lim, C.S., Chong, K.K., Karni, J., Buck, R., Pfahl, A., Bligh, T.P. (2004). Comparison of two sun tracking methods in the application of a heliostat field. *Journal of Solar Energy Engineering*, 126 (1), 638–644.
- Chen, Y.T., Lim, B.H., Lim, C.S. (2006). Complete solution of sun tracking for heliostat. *Communications in Theoretical Physics*, 45, 165–166.
- Chong, K.K. (2002). *Characterization of non-imaging focusing heliostat in University of Technology Malaysia*. Ph.D. Thesis, Faculty of Electrical Engineering, Universiti Teknologi Malaysia, Skudai, Malaysia.
- Chong, K.K. (2010a). Optimization of nonimaging focusing heliostat in dynamic correction of astigmatism for a wide range of incident angles. *Optics Letters*, 35 (10), 1614–1616.
- Chong, K.K. (2010b). Optical analysis for simplified astigmatic correction of non-imaging focusing heliostat. *Solar Energy*, 84 (8), 1356–1365.
- Chong, K.K., Lim, C.Y., Hiew, C.W. (2011). Cost-effective solar furnace system using fixed geometry non-imaging focusing heliostat and secondary parabolic concentrator. *Renewable Energy*, 36 (5), 1595–1602.

- Chong, K.K., Tan, B.K., Yunus, Jasmy. (2006). Characteristic study of hot spot in the new solar furnace comprising of non-imaging focusing heliostat and parabolic reflector. *Journal of Science and Technology in the Tropics*, 2, 27–34.
- Collado, F. J. (2009). Preliminary design of surrounding heliostat field. *Renewable Energy*, 34, 1359–1363.
- Collado, F. J., Turégano, J. A. (1989). Calculation of the annual thermal energy supplied by a defined heliostat field. *Solar Energy*, 42, 149–165.
- Corey J. Noone, A. Ghobeity, A. H. Slocum, G. Tzamtzis, A. Mitsos. (2011). Site selection for hillside central receiver solar thermal plants. *Solar Energy*, 85, 839–848.
- Dellin, T. A., M. J. Fish, C. L. Yang. (1981). A user manual for DELSOL2: A computer code for calculating the optical performance and optimal system design for solar thermal central receiver plants. *Sandia National Labs Report SAND 81-8237*.
- Guo, M., Wang, Z., Liang, W., Zhang, X., Zang, C., Lu, Z., Wei, X. (2010). Tracking formulas and strategies for a receiver oriented dual-axis tracking toroidal heliostat. *Solar Energy*, 84, 939–947.

Jespersion, J., J. Fitz-Randolph. (1977). From sundials to atomic clocks. *National Bureau of Standards Monograph*.

Li, L., Lim, C.S. (2009). Tracking speed analysis for heliostat using spinning-elevation tracking mode. *Journal of Solar Energy Engineering*, 131 (3), 034501–034505.

Lipps, F. W., L. L. Vant-Hull. (1978). A cellwise method for the optimization of large central receiver systems. *Solar Energy*, 30(6), 505–516.

Omar M. Al-Rabghi, Moustafa M. Elsayed. (1990). Heliostat minimum radial spacing for no blocking and no shadowing condition. *Renewable Energy*, 1, 37–47.

Sanchez, M., Romero, M. (2006). Methodology for generation of heliostat field layout in central receiver systems based on yearly normalized energy surfaces. *Solar Energy*, 80(7), 861–874.

Schramek, P., Mills, D. R., Wes Stein, Lievre, P.L. (2009). Design of the heliostat field of the CSIRO solar tower. *Journal of Solar Energy Engineering*, 131, 505–510

Schubnell, M., Ries, H. (1990). The optics of a two-stage solar furnace. *Solar Energy Materials*, 21, 213–217.

- Segal, A., Epstein, M. (1996). A model for optimization of a heliostat field layout in solar thermal concentrating technologies. *Proceedings of the Eighth International Symposium, Köln, Germany, Oct. 5–11, 1989–1998.*
- Siala, F. M. F. Elayeb, M. E. (2001). Mathematical formulation of a graphical method for a no-blocking heliostat field layout. *Renewable Energy*, 23(1), 77–92.
- Stine, W.B., Harrigan, R.W. (Eds.) (1985). *Solar Energy Fundamentals and Design with Computer Applications*. John Wiley, New York, 135-262.
- Vittitoe, C. N., F. Biggs. (1978). Terrestrial propagation loss, paper presented at the American section, *International Solar Energy Society Meeting*, Denver, Colorado.
- Woolf, H.M. (1968). On the computation of solar evaluation angles and the determination of sunrise and sunset times. *National Aeronautics and Space Administration Report NASA*.
- Zaibel, R., Dagan, E., Karni, J., Ries, H. (1995). An astigmatic corrected target-aligned heliostat for high concentration. *Solar Energy Materials and Solar Cells*, 37, 191–202.



Range of motion study for two different sun-tracking methods in the application of heliostat field

K.K. Chong*, M.H. Tan

Faculty of Engineering and Science, Universiti Tunku Abdul Rahman, Off Jalan Genting Kelang, Setapak, 53300 Kuala Lumpur, Malaysia

Received 20 December 2010; received in revised form 11 April 2011; accepted 23 April 2011

Communicated by: Associate Editor Dr. L. Vant-Hull

Abstract

Since the beginning of the history in the application of heliostats, the sun-tracking method is generally implemented using the Azimuth-Elevation method. Although Spinning-Elevation method was first proposed by Ries et al. and then popularized by Chen et al., it is still not widely applied in a large scale solar energy application especially in central tower system. This paper will study in more detail the implementation of the Spinning-Elevation method in the central tower system for a comparison to that of the typical Azimuth-Elevation method. The annual accumulated angles of the two different sun-tracking methods were analyzed in details for both the cases of a single heliostat and the heliostat field.

© 2011 Elsevier Ltd. All rights reserved.

Keywords: Azimuth-Elevation; Spinning-Elevation; Heliostat; Range of motion; Sun-tracking angles; Central power tower

1. Introduction

The largest fixed target solar collector which is also known as the central tower system involves the use of many individual sun-tracking mirrors (or heliostats) to reflect and to superpose the concentrated sunlight at a common target attached to the central tower. According to the thermodynamic law, high conversion efficiency from the solar energy to the electrical energy can only be reached by this type of solar power plant through Rankine cycle. Unfortunately, it requires a complex control system to operate and to monitor the motors fixed on each heliostat for sun-tracking.

Since the beginning of the history in the application of heliostats, the sun-tracking method has generally been implemented using the Azimuth-Elevation (AE) method (Stine and Harrigan, 1985). In this tracking method, one

of the tracking axes of the heliostat points towards the zenith namely azimuth-axis while the other axis is perpendicular to the first axis and tangent to the heliostat frame called elevation-axis. During the sun-tracking, the motions of the heliostat are operated by two motors: one motor for the azimuth which provides rotational movement in the azimuth direction, and another motor which rotates the heliostat in the elevation direction. The development of heliostat before year 1990 is fully dominant by this sun-tracking method due to its straightforward design learned from the steering mirror using in the optical system and in radar antennae.

The first idea of Spinning-Elevation (SE) method was proposed by Schubnell and Ries in the year 1990 for the application of heliostat in the solar furnace system and was then studied in various applications by several authors (Schubnell and Ries, 1990; Chen et al., 2001, 2002, 2003, 2004, 2005, 2006; Chong, 2002, 2010a,b; Chong et al., 2006, 2011; Guo et al., 2010; Li and Lim, 2009). In this tracking method, one of the tracking axes of the heliostat points towards the target namely spinning-axis in order

* Corresponding author. Tel.: +60 3 41079802; fax: +60 3 41079803.
E-mail addresses: chongkk@utar.edu.my, kokkeong_c@yahoo.com (K.K. Chong).

to maintains the heliostat normal within the tangential plane, while the other axis is perpendicular to the first axis and tangent to the heliostat frame in order to adjust the heliostat normal within the tangential plane until it bisects the sun position vector and the target position vector called elevation-axis. The motions of this type of heliostat are also

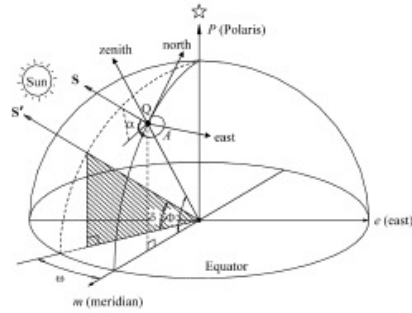


Fig. 1. Composite view of coordinate systems attached to both the earth-center and earth-surface reference frames.

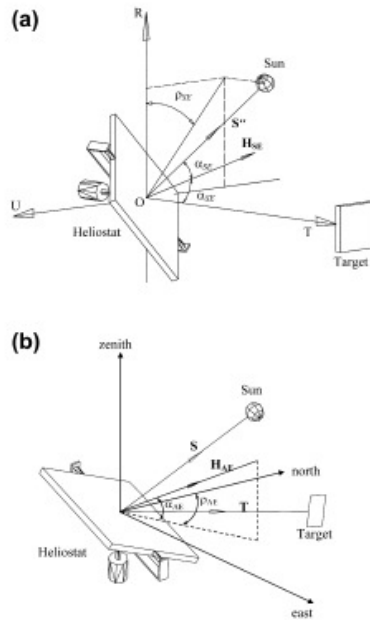


Fig. 2. (a) Coordinate system attached to the local heliostat reference frame for the Spinning-Elevation (SE) sun-tracking method. The heliostat normal vector H_{SE} is defined in the function of the angles α_{SE} and ρ_{SE} . (b) Coordinate system attached to the earth-surface reference frame for the Azimuth-Elevation (AE) sun-tracking method where the heliostat normal vector H_{AE} is defined in the function of the angles α_{AE} and ρ_{AE} .

operated by two different motors, the motor which provides rotational movement at spinning-axis and another motor which provides rotational movement at elevation-axis. Since year 2001, Chen et al. and Chong have collectively derived and developed the sun-tracking formula for the SE method by proposing a novel focusing heliostat called non-imaging focusing heliostat (Chen et al., 2001, 2002, 2003, 2004, 2005; Chong, 2002, 2010a,b; Chong et al., 2006, 2011). Unlike the conventional imaging heliostat design where a fixed geometry approximating spherical surface is used, the non-imaging focusing heliostat is comprised of an array of $m \times n$ facet mirrors which can be maneuvered in line-tilting manner instead of the trivial tip-tilting manner to dynamically correct the first-order astigmatism. Several years later, non-imaging focusing

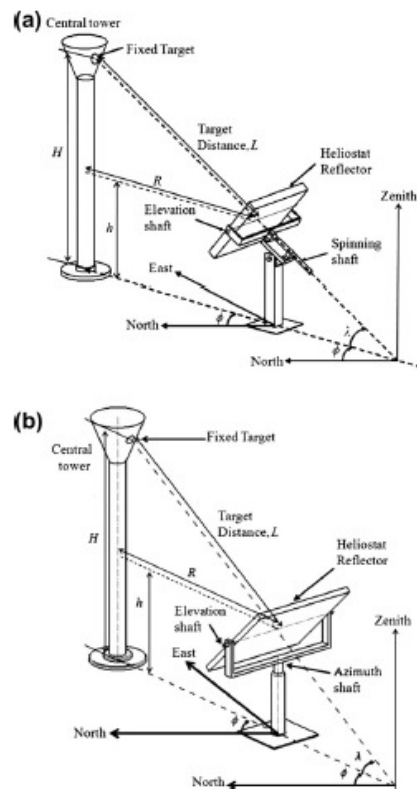


Fig. 3. Coordinate system attached to earth-surface reference frame in which the central tower and heliostat is located for two different sun-tracking methods where ϕ is the facing angle and λ is the target angle of the heliostat. (a) Spinning-Elevation sun-tracking method. (b) Azimuth-Elevation sun-tracking method.

Please cite this article in press as: Chong, K.K., Tan, M.H. Range of motion study for two different sun-tracking methods in the application of heliostat field. Sol. Energy (2011), doi:10.1016/j.solener.2011.04.024

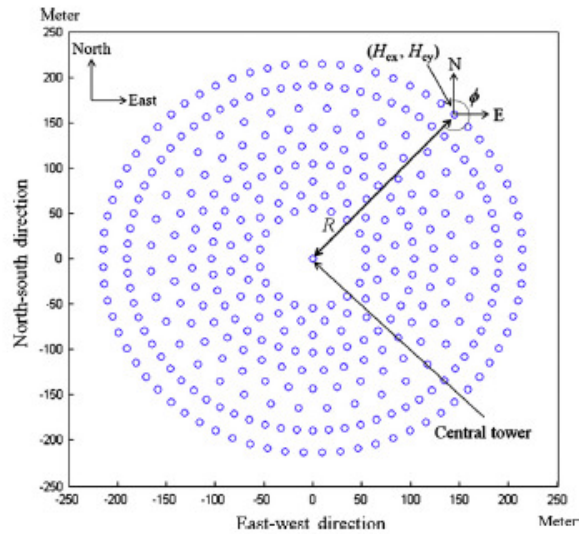


Fig. 4. Layout of the heliostat field consisted of one central tower at the origin and it is surrounded by 342 heliostats.

heliostat with a fixed geometry configuration has also been introduced to the solar power tower system as to minimize the complexity of the control system considerably in the heliostat field by excluding all the driving devices for correcting astigmatism (Chen et al., 2004).

With the newly published SE tracking formula, it preserves the vertical and horizontal sides of the heliostat frame to be always aligned with the tangential and sagittal planes respectively so that the astigmatism can be corrected using a non-symmetric heliostat with two different radii of curvature as proposed by Zaibel et al. (1995). The geometry of non-imaging focusing heliostat proposed by Chen et al. can be approximated to that of non-symmetric heliostat when the distance between the heliostat and the target is much greater compared to the dimension of the heliostat. In year 2004, Chen's group has studied the optical performance of the two different sun-tracking methods at the level of a single heliostat and a heliostat field (Chen et al., 2004). The two types of heliostat design are the fixed geometry non-imaging focusing heliostat using SE tracking method and the typical spherical geometry heliostat using AE tracking method. They concluded that the SE tracking method can reduce the receiver spillage loss by 10–30% and also provide a much more uniform concentrated sunlight at the receiver without huge variations with the time of day compared to the AE tracking method. Despite the SE method is more superior than the AE method in the aspect of optical performance, the range of motion of the two sun-tracking methods still remain unknown to us. In this paper, we would like to further explore on the range of motion for the two different sun-tracking methods implemented in the heliostat field. In this study, the characteristics of both

rotational angles in the AE and SE methods are analyzed to justify which sun-tracking method has the minimum accumulated rotational angles throughout the year.

2. Methodology

2.1. Sun-tracking formulas

To analyze range of motion for two different sun-tracking methods in the application of central tower system, the formulas of sun-tracking angles of both methods must be obtained first. In fact, the mathematical expressions of the sun-tracking formulas for AE and SE methods were previously derived by Stine and Harrigan (1985), Chen et al. (2001) respectively. The derivations of both sun-tracking formulas are revised in this paper for the sake of standardization in the definition of parameters for both methods as well as for the completeness of the mathematical analysis in the later section.

In the central tower system, the sun rays that impinge on a field of heliostats (each heliostat is an array of $m \times n$ facet

Table 1

Specification and design parameters of the heliostat.

Reflective area of heliostat	11 m × 11 m
Height of heliostat, h	7 m
Gear ratio of the gear train in the azimuth or spinning drive, G_p	4400
Gear ratio of the gear train in the elevation drive, G_e	4400
Angular speed of the azimuth or spinning motor, ω_p	120 rpm
Angular speed of the elevation motor, ω_e	120 rpm
Power rating of azimuth or spinning motor, P_p	66 W
Power rating of the elevation motor, P_e	99 W

Table 2
Specification of central power tower and heliostat field layout.

Total number of heliostats	342								
Target (or tower) height, H	95 m								
Total reflective area of heliostat field	41,382 m ²								
Total land area	156,016.6 m ² (15.60166 hectare)								
Ring Number	1	2	3	4	5	6	7	8	9
Radial distances of heliostats from the central tower, R (m)	55	70	85	104	124	144	166	190	216
Target angle, λ (°)	57.99	51.50	45.99	40.24	35.36	31.43	27.93	24.85	22.26
Field layout (number of heliostats per ring)	18	18	18	36	36	36	36	72	72

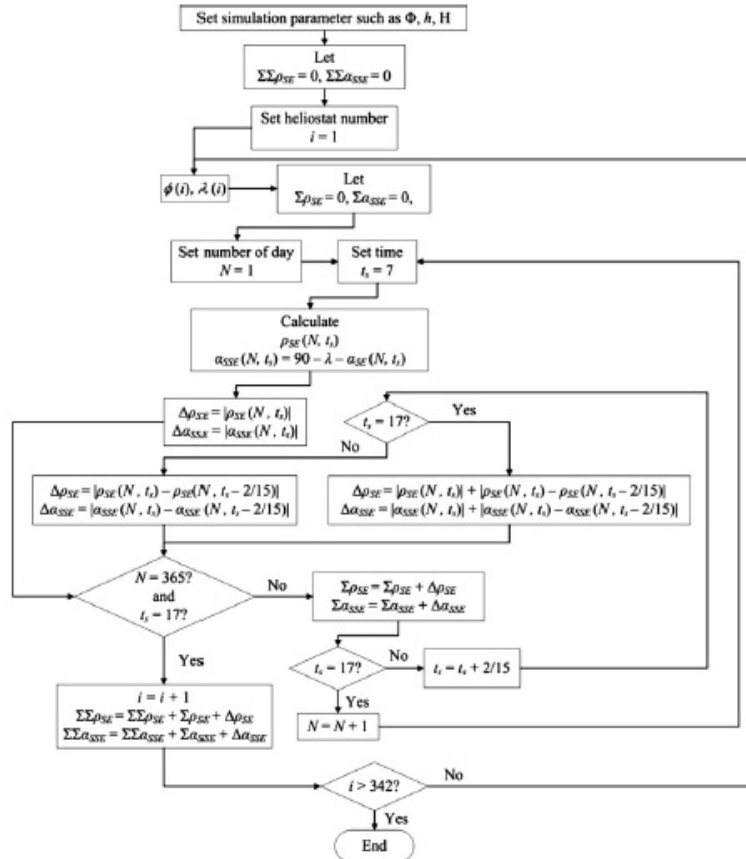


Fig. 5. The flow chart to show the algorithm of computing the annual accumulated sun-tracking angles for two different methods. (a) Spinning-Elevation sun-tracking method. (b) Azimuth-Elevation sun-tracking method.

mirrors attached to a movable mechanical frame) are reflected to a single point in space namely fixed target or central receiver. Thus, sun-tracking formulas of both meth-

ods have to involve a sun position vector (incident sun ray), a target position vector (reflected sun ray) and a heliostat normal vector. Since the sun is a moving object and the

Please cite this article in press as: Chong, K.K., Tan, M.H. Range of motion study for two different sun-tracking methods in the application of heliostat field. Sol. Energy (2011), doi:10.1016/j.solener.2011.04.024

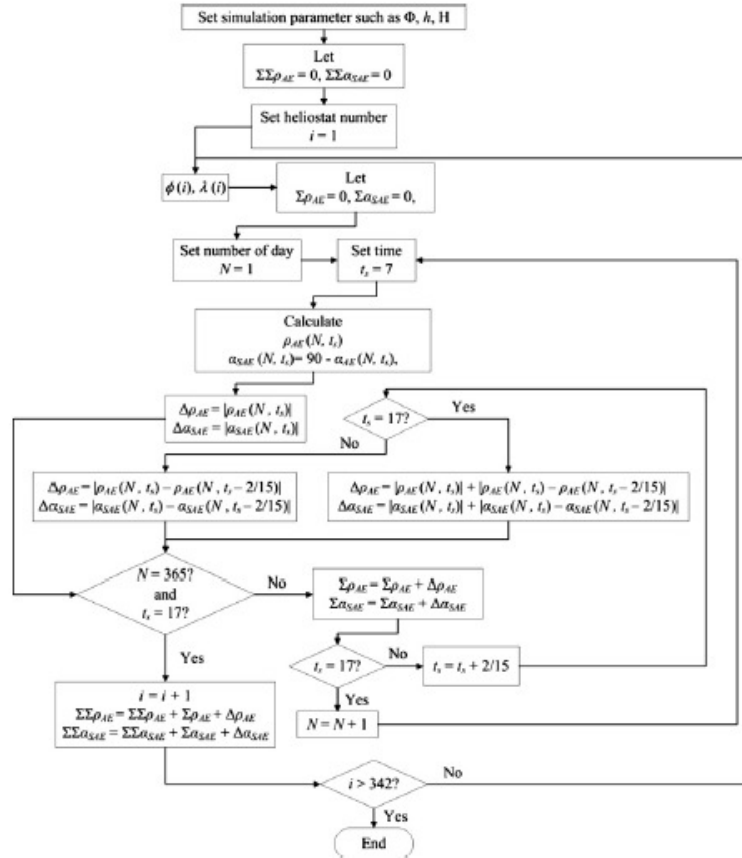


Fig 5. (continued)

target is a fixed object, the heliostat normal must be adjusted from time to time when the sun position changes with time. The sun position relative to any location on the earth surface can be mathematically described as sun altitude angle (α) and sun azimuth angle (A). The ultimate position of the heliostat normal regardless of any sun-tracking method should be the same during sun-tracking whilst the only difference between the AE and the SE methods is the orientation of tracking axes for rotating the heliostat normal to that position. Before deriving the sun-tracking formulas of both methods, the sun position angles must be presented first. Fig. 1 shows composite view of coordinate systems attached to both the earth-center and earth-surface reference frames. In earth-center frame, the vector S' that points towards the sun is described in terms of hour angle ω and declination angle δ . Given that the observer Q is

located on the earth surface with latitude Φ , the sun position vector S is defined in the earth-surface frame in terms of the sun altitude angle α and the sun azimuth angle A . According to Stine and Harrigan (1985), the derivation of sun altitude and azimuth angles can be obtained by multiplying the latitude transformation matrix Φ on the vector S' as follow:

$$\begin{bmatrix} \sin \alpha \\ \cos \alpha \sin A \\ \cos \alpha \cos A \end{bmatrix} = \begin{bmatrix} \cos \Phi & 0 & \sin \Phi \\ 0 & 1 & 0 \\ -\sin \Phi & 0 & \cos \Phi \end{bmatrix} \begin{bmatrix} \cos \delta \cos \omega \\ -\cos \delta \sin \omega \\ \sin \delta \end{bmatrix} \quad (1)$$

$$\begin{bmatrix} \sin \alpha \\ \cos \alpha \sin A \\ \cos \alpha \cos A \end{bmatrix} = \begin{bmatrix} \sin \delta \sin \Phi + \cos \delta \cos \omega \cos \Phi \\ -\cos \delta \sin \omega \\ \sin \delta \cos \Phi - \cos \delta \cos \omega \sin \Phi \end{bmatrix} \quad (2)$$

Please cite this article in press as: Chong, K.K., Tan, M.H. Range of motion study for two different sun-tracking methods in the application of heliostat field. Sol. Energy (2011), doi:10.1016/j.solener.2011.04.024

The sun altitude angle is defined as

$$\alpha = \sin^{-1}(\sin \delta \sin \Phi + \cos \delta \cos \omega \cos \Phi) \quad (3)$$

The sun azimuth angle is defined as

$$A = \cos^{-1} \left(\frac{\sin \delta \cos \Phi - \cos \delta \cos \omega \sin \Phi}{\cos \alpha} \right) \quad (4)$$

$$\text{If } \sin \omega > 0 \text{ then } A = 2\pi - A. \quad (5)$$

The declination angle, δ , can be calculated by using the following formula:

$$\delta = \sin^{-1}[0.39795 \times \cos(0.98563 \times (N - 173))] \quad (6)$$

The hour angle, ω , can be calculated as follow:

$$\omega = 15 \times (t_s - 12) \quad (7)$$

where N is number of day where $N = 1$ for January 1 and $N = 42$ for February 11, t_s is the solar time in 24-h rather than AM/PM.

For the Spinning-Elevation (SE) sun-tracking method, the coordinate system attached to the local heliostat reference frame as shown in Fig. 2a with the origin, O, defined as the cross section point of the two sun-tracking axes.

The OR, OU and OT are three fixed orthogonal axes with the OT axis pointing out from the origin towards the target direction. The initial orientation of heliostat is defined in such a way that the mirrors along the central column and central row are aligned to be parallel with the OR and OU axes respectively. The heliostat normal vector \mathbf{H}_{SE} is defined in the function of the angles α_{SE} and ρ_{SE} . From Fig. 3a, the spinning angle (ρ_{SE}) and elevation angle (α_{SE}) of the heliostat can be interrelated to the sun position vector through the coordinate transformations of facing angle, ϕ , and then followed with that of target angle, λ , as expressed in the following:

$$\begin{bmatrix} \cos(\frac{\pi}{2} - 2\alpha_{SE}) \cos \rho_{SE} \\ -\cos(\frac{\pi}{2} - 2\alpha_{SE}) \sin \rho_{SE} \\ \sin(\frac{\pi}{2} - 2\alpha_{SE}) \end{bmatrix} = \begin{bmatrix} \cos \lambda & 0 & -\sin \lambda \\ 0 & 1 & 0 \\ \sin \lambda & 0 & \cos \lambda \end{bmatrix} \begin{bmatrix} 1 & 0 & 0 \\ 0 & \cos \phi & -\sin \phi \\ 0 & \sin \phi & \cos \phi \end{bmatrix} \begin{bmatrix} \sin \alpha \\ \cos \alpha \sin A \\ \cos \alpha \cos A \end{bmatrix} \quad (8)$$

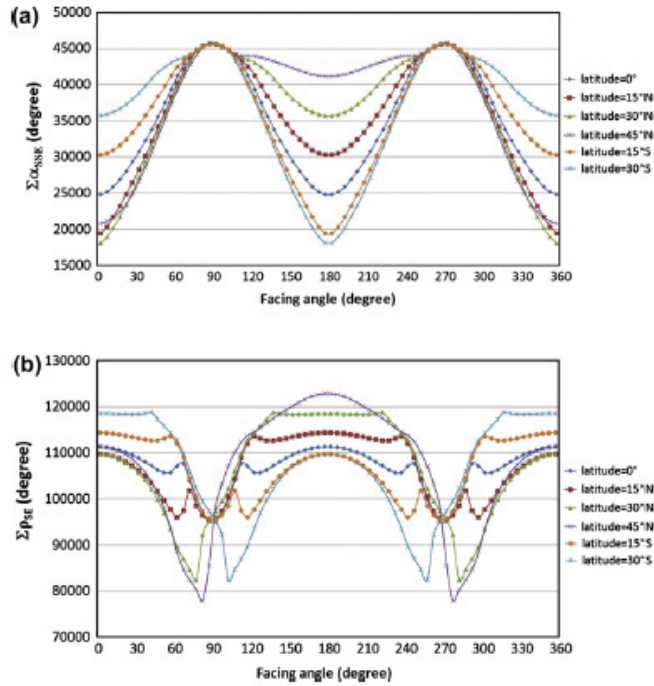


Fig. 6. The annual accumulated tracking angle of a single heliostat versus facing angle in the case of target angle 22.26°, and latitudes 0°, 15°N, 30°N, 45°N, 15°S, 30°S. (a) The annual accumulated elevation angle for SE method ($\Sigma\alpha_{SE}$). (b) The annual accumulated spinning angle for SE method ($\Sigma\rho_{SE}$). (c) The annual accumulated elevation angle for AE method ($\Sigma\alpha_{AE}$). (d) The annual accumulated azimuth angle for AE method ($\Sigma\rho_{AE}$).

Please cite this article in press as: Chong, K.K., Tan, M.H. Range of motion study for two different sun-tracking methods in the application of heliostat field. Sol. Energy (2011), doi:10.1016/j.solener.2011.04.024

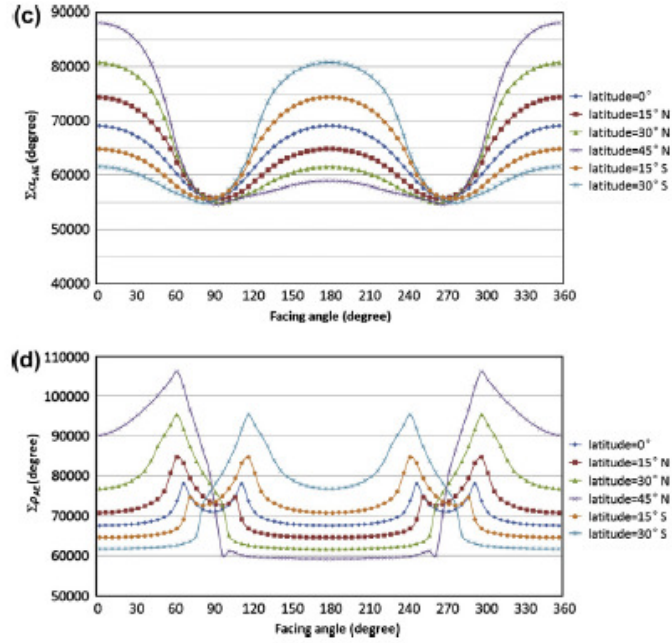


Fig 6. (continued)

$$\begin{aligned}
 & \begin{bmatrix} \cos(\frac{\pi}{2} - 2\alpha_{SE}) \cos \rho_{SE} \\ -\cos(\frac{\pi}{2} - 2\alpha_{SE}) \sin \rho_{SE} \\ \sin(\frac{\pi}{2} - 2\alpha_{SE}) \end{bmatrix} \\
 & = \begin{bmatrix} \cos \lambda \sin \alpha - \sin \lambda \sin \phi \cos \alpha \sin A - \sin \lambda \cos \phi \cos \alpha \cos A \\ \cos \phi \cos \alpha \sin A - \sin \phi \cos \alpha \cos A \\ \sin \lambda \sin \alpha + \cos \lambda \sin \phi \cos \alpha \sin A + \cos \lambda \cos \phi \cos \alpha \cos A \end{bmatrix} \quad (9)
 \end{aligned}$$

where $\phi = 0^\circ$ when the heliostat is due south of the target and it is positive value if the spinning-axis is rotated from north to east direction; $\lambda = 0^\circ$ if the heliostat is of the same height as the target and it is positive value when the spinning-axis is rotated so that the target is higher than the heliostat. Please note that the angle λ in this paper is defined to be in the opposite direction compared to that of definition by Chen et al. (2001, 2002, 2003, 2004, 2005, 2006). It is important to redefine the direction of λ here in order to suit the application of central tower system of which heliostat field surrounded a much higher central tower in which the target is placed on top.

The elevation and spinning angles of heliostat using the SE method can be expressed as follow:

$$\begin{aligned}
 \alpha_{SE} &= \frac{\pi}{4} - \frac{1}{2} \sin^{-1} (\sin \lambda \sin \alpha + \cos \lambda \sin \phi \cos \alpha \sin A \\
 & \quad + \cos \lambda \cos \phi \cos \alpha \cos A) \quad (10)
 \end{aligned}$$

In the case of $\cos \rho_{SE} > 0$,

$$\rho_{SE}^+ = \sin^{-1} \left\{ \frac{\sin \phi \cos \alpha \cos A - \cos \phi \cos \alpha \sin A}{\cos(\frac{\pi}{2} - 2\alpha_{SE})} \right\} \quad (11a)$$

In the case of $\cos \rho_{SE} < 0$,

$$\rho_{SE}^- = \pi - \rho_{SE}^+ \quad (11b)$$

where $\cos \rho =$

$$\frac{\cos \lambda \sin \alpha - \sin \lambda \sin \phi \cos \alpha \sin A - \sin \lambda \cos \phi \cos \alpha \cos A}{\cos(\frac{\pi}{2} - 2\alpha_{SE})} \quad (12)$$

Note: Eq. (10) is obtained from the third row of Eq. (9); Eqs. (11a) and (11b) are derived from second row of Eq. (9); and Eq. (12) is derived from the first row of Eq. (9).

From the above equation, both the angles ρ_{SE} and α_{SE} are exactly 0° when the elevation axis is aligned to be parallel with the OU axis and the top of heliostat frame facing towards OR axis.

For the Azimuth-Elevation (AE) sun-tracking method, Fig. 2b shows the coordinate system attached to the

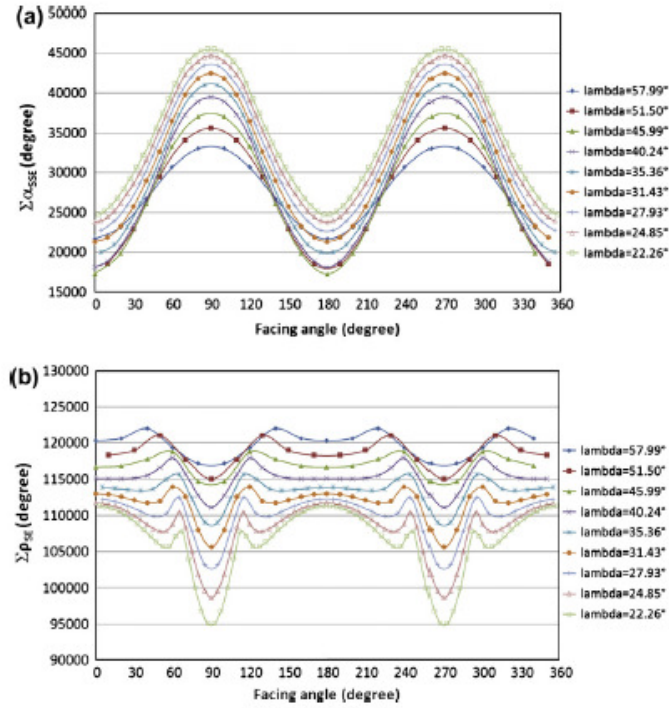


Fig. 7. The annual accumulated tracking angle of a single heliostat versus facing angle in the case of latitude 0° . (a) The annual accumulated elevation angle for SE method ($\Sigma\alpha_{SSE}$). (b) The annual accumulated spinning angle for SE method ($\Sigma\rho_{SSE}$). (c) The annual accumulated elevation angle for AE method ($\Sigma\alpha_{AER}$). (d) The annual accumulated azimuth angle for AE method ($\Sigma\rho_{AER}$).

earth-surface reference frame where the heliostat normal vector \mathbf{H}_{AE} is defined in the function of the angles α_{AE} and ρ_{AE} . The azimuth angle ρ_{AE} and the elevation angle α_{AE} can be derived solely based on the reflection law that relates the sun position vector, the target position vector and the heliostat normal vector in the earth-surface coordinate system. The sun position vector can be recalled from the Eq. (1) in the matrix form as follow:

$$\mathbf{S} = \begin{bmatrix} \sin \alpha \\ \cos \alpha \sin A \\ \cos \alpha \cos A \end{bmatrix} \quad (13)$$

The target position vector expressed in terms of angles λ and ϕ is as follow:

$$\mathbf{T} = \begin{bmatrix} \sin \lambda \\ \cos \lambda \sin \phi \\ \cos \lambda \cos \phi \end{bmatrix} \quad (14)$$

The heliostat normal vector expressed in terms of angles α_{AE} and ρ_{AE} is as follow:

$$\mathbf{H}_{AE} = \begin{bmatrix} \sin \alpha_{AE} \\ \cos \alpha_{AE} \sin \rho_{AE} \\ \cos \alpha_{AE} \cos \rho_{AE} \end{bmatrix} \quad (15)$$

From the reflection law, the relationship of the three vectors is as follow:

$$\mathbf{H}_{AE} = \frac{1}{2 \cos \theta} (\mathbf{S} + \mathbf{T})$$

$$\begin{bmatrix} \sin \alpha_{AE} \\ \cos \alpha_{AE} \sin \rho_{AE} \\ \cos \alpha_{AE} \cos \rho_{AE} \end{bmatrix} = \frac{1}{2 \cos \theta} \begin{bmatrix} \sin \alpha + \sin \lambda \\ \cos \alpha \sin A + \cos \lambda \sin \phi \\ \cos \alpha \cos A + \cos \lambda \cos \phi \end{bmatrix} \quad (16)$$

where $\cos 2\theta = (\mathbf{S} \cdot \mathbf{T})$ so that the incident angle can be obtained as

$$\theta = \frac{1}{2} \cos^{-1} (\sin \alpha \sin \lambda + \cos \alpha \sin A \cos \lambda \sin \phi + \cos \alpha \cos A \cos \lambda \cos \phi) \quad (17)$$

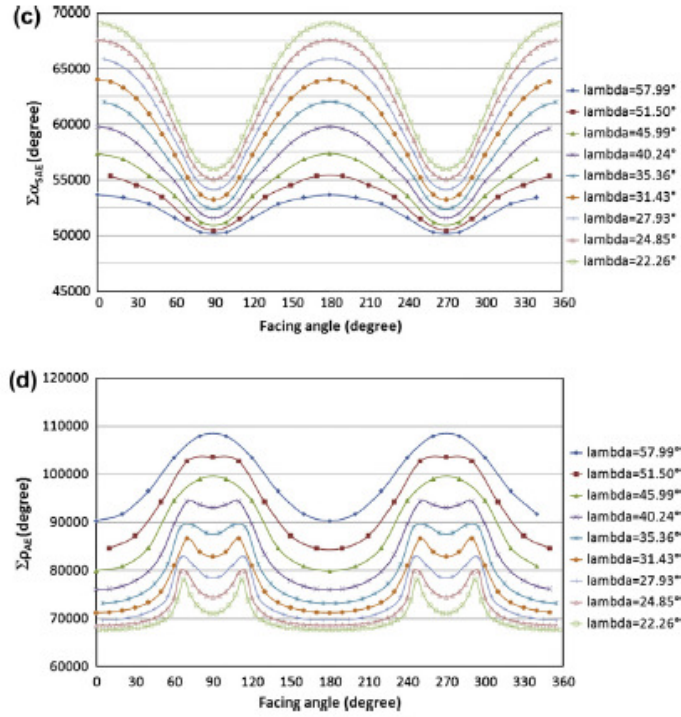


Fig 7. (continued)

From Eq. (16), the elevation and azimuth angles of AE method can be derived as follow:

$$\alpha_{AE} = \sin^{-1} \left(\frac{\sin \alpha + \sin \lambda}{2 \cos \theta} \right) \quad (18)$$

In the case of $\cos \rho_{AE} > 0$,

$$\rho_{AE}^+ = \sin^{-1} \left(\frac{\cos \alpha \sin A + \cos \lambda \sin \phi}{2 \cos \theta \cos \alpha_{AE}} \right) \quad (19a)$$

In the case of $\cos \rho_{AE} < 0$,

$$\rho_{AE}^- = \pi - \rho_{AE}^+ \quad (19b)$$

$$\text{given that } \cos \rho_{AE} = \frac{\cos \alpha \cos A + \cos \lambda \cos \phi}{2 \cos \theta \cos \alpha_{AE}} \quad (20)$$

Note: Eq. (18) is obtained from the first row of Eq. (16); Eqs. (19a) and (19b) are derived from second row of Eq. (16); and Eq. (20) is derived from the third row of Eq. (16).

From the above equations, both the angles ρ_{AE} and α_{AE} are exactly 0° when the elevation axis is aligned to be parallel along the east–west axis and heliostat frame facing towards north.

Those heliostats located in the north, east and west fields of the central tower will encounter problem of large azi-

imuth angle because the initial position of heliostat reflector is defined facing towards the north direction as shown in Fig. 3b instead of facing towards the central tower and hence it will require additional power consumption to the azimuth motor for driving the heliostat reflector to face the central tower during sun-tracking. In order to avoid the aforementioned problem, the initial orientation of heliostat reflector is redefined to face the central tower and thus the azimuth angle has to be rewritten as

$$\rho_{AE} = \rho_{AE} - \phi \quad (21)$$

2.2. Heliostat field layout

In Fig. 4, a layout of heliostat field consisted of central tower surrounded by 342 heliostats with the specifications as listed in Tables 1 and 2 is designed for the range of motion study. In the field layout, the heliostats are arranged into nine rings with radial stagger pattern encircled the central tower. The specifications of each ring, such as number of heliostats per ring, radial distance and target angle, are listed in Table 2 and the heliostats along each ring are separated with equal radial spacing. According

Please cite this article in press as: Chong, K.K., Tan, M.H. Range of motion study for two different sun-tracking methods in the application of heliostat field. Sol. Energy (2011), doi:10.1016/j.solener.2011.04.024

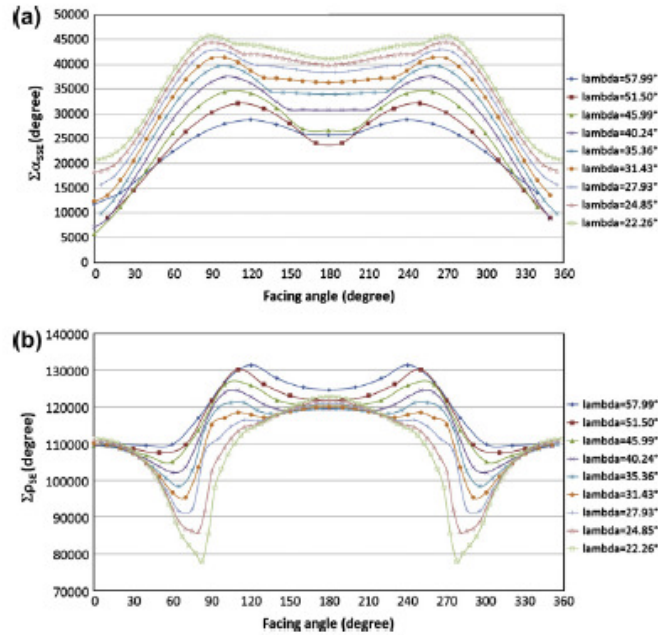


Fig. 8. The annual accumulated tracking angle of a single heliostat versus facing angle in the case of latitude 45°. (a) The annual accumulated elevation angle for SE method ($\Sigma\alpha_{SE}$). (b) The annual accumulated spinning angle for SE method ($\Sigma\rho_{SE}$). (c) The annual accumulated elevation angle for AE method ($\Sigma\alpha_{AE}$). (d) The annual accumulated azimuth angle for AE method ($\Sigma\rho_{AE}$).

to the sun-tracking formulas stated earlier, the local coordinate of the heliostat can be represented by two position angles, i.e. the facing angle ϕ and the target angle λ . Alternatively, we can also represent the position of the heliostat's central point (defined as the cross section point of two sun-tracking axes) with Cartesian coordinate of (H_{ex} , H_{ey} , H_{ez}) and the position of target located at the center of heliostat field as $(0, 0, H)$. The relationship between the Cartesian coordinate and the position angles of heliostat are as below:

$$H_{ex} = -R \sin \phi \quad (22)$$

$$H_{ey} = -R \cos \phi \quad (23)$$

$$H_{ez} = h \quad (24)$$

provided that

$$R = \frac{H - h}{\tan \lambda} \quad (25)$$

where H_{ex} is the distance of the concerned heliostat in east-west direction (it is positive value if the heliostat is located on the east of the tower), H_{ey} is the distance of the concerned heliostat in north-south direction (it is positive value if the heliostat is located on the north of the tower), R is perpendicular distance between the central point of con-

cerned heliostat and the central line of central tower or radial distance, H is the target height, and h is the height of the concerned heliostat.

2.3. Annual accumulated sun-tracking angles

Since the orientation of sun-tracking axes for AE and SE methods are quite different, the sun-tracking angles, α_{AE} and ρ_{AE} of AE method will be definitely different from α_{SE} and ρ_{SE} of SE method. In practice, the reflector of the heliostat is set to be in the stowed orientation also known as the storage position, i.e. facing the sky, when it is not in operation for minimizing the wind load acting on the reflector. Hence, to simulate the actual operation of heliostat field, the computation of accumulated sun-tracking angle should be started from the stowed orientation during the sunrise as well as returned back to this orientation during the sunset. To fully understand the range of motion for the two different methods, the annual accumulated sun-tracking angles are calculated for both the cases of a single heliostat and the heliostat field.

The annual accumulated sun-tracking angle of any heliostat is defined as a summation of angular movement of the particular heliostat for the daily operation with solar time from 0700 h (or $t_s = 7$) to 1700 h (or $t_s = 17$)

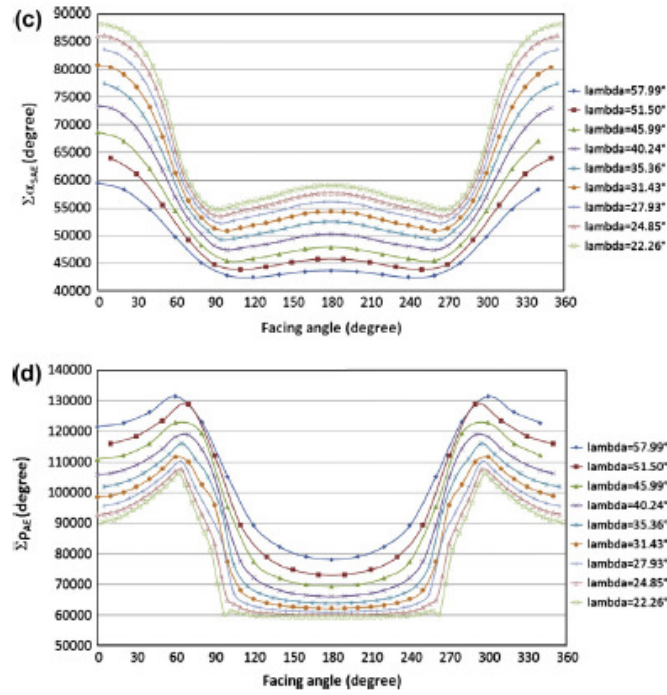


Fig 8. (continued)

and throughout the year with the calendar day from 1st January (or $N=1$) to 31st December (or $N=365$) provided that the heliostat is started from and returned to the stowed position during the daily tracking. Furthermore, we only consider the heliostat that adopts open-loop sun-tracking system that means the angular movement of heliostat is strictly based on the calculated tracking angles using two optical encoders as position sensors and therefore the heliostat movement is not affected by windy or cloudy weather.

To differentiate with the elevation angles relative to their respective origins that are α_{AE} and α_{SE} as defined in Fig. 2a and b, we define α_{SAE} and α_{SSE} as the elevation angles relative to the stowed orientation for AE and SE methods respectively in which $\alpha_{SAE} = 90^\circ - \alpha_{AE}$ and $\alpha_{SSE} = 90^\circ - \lambda - \alpha_{SE}$. The annual accumulated elevation and azimuth angles of a single heliostat for AE method are represented by $\Sigma\alpha_{SAE}$ and $\Sigma\rho_{AE}$ respectively, while the annual accumulated elevation and spinning angles of a single heliostat for SE method are represented by $\Sigma\alpha_{SSE}$ and $\Sigma\rho_{SE}$ respectively. To differentiate from the case of a single heliostat, the annual accumulated angles of heliostat field are indicated by using a double sum, i.e. $\Sigma\Sigma\alpha_{SAE}$, $\Sigma\Sigma\rho_{AE}$, $\Sigma\Sigma\alpha_{SSE}$ and $\Sigma\Sigma\rho_{SE}$.

Algorithm of computing the annual accumulated sun-tracking angles of the heliostat field is presented in the flow chart as illustrated in Fig. 5a and b. In this algorithm, it always considers the computation of shortest pathway for the heliostat to reach the tracking position in each interval during period of sun-tracking in order to optimize the annual accumulated sun-tracking angles.

2.4. Annual power consumption of heliostat field on sun-tracking system

For AE method, the annual power consumption of the heliostat field on the sun-tracking system can be computed using the following formula:

$$\Sigma P_{AE} = \left(\frac{\Sigma\Sigma\alpha_{SAE} \times G_a}{\omega_a(\text{rpm}) \times 60 \times 360} \times P_a(\text{kW}) \right) + \left(\frac{\Sigma\Sigma\rho_{AE} \times G_p}{\omega_p(\text{rpm}) \times 60 \times 360} \times P_p(\text{kW}) \right) \quad (26)$$

For SE method, the annual power consumption of the heliostat field can be obtained by simply replacing $\Sigma\Sigma\alpha_{SAE}$ and $\Sigma\Sigma\rho_{AE}$ with $\Sigma\Sigma\alpha_{SSE}$ and $\Sigma\Sigma\rho_{SE}$ respectively in Eq. (26). G_p is gear ratio of the gear train in the azimuth or

spinning drive; G_g is gear ratio of the gear train in the elevation drive; ω_e is angular speed of the elevation motor; ω_p is angular speed of the azimuth or spinning motor; P_e is power rating of the elevation motor; and P_p is power rating of azimuth or spinning motor.

3. Result and discussion

To simulate the annual accumulated angles of the two different sun-tracking methods, the algorithm as shown in Fig. 5a and b are applied in which Eqs. (10), (11a), (11b), (12) and Eqs. (18), (19a), (19b), (20), (21) are used for SE and AE methods respectively. The three major parameters that affect the annual accumulated tracking angles are analyzed in this study, which are latitude (Φ), facing angle (ϕ) and target angle (λ). Besides that, a detailed comparison study has also been carried out for both cases of a single heliostat and the heliostat field.

3.1. Comparison of two methods for a single heliostat

The simulation of the annual accumulated angles of a single heliostat has been performed to calculate $\Sigma\alpha_{SSE}$ and $\Sigma\rho_{SE}$ for SE method and $\Sigma\alpha_{SAE}$ and $\Sigma\rho_{AE}$ for AE method based on the specification as listed in Table 1. At first, the characteristic of the annual accumulated angle of a single heliostat at different latitudes is analyzed. For the case of SE method, Fig. 6a and b are plotted to show the annual accumulated elevation ($\Sigma\alpha_{SSE}$) and spinning angles ($\Sigma\rho_{SE}$) of a single heliostat versus facing angle in the case of target angle fixed at 22.26°. Similarly, Fig. 6c and d are plotted for the case of AE method. For the equator (or latitude 0°), the graphs in Fig. 6a–d have shown perfect symmetrical patterns between north field and south field as well as east field and west field. On the other hand,

for the other latitudes, such as 15°N, 30°N, 45°N, 15°S and 30°S, the graphs only show symmetrical patterns between east field and west field. There is another remarkable relationship between the corresponding latitudes in northern and southern hemispheres shown in Fig. 6a–d where the graphs of annual accumulated tracking angles at northern hemisphere will be identical to that of southern hemisphere by simply displacing one of them with 180° of facing angle. In other words, the north field in the northern hemisphere behaves identically to the south field in the southern hemisphere. For a comparison of the annual accumulated elevation angle between SE and AE methods, it is obvious that $\Sigma\alpha_{SSE}$ with the range of 18,088–45,718° is about half of $\Sigma\alpha_{SAE}$ with the range of 54,641–88,113°. Nevertheless, $\Sigma\rho_{SE}$ with the range of 77,977–122,842° is about 20% more than $\Sigma\rho_{AE}$ with the range of 59,298–106,247°.

Furthermore, the characteristic of the annual accumulated angle of a single heliostat with different position angles (combination of target angle and facing angle) is carefully analyzed as well. All the possible position angles of 342 heliostats in the field layout as shown in Fig. 4 are considered in our analysis for the latitudes 0° and 45°N. This study can also facilitate us to understand more about the contribution of individual heliostat with different position angles to the total annual accumulated angles of the heliostat field. Since the simulated graphs of the heliostat located at southern hemisphere can be deduced from that of northern hemisphere, it will be sufficient that we only show the graphs of the heliostat located at equator and northern hemisphere.

For the latitude 0°, Fig. 7a–d show the annual accumulated sun-tracking angles varying against both facing angle and target angle for two different methods. The figures have shown perfect symmetry between the east and west fields as well as between the north and south fields for all target angles. Fig. 7c shows that $\Sigma\alpha_{SAE}$ is inversely pro-

Table 3
Annual accumulated sun-tracking angles and power consumption of heliostat field.

Latitude	SE method		Annual power consumption on elevation movement (MWh)	Annual power consumption on spinning movement (MWh)	Annual total power consumption (MWh)
	$\Sigma\alpha_{SSE}$ (°)	$\Sigma\rho_{SE}$ (°)			
0°	10,898,727	38,068,016	1.83	4.27	6.10
15°N	10,930,488	38,036,573	1.84	4.26	6.10
30°N	11,040,512	37,957,837	1.86	4.25	6.11
45°N	11,161,685	37,990,854	1.88	4.26	6.13
15°S	10,930,488	38,036,573	1.84	4.26	6.10
30°S	11,040,512	37,957,837	1.86	4.25	6.11
AE method					
	$\Sigma\alpha_{SAE}$ (°)	$\Sigma\rho_{AE}$ (°)	Annual power consumption on elevation movement (MWh)	Annual power consumption on azimuth movement (MWh)	Annual total power consumption (MWh)
0°	20,379,193	26,672,585	3.42	2.99	6.41
15°N	20,404,920	27,058,546	3.43	3.03	6.46
30°N	20,491,149	28,092,050	3.44	3.15	6.59
45°N	20,620,319	29,445,112	3.47	3.30	6.76
15°S	20,404,920	27,058,546	3.43	3.03	6.46
30°S	20,491,149	28,092,050	3.44	3.15	6.59

Please cite this article in press as: Chong, K.K., Tan, M.H. Range of motion study for two different sun-tracking methods in the application of heliostat field. Sol. Energy (2011), doi:10.1016/j.solener.2011.04.024

portional to the target angle (or lambda) at all facing angles. Contrarily, Fig. 7d shows that $\Sigma\rho_{SAE}$ is proportional to the target angle (or lambda) at all facing angles. From Fig. 7a and b, SE method has also shown the same tendency as that of AE method except for the facing angles around both 0° and 180° . For a comparison between SE and AE methods as shown in Fig. 7a and c respectively, it is obvious that $\Sigma\alpha_{SSE}$ with the range of $17,311\text{--}45,502^\circ$ is lesser than $\Sigma\alpha_{SAE}$ with the range of $50,303\text{--}69,080^\circ$. Nonetheless, for Fig. 7b and d, $\Sigma\rho_{SE}$ with the range of $95,075\text{--}122,055^\circ$ is more than $\Sigma\rho_{AE}$ with the range of $67,704\text{--}107,962^\circ$.

Fig. 8a–d show the annual accumulated sun-tracking angles varying against both facing and target angles for two different methods at the latitude 45°N . In northern hemisphere, the graphs of the annual accumulated angle show perfect symmetry between east and west fields for all target angles. Fig. 8c shows that $\Sigma\alpha_{SAE}$ is inversely proportional to the target angle at all facing angles. Contrarily, Fig. 8d shows that $\Sigma\rho_{SAE}$ is proportional to the target angle at all facing angles. From Fig. 8a and b, SE method has also shown the same tendency as that of AE method except the heliostat located at north and south fields. To compare between SE and AE methods as shown in Fig. 8a and c respectively, it is obvious that $\Sigma\alpha_{SSE}$ with the range of $5732\text{--}45,718^\circ$ is lesser than $\Sigma\alpha_{SAE}$ with the range of $42,478\text{--}88,113^\circ$. For Fig. 8b and d, $\Sigma\rho_{SE}$ with the range of $77,977\text{--}131,400^\circ$ is more than $\Sigma\rho_{AE}$ with the range of $59,298\text{--}131,400^\circ$.

3.2. Comparison of two methods for heliostat field

The simulation of the annual accumulated angles of heliostat field has been performed to compute $\Sigma\Sigma\alpha_{SSE}$ & $\Sigma\Sigma\rho_{SE}$ and $\Sigma\Sigma\alpha_{SAE}$ & $\Sigma\Sigma\rho_{AE}$ for both SE and AE methods correspondingly based on the specification as revealed in Table 2 and Fig. 4. Fig. 5a and b show the complete algorithms of simulation programs designed to compute the annual accumulated tracking angles of heliostat field for SE and AE tracking methods respectively. The simulated results of $\Sigma\Sigma\alpha_{SAE}$, $\Sigma\Sigma\rho_{AE}$, $\Sigma\Sigma\alpha_{SSE}$ and $\Sigma\Sigma\rho_{SE}$ at different latitudes, i.e. 0° , 15°N , 30°N , 45°N , 15°S and 30°S , are listed in Table 3. In overall, the annual accumulated elevation angle for the SE method $\Sigma\Sigma\alpha_{SSE}$ is about $53.5\text{--}54.1\%$ of the annual accumulated elevation angle for the AE method $\Sigma\Sigma\alpha_{SAE}$. Meanwhile, the annual accumulated azimuth angle for the AE method $\Sigma\Sigma\rho_{AE}$ is about $70.1\text{--}74.0\%$ of the annual accumulated spinning angle for the SE method $\Sigma\Sigma\rho_{SE}$. To be more practical concern, the corresponded power consumption of the heliostat field for both sun-tracking methods is also calculated based on the annual accumulated angles. From the computed result, central tower system located at latitude at 0° consumes the lowest annual power consumption on sun-tracking system compared to those of other latitudes. In general, the annual power consumption for SE method is lower than that of AE method in all latitudes.

4. Conclusions

Study on the range of motion for two different sun-tracking methods at the level of single heliostat and heliostat field has been conducted in details. The algorithms to analyze the annual accumulated sun-tracking angles for both methods have also been developed. For a comparison of two tracking methods, $\Sigma\Sigma\alpha_{SSE}$ is about half of $\Sigma\Sigma\alpha_{SAE}$ but $\Sigma\Sigma\rho_{AE}$ is about $70\text{--}74\%$ of $\Sigma\Sigma\rho_{SE}$. As a result, total power consumption on the sun-tracking system of SE method can be about $4.8\text{--}9.3\%$ lesser than that of AE method. Despite the mechanical design of the heliostat using SE sun-tracking method is different from that of the AE sun-tracking method, both types of heliostats in fact contains exactly the same basic driving mechanism such as motor, gearbox, optical encoder and control system. The necessitated manufacturing, assembly and alignment procedures are quite similar for both methods. Comparing the construction cost of both SE and AE methods is not the main aim of this paper because it depends on many factors such as the mechanical design, optical design, labor cost (very much dependent on the country), the quantity of heliostat to be manufactured, quality of materials, etc. However, the materials cost for the heliostat with different tracking methods could be almost the same because both tracking methods require almost the same types of materials such as steel structure, driving mechanism, sensors, and mirrors. Therefore, the final construction cost can be very much dependent on the innovative design of the heliostat and it will remain as a great challenge for the solar energy engineering in the future.

Acknowledgements

The authors would like to express their gratitude to Fundamental Research Grant Scheme (FRGS) by the Ministry of Higher Education with Project Number FRGS/1/10/SG/UTAR/03/4 and UTAR Research Fund with Project Number IPSR/RMC/UTARRF/C2-10/C6 for the financial support in this study.

References

- Chen, Y.T., Chong, K.K., Bligh, T.P., Chen, L.C., Yunus, J., Kannan, K.S., Lim, B.H., Lim, C.S., Alias, M.A., Bidin, N., Aliman, O., Salehan, S., Rezan, S.A.H. Shk. Abd., Tam, C.M., Tan, K.K., 2001. Non-imaging focusing heliostat. *Solar Energy* 71 (3), 155–164.
- Chen, Y.T., Chong, K.K., Lim, C.S., Lim, B.H., Tan, K.K., Aliman, Omar, Bligh, T.P., Tan, B.K., Ismail, Ghazally, 2002. Report of the first prototype of non-imaging focusing heliostat and its application in high temperature solar furnace. *Solar Energy* 72 (6), 531–544.
- Chen, Y.T., Chong, K.K., Lim, B.H., Lim, C.S., 2003. Study of residual aberration for non-imaging focusing heliostat. *Solar Energy Materials and Solar Cells* 79 (1), 1–20.
- Chen, Y.T., Kribus, A., Lim, B.H., Lim, C.S., Chong, K.K., Kami, J., Buck, R., Pfahl, A., Bligh, T.P., 2004. Comparison of two sun tracking methods in the application of a heliostat field. *Journal of Solar Energy Engineering* 126 (1), 638–644.

- Chen, Y.T., Chong, K.K., Lim, C.S., Lim, B.H., Tan, B.K., Lu, Y.F., 2005. Report on the second prototype of non-imaging focusing heliostat and its application in food processing. *Solar Energy* 79 (3), 280–289.
- Chen, Y.T., Lim, B.H., Lim, C.S., 2006. Complete solution of sun tracking for heliostat. *Communications in Theoretical Physics* 45, 165–166.
- Chong, K.K., 2002. Characterization of non-imaging focusing heliostat in University of Technology Malaysia. Ph.D. Thesis, Faculty of Electrical Engineering, Universiti Teknologi Malaysia, Skudai, Malaysia.
- Chong, K.K., 2010a. Optimization of nonimaging focusing heliostat in dynamic correction of astigmatism for a wide range of incident angles. *Optics Letters* 35 (10), 1614–1616.
- Chong, K.K., 2010b. Optical analysis for simplified astigmatic correction of non-imaging focusing heliostat. *Solar Energy* 84 (8), 1356–1365.
- Chong, K.K., Tan, B.K., Yunus, J., 2006. Characteristic study of hot spot in the new solar furnace comprising of non-imaging focusing heliostat and parabolic reflector. *Journal of Science and Technology in the Tropics* 2, 27–34.
- Chong, K.K., Lim, C.Y., Hiew, C.W., 2011. Cost-effective solar furnace system using fixed geometry non-imaging focusing heliostat and secondary parabolic concentrator. *Renewable Energy* 36 (5), 1595–1602.
- Guo, M., Wang, Z., Liang, W., Zhang, X., Zang, C., Lu, Z., Wei, X., 2010. Tracking formulas and strategies for a receiver oriented dual-axis tracking toroidal heliostat. *Solar Energy* 84, 939–947.
- Li, L., Lim, C.S., 2009. Tracking speed analysis for heliostat using spinning-elevation tracking mode. *Journal of Solar Energy Engineering* 131 (3), 034501–034505.
- Schubnell, M., Ries, H., 1990. The optics of a two-stage solar furnace. *Solar Energy Materials* 21, 213–217.
- Stine, W.B., Harrigan, R.W. (Eds.), 1985. *Solar Energy Fundamentals and Design with Computer Applications*. John Wiley, New York, pp. 135–262.
- Zaibel, R., Dagan, E., Karni, J., Ries, H., 1995. An astigmatic corrected target-aligned heliostat for high concentration. *Solar Energy Materials and Solar Cells* 37, 191–202.